



**HAL**  
open science

## **Association of snR190 snoRNA chaperone with early pre-60S particles is regulated by the RNA helicase Dbp7 in yeast**

Mariam Jaafar, Julia Contreras, Carine Dominique, Sara Martín-Villanueva, Régine Capeyrou, Patrice Vitali, Olga Rodríguez-Galán, Carmen Velasco, Odile Humbert, Nicholas Watkins, et al.

### ► To cite this version:

Mariam Jaafar, Julia Contreras, Carine Dominique, Sara Martín-Villanueva, Régine Capeyrou, et al.. Association of snR190 snoRNA chaperone with early pre-60S particles is regulated by the RNA helicase Dbp7 in yeast. *Nature Communications*, 2021, 12 (1), pp.6153. 10.1038/s41467-021-26207-w . hal-03775895

**HAL Id: hal-03775895**

**<https://hal.science/hal-03775895>**

Submitted on 9 Nov 2022

**HAL** is a multi-disciplinary open access archive for the deposit and dissemination of scientific research documents, whether they are published or not. The documents may come from teaching and research institutions in France or abroad, or from public or private research centers.

L'archive ouverte pluridisciplinaire **HAL**, est destinée au dépôt et à la diffusion de documents scientifiques de niveau recherche, publiés ou non, émanant des établissements d'enseignement et de recherche français ou étrangers, des laboratoires publics ou privés.

1 **Association of snR190 snoRNA chaperone with early pre-60S particles is regulated by the RNA**  
2 **helicase Dbp7 in yeast**

3  
4 Mariam Jaafar<sup>1,2,9</sup>, Julia Contreras<sup>3,4</sup>, Carine Dominique<sup>1</sup>, Sara Martin Villanueva<sup>3</sup>, Régine  
5 Capeyrou<sup>1</sup>, Patrice Vitali<sup>1</sup>, Olga Rodríguez-Galán<sup>3,4</sup>, Carmen Velasco<sup>3,5</sup>, Odile Humbert<sup>1</sup>, Nicholas  
6 J. Watkins<sup>6</sup>, Eduardo Villalobo<sup>3,5</sup>, Katherine E. Bohnsack<sup>7</sup>, Markus T. Bohnsack<sup>7,8</sup>, Yves Henry<sup>1</sup>,  
7 Raghida Abou Merhi<sup>2</sup>, Jesús de la Cruz<sup>3,4</sup> and Anthony K. Henras<sup>1\*</sup>

8  
9 <sup>1</sup> Molecular, Cellular and Developmental Biology Unit (MCD), Centre de Biologie Intégrative (CBI),  
10 Université de Toulouse, CNRS, UPS, 31062 Toulouse, France.

11 <sup>2</sup> Genomic Stability and Biotherapy (GSBT) Laboratory, Faculty of Sciences, Rafik Hariri Campus,  
12 Lebanese University, Lebanon.

13 <sup>3</sup> Instituto de Biomedicina de Sevilla (IBiS), Hospital Universitario Virgen del  
14 Rocío/CSIC/Universidad de Sevilla, 41013 Seville, Spain.

15 <sup>4</sup> Departamento de Genética, Facultad de Biología, Universidad de Sevilla, 41012 Seville, Spain.

16 <sup>5</sup> Departamento de Microbiología, Facultad de Biología, Universidad de Sevilla, 41012 Seville,  
17 Spain.

18 <sup>6</sup> Institute for Cell and Molecular Biosciences, The Medical School, Newcastle University,  
19 Newcastle upon Tyne, NE1 7RU, UK.

20 <sup>7</sup> Department of Molecular Biology, University Medical Centre Göttingen, 37073 Göttingen,  
21 Germany.

22 <sup>8</sup> Göttingen Center for Molecular Biosciences, Georg-August University Göttingen, 37077  
23 Göttingen, Germany.

24 <sup>9</sup> Present address: Cancer Research Center of Lyon (CRCL), 69 008 Lyon, France.

25  
26 \*: Corresponding author: [anthony.henras@univ-tlse3.fr](mailto:anthony.henras@univ-tlse3.fr)

1 **Abstract**

2 Synthesis of eukaryotic ribosomes involves the assembly and maturation of precursor particles  
3 (pre-ribosomal particles) containing ribosomal RNA (rRNA) precursors, ribosomal proteins (RPs)  
4 and a *plethora* of assembly factors (AFs). Formation of the earliest precursors of the 60S  
5 ribosomal subunit (pre-60S r-particle) is among the least understood stages of ribosome  
6 biogenesis. It involves the Npa1 complex, a protein module suggested to play a key role in the  
7 early structuring of the pre-rRNA. Npa1 displays genetic interactions with the DExD-box protein  
8 Dbp7 and interacts physically with the snR190 box C/D snoRNA. We show here that snR190  
9 functions as a snoRNA chaperone, which likely cooperates with the Npa1 complex to initiate  
10 compaction of the pre-rRNA in early pre-60S r-particles. We further show that Dbp7 regulates  
11 the dynamic base-pairing between snR190 and the pre-rRNA within the earliest pre-60S r-  
12 particles, thereby participating in structuring the peptidyl transferase center (PTC) of the large  
13 ribosomal subunit.

## 1 **Introduction**

2 Ribosomes are universal molecular machines responsible for protein synthesis. The first crystal  
3 structures of ribosomal subunits (r-subunits)<sup>1,2</sup> revealed that the ribosome is a ribozyme<sup>3</sup>, namely  
4 an RNA-based enzyme. This implies that an essential aspect of ribosome biogenesis is the  
5 accurate folding of the rRNAs to generate their functional structure. In yeast, rRNAs contained in  
6 the 40S (18S) and 60S (5S, 5.8S and 25S) r-subunits are generated by transcription of rDNA genes  
7 by RNA polymerases I and III (Pol I and Pol III). Pol I-mediated transcription generates a primary  
8 transcript containing the sequences of 18S, 5.8S and 25S rRNAs. Maturation of this pre-rRNA  
9 occurs within a series of pre-ribosomal particles containing also RPs and numerous AFs. This  
10 process comprises pre-rRNA nucleotide modifications, cleavage and folding events and the  
11 incorporation and proper positioning of RPs that gradually lead to the formation of mature r-  
12 subunits<sup>4-6</sup>.

13 Assembly of the earliest precursors to the large (60S) r-subunit is the least understood  
14 step of eukaryotic ribosome biogenesis. These particles contain numerous small nucleolar  
15 ribonucleoprotein particles (snoRNPs)<sup>7</sup>, which belong to the C/D- and H/ACA-type families. C/D-  
16 type snoRNPs typically catalyze the 2'-O-methylation of selected nucleotides. They contain a box  
17 C/D small nucleolar RNA (snoRNA) associated with a protein core including the methyltransferase  
18 Nop1. H/ACA-type snoRNPs are composed of a box H/ACA snoRNA and several proteins including  
19 the pseudouridine synthase Cbf5, which isomerizes uridines into pseudouridines. In both cases,  
20 the snoRNAs contain antisense elements that base-pair to target sequences on the pre-rRNA,  
21 and function as a guide for specific nucleotide modifications<sup>8,9</sup>. A subset of snoRNAs from both  
22 families do not function as modification guides but as RNA chaperones, assisting folding of the  
23 pre-rRNA to promote proper processing. In yeast, four snoRNP chaperones, containing U3, U14,  
24 snR30 and snR10 snoRNAs, are involved in the biogenesis of the small r-subunit<sup>10-13</sup>. An  
25 important issue that remains to be addressed is when and how snoRNA base-pairings with the  
26 pre-rRNA are disrupted, given that some of these interactions are thermodynamically highly  
27 stable. NTP-dependent RNA helicases have the potential to dissociate snoRNA-pre-rRNA  
28 interactions. Twelve RNA helicases (Dbp2, Dbp3, Dbp6, Dbp7, Dbp9, Dbp10, Drs1, Mak5, Mtr4,  
29 Spb4, Prp43 and Has1) participate in the synthesis of the large r-subunit<sup>14,15</sup> and interestingly,

1 eight of them (Dbp3, Dbp6, Dbp7, Dbp9, Drs1, Has1, Mak5 and Prp43) are present in early pre-  
2 60S r-particles<sup>7</sup>. These proteins are believed to fulfill various functions in the remodeling events  
3 occurring within pre-60S r-particles, such as promoting formation, stability or dissociation of RNA  
4 secondary structures or regulating the binding or dissociation of proteins<sup>16,17</sup>. Among these  
5 enzymes, only the RNA helicase Prp43 and Dbp3 have been shown to function in the release of  
6 snoRNAs<sup>18,19</sup>.

7         The structural organization of the RNA components of the earliest pre-60S r-particles  
8 remains ill-defined. In the mature 60S r-subunit, the 25S and 5.8S rRNAs are organized in 6  
9 structural domains (I to VI), each beginning with short stems referred to as root helices  
10 (Supplementary Fig. 1). These root helices are clustered in the mature particles and their  
11 clustering and compaction has been proposed to occur early during assembly of pre-60S r-  
12 particles<sup>20</sup>. In the earliest pre-60S r-particles, root helix I and base-pairing interactions between  
13 the 25S and 5.8S rRNAs, key determinants of domain I folding, are already established<sup>21</sup>. In the  
14 earliest pre-60S particle cryo-electron microscopy structure reported to date (State A<sup>22</sup>), the root  
15 helix of domain I is formed, and domains I, II and part of domain VI have acquired their final  
16 secondary structure. These structured domains form a rigid platform, corresponding to the  
17 solvent-exposed side of the mature subunit, onto which takes place assembly and compaction of  
18 the other domains<sup>22</sup>. Failure to correctly complete these early folding events is believed to lead  
19 to turnover of pre-60S r-particles.

20         Formation and/or stability of the earliest pre-60S r-particles in yeast requires the Npa1  
21 complex, a protein module composed of 5 AFs: Npa1, Npa2, Nop8, Rsa3 and the RNA helicase  
22 Dbp6<sup>7,23,24</sup>. Mapping of RNA interaction sites of Npa1 using the crosslinking and analysis of cDNA  
23 approach (CRAC) revealed that Npa1 interacts with both the 5' (domain I) and 3' (domains V and  
24 VI) regions of the 25S rRNA (Supplementary Fig. 1), and has therefore the potential to act as a  
25 long-range, physical link between domains I, V and VI<sup>25</sup>. The Npa1 complex may therefore  
26 promote or stabilize circularization of the 25S rRNA in the earliest stages of pre-60S r-particle  
27 assembly, by tethering the 5' and 3' domains. Npa1 also crosslinks to a subset of C/D- and H/ACA-  
28 type snoRNAs involved in the chemical modification of nucleotides of the decoding center and  
29 PTC of the large r-subunit. Interestingly, the snR190 box C/D snoRNA is particularly efficiently

1 crosslinked to Npa1. Its antisense sequence upstream of box D' (box A, Supplementary Fig. 2a) is  
2 complementary to a sequence embedded within helix H73 in domain V of the 25S rRNA and it is  
3 predicted to guide ribose 2'-*O*-methylation at position G2395 (Supplementary Fig. 1). However,  
4 this methylation has not been detected in recent large scale studies<sup>26–28</sup>. snR190 also contains  
5 another 15 nucleotide sequence (box B, Supplementary Fig. 2a) that is perfectly complementary  
6 to a sequence in domain I of 25S rRNA near the Npa1 binding site (Supplementary Fig. 1). Like  
7 the Npa1 complex, snR190 therefore also has the potential to make a physical link between the  
8 5' and 3' domains of the 25S rRNA.

9         Here, we provide evidence that yeast snR190 does not function as a methylation guide  
10 snoRNP, but rather as a placeholder preventing specific 25S rRNA sequences from establishing  
11 inappropriate interactions during pre-rRNA folding. Moreover, our data strongly support the  
12 model that Dbp7 regulates the dynamics of base-pairing between snR190 and the 25S rRNA  
13 within early pre-60S r-particles.

## 1 Results

### 2 Genetic link between Dbp7 and snR190 base-pairing site on 25S rRNA

3 The absence of Dbp7 impairs production of the 27S and 7S pre-rRNA intermediates during early  
4 pre-60S r-particle maturation, and compromises synthesis of mature 25S and 5.8S rRNAs and the  
5 60S subunit<sup>29,30</sup>. The precise molecular function of Dbp7 in this process remains elusive. *DBP7*  
6 displays genetic interactions with most genes encoding members of the Npa1 complex<sup>24</sup>,  
7 suggesting that Dbp7 function may be related to these AFs<sup>25</sup>. To gain further insight into the  
8 function of Dbp7, we exploited the severe growth defect of the *dbp7Δ* strain to isolate  
9 suppressors bearing mutations in rRNAs. We made use of the yeast strain NOY891<sup>31</sup>, in which all  
10 the chromosomal rDNA genes are deleted and the 35S pre-rRNA is expressed from a plasmid  
11 (pNOY353, 2 $\mu$ , *TRP1*) driven by the galactose-inducible *GAL7* promoter<sup>31</sup>. We further engineered  
12 this strain to express a HA-tagged version of Dbp7 under control of another galactose-inducible  
13 promoter (*GAL1::HA-DBP7*, strain EMY65). To identify rRNA suppressors of Dbp7 loss-of-function,  
14 a mutant library of a second plasmid, (pNOY373, 2 $\mu$ , *LEU2*) expressing the 35S pre-rRNA from its  
15 natural Pol I-dependent promoter, was transformed into strain EMY65. Transformants were  
16 screened on selective SD medium for faster-growing clones, condition where neither pNOY353  
17 nor the *GAL1::HA-DBP7* construct are expressed (Supplementary Fig. 3). Only two plasmids  
18 recovered from candidate clones, referred to as Sup. #2 and Sup. #10, reproducibly improved the  
19 growth of strain EMY65 when re-transformed (Fig. 1a). Their rDNA inserts were found to carry  
20 different mutations (Supplementary Table 1). Strikingly, both featured, among others, the same  
21 rRNA mutation, a C-to-U transition at position C2392 in helix H73 of the 25S rRNA sequence. To  
22 confirm that C2392U was itself responsible for the suppression effect, we specifically introduced  
23 the C2392T mutation in the wild-type pNOY373 plasmid. In parallel, we also introduced the  
24 T2392C reversion in the Sup. #2 and Sup. #10 plasmids. Growth of the resulting strains at 30 °C  
25 on selective SGal and SD media showed that the C2392U substitution was both necessary and  
26 sufficient to rescue the growth defect of the *dbp7Δ* strain (Fig. 1a). This suppression effect was  
27 not complete, as growth of the EMY65 strain transformed with the Sup. #10 plasmid on SD  
28 medium was slower than that of the original NOY891 strain expressing Dbp7 (Fig. 1b).

1 Helix H73 corresponds to the root helix of domain V of the 25S rRNA, which forms the PTC  
2 of the mature 60S r-subunit (Fig. 1c and Supplementary Fig. 1). Interestingly, the C2392U  
3 substitution lies in the immediate vicinity of G2395, predicted to undergo ribose 2'-O-  
4 methylation guided by the snR190 box C/D snoRNA (Supplementary Fig. 1) and is expected to  
5 weaken the base-pairing between snR190 and its complementary sequence on the pre-rRNA.  
6 snR190 is the snoRNA most efficiently crosslinked to Npa1 in CRAC experiments<sup>25</sup>. This intimate  
7 biochemical relationship between Npa1 and snR190 along with (i) the genetic interaction  
8 between Dbp7 and Npa1 and (ii) the suppression of the growth defect of the loss-of-function of  
9 Dbp7 by a mutation in the 25S rRNA predicted to weaken the base-pairing with snR190, led us to  
10 hypothesize that the function of Dbp7 might be linked to that of snR190.

11

### 12 **snR190 is required for optimal 60S r-subunit biogenesis**

13 In yeast, snR190 is expressed from a dicistronic precursor transcript also supporting expression  
14 of U14, an essential box C/D snoRNA that functions as an RNA chaperone in the maturation of  
15 the 18S rRNA<sup>32</sup>. This particular context precluded using conventional genomic knockout  
16 approaches to inactivate snR190 expression. To interfere with snR190 expression post-  
17 transcriptionally, we mutagenized the genomic sequences encoding box C and the terminal stem  
18 of the snoRNA (*snr190-[mut.C]*, Supplementary Fig. 2b) using the CRISPR-Cas9 approach<sup>33</sup> (see  
19 "Materials and Methods" section for details). We selected two independent *snr190-[mut.C]*  
20 clones in two different yeast genetic backgrounds, W303 and BY4741, and confirmed snR190  
21 depletion by northern blotting (Fig. 2a and Supplementary Fig. 4a). Strains having undergone the  
22 mutagenesis procedure, but which lacked mutations in *SNR190* were used as controls (referred  
23 to as "WT" on the figures).

24 To assess the impact of the loss-of-function of snR190 on cell fitness, we carried out  
25 growth tests in liquid YPD medium at 30 °C. We observed that the *snr190-[mut.C]* strains showed  
26 a moderate but reproducible decrease in growth rate (Supplementary Table 2 and  
27 Supplementary Fig. 15). In order to verify that this defect was not due to off-target mutations  
28 introduced by the CRISPR-Cas9 approach, we rescued snR190 expression in these strains. The  
29 *U14-SNR190* gene was PCR amplified from yeast genomic DNA and inserted into a centromeric

1 vector. The resulting plasmid, as well as an empty vector (*E.V.*), as a negative control, were  
2 transformed into the *snr190-[mut.C]* strains. We confirmed by northern blotting re-expression of  
3 snR190 in the *snr190-[mut.C]* strain in the W303 background (Fig. 2b). Ectopic expression of  
4 snR190 in the *snr190-[mut.C]* strains (BY4741 and W303 backgrounds) fully restored wild-type  
5 growth rates (Supplementary Table 2 and Supplementary Fig. 15). These results indicated that,  
6 in contrast to numerous box C/D snoRNAs functioning as methylation guides, snR190 is required  
7 for optimal yeast proliferation.

8 In yeast, the few known examples of snoRNAs required for yeast proliferation (U3, U14,  
9 snR10 and snR30) function as chaperones in the 40S r-subunit biogenesis<sup>10-13</sup>. We next tested  
10 whether snR190 might function as a snoRNA chaperone in the maturation of pre-60S r-particles  
11 by analyzing pre-rRNA processing in the absence of snR190. Total RNA was extracted from  
12 *snr190-[mut.C]* strains and steady-state levels of pre-rRNA species were analyzed using northern  
13 blotting. Loss-of-function of snR190 resulted in a strong increase in the steady-state levels of the  
14 35S and 33S/32S pre-rRNAs in the *snr190-[mut.C]* mutant compared to the wild-type strains (Fig.  
15 2a and Supplementary Fig. 5a for the W303 background; Supplementary Fig. 4a and  
16 Supplementary Fig. 5b for the BY4741 background), indicating that the maturation of early 90S  
17 r-particles was delayed. We further observed a slight increase in the 27SA<sub>2</sub> precursor levels and  
18 reduced accumulation of the 27SB pre-rRNAs. The 27SB/27SA<sub>2</sub> ratios therefore substantially  
19 decreased in the absence of snR190 in both genetic backgrounds (Supplementary Fig. 5c, d). We  
20 conclude that snR190 loss-of-function impairs conversion of 27SA<sub>2</sub> to 27SB pre-rRNA within pre-  
21 60S r-particles. Low-molecular-weight rRNAs were also studied to determine whether the  
22 absence of snR190 also influences production of the downstream intermediates. The levels of  
23 the 7S pre-rRNAs did not show any apparent change (Supplementary Fig. 6a, b) nor did the levels  
24 of the mature 5.8S rRNAs (Supplementary Fig. 7a, b). Furthermore, no change in the level of 20S  
25 pre-rRNA was observed in absence of snR190, suggesting that snR190 is not involved in pre-40S  
26 r-particle maturation. Importantly, loss-of-function of snR190 slightly affected production of the  
27 mature 25S rRNA (Fig. 2a and Supplementary Fig. 4a). These phenotypes are not due to off-target  
28 mutations introduced by the CRISPR-Cas9 approach, as ectopic re-expression of snR190 in the  
29 *snr190-[mut.C]* strain partially rescued the pre-rRNA processing defects as shown by the reduced

1 levels of the 35S and 27SA<sub>2</sub> intermediates (Fig. 2b). Although these levels did not drop to those  
2 observed in the wild-type W303 strain, accumulation of the 27SB intermediate appeared fully  
3 restored to wild-type levels (Fig. 2b and Supplementary Fig. 8a). Similar observations were made  
4 in the BY4741 background (Supplementary Fig. 8b and Supplementary Fig. 8c), indicating that  
5 although these phenotypes are relatively weak, they are highly reproducible.

6 To determine whether the pre-rRNA processing defects observed in the absence of  
7 snR190 impact 60S r-subunit biogenesis, we analyzed polysome profiles from cell extracts of the  
8 *snr190-[mut.C]* strains in both genetic backgrounds. We observed that loss-of-function of snR190  
9 resulted in a minor deficit in 60S r-subunits, as judged from the slight reduction in the levels of  
10 free 60S relative to 40S r-subunits, and the appearance of half-mer polysomes indicative of a  
11 shortage in 60S subunit and/or translation defects<sup>34,35</sup> (Fig. 2c, W303 background). Re-expression  
12 of snR190 restored a close to wild-type polysome profile, clearly reducing the presence of half-  
13 mer peaks (Fig. 2d). Similar results were obtained in a strain derived from BY4741  
14 (Supplementary Fig. 4b). These results indicate that loss-of-function of snR190 induces minor but  
15 significant pre-rRNA processing defects in the maturation pathway of the 25S rRNA, thus  
16 affecting production of 60S r-subunits and possibly also translation.

17

### 18 **snR190 does not function as a ribose 2'-O-methylation guide**

19 snR190 contains an antisense element upstream of its box D' that is complementary to a  
20 sequence embedded within the root helix (helix H73) of domain V of the 25S rRNA (box A,  
21 Supplementary Fig. 2a). This antisense sequence is predicted to guide methylation of G2395 in  
22 the 25S rRNA<sup>36,37</sup>. Several large scale studies have been undertaken to exhaustively detect and  
23 quantify rRNA methylations in yeast<sup>26-28</sup>, but none of them detected a ribose 2'-O-methylation  
24 at position G2395. To verify these data with a specific emphasis on G2395 methylation, we  
25 mapped methylations in this region of the 25S rRNA using primer extensions at low dNTP  
26 concentration<sup>38</sup>. Two different primers, proximal and distal, were used in these experiments,  
27 located 19 and 40 nucleotides upstream of G2395 respectively (Supplementary Fig. 9). For this  
28 experiment, we used the *snr190-[mut.C]* strain (BY4741 background) transformed with the  
29 *SNR190-U14* expression plasmid (*WT*) or the empty vector (*E.V.*) as a control. Primer extension

1 using the distal primer revealed two expected signals corresponding to methylations of  
2 nucleosides U2417 and U2421 (Fig. 3, right panel). No clear signal located further upstream at  
3 G2395 was observed. Primer extension with the proximal primer (Fig. 3, left panel) confirmed the  
4 absence of a strong, snR190-dependent signal at position G2395. Analysis of snR190 putative  
5 secondary structure revealed that a potential internal stem can be formed between part of the  
6 antisense sequence and a region of the snoRNA including box C' and the downstream sequence  
7 (Supplementary Fig. 2a), possibly inactivating the guide element. To test whether this internal  
8 stem prevents methylation of G2395, we introduced mutations in the *SNR190-U14* expression  
9 plasmid to destabilize the stem (*snr190-[mut.S]*, Supplementary Fig. 2b). These mutations did not  
10 provoke any change in the signal obtained at position G2395 (Fig. 3). We conclude that snR190  
11 does not direct 25S rRNA modification at position G2395.

12

### 13 **snR190 functions as a chaperone in pre-60S r-particle maturation**

14 In addition to its antisense box A, snR190 contains another 15 nucleotide-long potential antisense  
15 element showing perfect complementarity to a sequence within domain I of the 25S rRNA,  
16 located in the vicinity of one of the Npa1 cross-linking sites<sup>25</sup> (box B, Supplementary Fig. 1 and  
17 2a). In the mature 60S r-subunit, this 25S rRNA sequence is base-paired to the 5.8S rRNA. Part of  
18 snR190 box B has been described previously to reinforce the base-pairing of box A in the vicinity  
19 of G2395<sup>39</sup>. In any case, snR190 contains two long antisense elements with the potential to base-  
20 pair to two different regions of the 25S rRNA in domains I and V. In order to test whether boxes  
21 A and B are required for snR190 function in the maturation of pre-60S r-particles, we introduced  
22 drastic mutations in boxes A and/or B on the *U14-SNR190* expression vector described above  
23 (*snr190-[mut.A]*, *snr190-[mut.B]* or *snr190-[mut.AB]*, Supplementary Fig. 2c). The resulting  
24 plasmids were used to transform the *snr190-[mut.C]* strain in the BY4741 or W303 genetic  
25 background. Mutation of box A or box B did not affect yeast cell proliferation as both mutant  
26 strains displayed a doubling time very similar to that of the *snr190-[mut.C]* strain rescued by the  
27 plasmid expressing wild-type snR190 (Supplementary Table 2 and Supplementary Fig. 15). In  
28 contrast, simultaneous mutation of boxes A and B induced a reproducible growth defect in both  
29 genetic backgrounds, with a doubling time intermediate between those of the wild-type and

1 *snr190-[mut.C]* strains (Supplementary Table 2 and Supplementary Fig. 15). In no case was this  
2 the result of reduced steady-state levels of the mutated snoRNAs (Fig. 4b). We next analyzed r-  
3 particle profiles in these mutants after fractionation of total cell extracts on density gradients.  
4 Mutation of boxes A or B alone showed polysome profiles very similar to that of the wild-type  
5 W303 strain (Fig. 4a). In contrast, mutation of both boxes A and B induced a minor imbalance of  
6 free 40S and 60S r-subunits, comparable to that observed in the *snr190-[mut.C]* strain, and the  
7 appearance of half-mer polysomes. Pre-rRNA processing analyses in the different strains gave  
8 results consistent with the polysome profiles (Fig. 4b, W303 background). The 27SB/27SA<sub>2</sub> ratio  
9 dropped to approximately half that of the wild-type in the absence of snR190 (Supplementary  
10 Fig. 8a), reflecting the accumulation of the 27SA<sub>2</sub> and depletion of the 27SB species. Ectopic  
11 expression of wild-type snR190, or the mutations of box A or box B alone, restored a close to  
12 wild-type 27SB/27SA<sub>2</sub> ratio. In contrast, mutation of both boxes resulted in a 27SB/27SA<sub>2</sub> ratio  
13 close to that of the *snr190-[mut.C]* strain (Fig. 4b and Supplementary Fig. 8a). These results were  
14 also reproduced in the BY4741 background (Supplementary Fig. 8b, c).

15         Altogether, these data show that individual mutation of box A or B does not negatively  
16 affect the function of snR190 whereas simultaneous mutation of both boxes induces pre-60S r-  
17 particle maturation defects.

18

### 19 **snR190 is retained in pre-ribosomal particles in absence of Dbp7**

20 The genetic screen described in Fig. 1 suggests that Dbp7 may contribute to the dissociation of  
21 snR190 from its 25S rRNA target(s) within pre-60S r-particles. To further test this hypothesis, we  
22 used a strain expressing an HTP-tagged version of Nop7, a component of 90S and pre-60S r-  
23 particles<sup>40,41</sup> to purify these particles in both a *dbp7Δ* strain and its isogenic wild-type counterpart  
24 (Fig. 5a). Then, we compared by northern blotting the association of snR190 and other snoRNAs  
25 previously found efficiently crosslinked to Npa1 by CRAC<sup>25</sup> with these particles. As shown in Fig.  
26 5a, b, snR190 clearly co-immunoprecipitated with Nop7-HTP in both tagged strains, but the  
27 efficiency of co-immunoprecipitation was much higher in the *dbp7Δ* strain. In contrast, the box  
28 H/ACA snoRNAs snR5, snR42 and snR10 were weakly co-immunoprecipitated with Nop7-HTP in  
29 both conditions, although snR42 and snR10 base-pair to domain V of the 25S rRNA, close to one

1 of the base-pairing sites of snR190. Strikingly, however, the box H/ACA snoRNA snR37, and the  
2 box C/D snoRNAs snR38 and snR71 were also preferentially retained within the pre-ribosomal  
3 particles containing Nop7-HTP in the *dbp7Δ* strain (Fig. 5a, b). These results indicate that the  
4 absence of Dbp7 alters the steady-state association of snR190 with early pre-ribosomes, as well  
5 as that of some, but not all, snoRNAs interacting with domain V of the 25S rRNA.

6 To further confirm snR190 retention in 90S and pre-60S r-particles in the absence of Dbp7,  
7 the sedimentation profiles of snR190 on density gradients were compared in *dbp7Δ* and wild-  
8 type cells. Polysome profile analyses revealed that lack of Dbp7 caused a robust decrease in the  
9 amount of free 60S r-subunits (Fig. 5c) and formation of prominent half-mer polysomes, in  
10 agreement with the previously reported function of Dbp7 in 60S r-subunit production<sup>29,30</sup>. RNA  
11 was isolated from gradient fractions and the sedimentation profile of snR190 analyzed by  
12 northern blotting (Fig. 5c). In wild-type cells, snR190 sedimented both with free snoRNPs in the  
13 top fractions of the gradient and with pre-ribosome-bound snoRNPs in denser fractions  
14 containing 90S and pre-60S r-particles. Deletion of *DBP7* induced a clear increase in the  
15 proportion of pre-ribosome-bound snR190. Similarly, the sedimentation profile of snR37 also  
16 appeared affected to the same extent, whereas that of snR5 and snR42 did not show the same  
17 pre-ribosome enrichment (Fig. 5c). Quantification of the signals detected in the top (1-5) or pre-  
18 ribosome-bound (7-18) fractions of the gradients for each snoRNA confirmed an increase in the  
19 bound/free ratios for snR190 and snR37, but not for snR42 and snR5 (Supplementary Fig. 10a).

20 These data were further supported using sedimentations through low magnesium (low-  
21 Mg<sup>2+</sup>) sucrose gradients, in which polysomes are dissociated into free 40S and 60S r-subunits.  
22 Compared to the wild-type control, lack of Dbp7 resulted in an increase in the proportion of the  
23 snR190, snR71, snR37 and snR38 snoRNAs co-sedimenting with pre-60S and 90S r-particles  
24 (Supplementary Fig. 11a). In contrast, the sedimentation profile of other snoRNAs such as snR42,  
25 snR5, snR10, snR61 and the 5S RNP, were less affected. Quantification of the radioactive signals  
26 detected in the different fractions of the gradient confirmed the increased sedimentation in  
27 fractions 9-13 of the gradient of snR190, snR71, snR37 and snR38 snoRNAs in absence of Dbp7  
28 (Supplementary Fig. 11b).

1 As a member of the DExD-box family of putative ATP-dependent RNA helicases, Dbp7 is  
2 expected to possess ATPase activity, which may contribute to release of snR190 from the pre-  
3 rRNA. We tested in vitro the ATPase activity of recombinant wild-type Dbp7 protein (Dbp7<sub>WT</sub>)  
4 and a mutant version carrying a lysine to alanine amino acid substitution in the conserved motif  
5 I (also referred to as Walker motif A) of the RecA1 domain (Dbp7<sub>K197A</sub>). Recombinant His-ZZ  
6 tagged Dbp7<sub>WT</sub> and Dbp7<sub>K197A</sub> proteins were expressed and purified to apparent homogeneity  
7 from *Escherichia coli* (Fig. 6a) and their in vitro ATPase activity was tested using a NADH-coupled  
8 ATPase assay in the presence or absence of model RNA (Fig. 6b). We observed that Dbp7 on its  
9 own displayed a very weak ATPase activity, which was strongly stimulated by RNA. In contrast  
10 the Dbp7<sub>K197A</sub> mutant displayed a greatly reduced activity in the same conditions (Fig. 6b).

11 To determine whether the ATPase activity of Dbp7 is required in vivo for release of snR190  
12 from pre-ribosomes, a yeast strain expressing Dbp7<sub>K197A</sub> was generated. This strain showed a  
13 sedimentation profile of r-particles very similar to that of the *dbp7Δ* strain (Fig. 6c) but, compared  
14 to a wild-type strain, a milder growth defect than was observed for the *dbp7Δ* strain  
15 (Supplementary Fig. 12). Analysis of the levels of free versus pre-ribosome-bound snoRNAs  
16 showed a strong accumulation of snR190 into pre-ribosomes in the strain expressing Dbp7<sub>K197A</sub>,  
17 similar to that previously observed in the *dbp7Δ* strain. In contrast, the sedimentation profile of  
18 two other snoRNAs, snR10 and snR42, were not drastically changed upon expression of  
19 Dbp7<sub>K197A</sub>. Quantification of the signals detected in the top or pre-ribosome-bound fractions of  
20 the gradients clearly revealed an increase in the bound/free ratios for snR190 but not for snR10  
21 and snR42 (Supplementary Fig. 10b). We conclude that the enzymatic activity of Dbp7 is required  
22 for efficient release of snR190 from pre-ribosomal particles.

23

#### 24 **snR190 mutations alleviate the growth defect of the *dbp7Δ* strain**

25 We hypothesized that the growth and processing defects observed in the *dbp7Δ* strain may be  
26 due to the aberrant retention of snR190 and other snoRNAs in early pre-ribosomal particles. In  
27 order to test this, we eliminated snR190 in the *dbp7Δ* strain and analyzed the phenotypes of the  
28 resulting double mutant. The absence of snR190 slightly alleviated the growth defect of a *dbp7Δ*  
29 strain at 30 °C (Fig. 7a and Supplementary Table 2 and Supplementary Fig. 15), and the recovery

1 was even more evident at 37 °C. Loss of snR190 also improved the growth rate of the strain  
2 expressing Dbp7<sub>K197A</sub> at 22, 25 and 30°C (Supplementary Fig. 12). This result indicates that the  
3 absence of snR190 alleviates the phenotypes resulting from the loss of the ATPase activity of  
4 Dbp7, in line with the model that Dbp7 contributes to the release of snR190 from its base-pairing  
5 sites with the pre-rRNA.

6 We next determined whether weakening of the base-pairing between snR190 and the  
7 25S rRNA was responsible for this phenotypic rescue. We expressed in the *dbp7Δ snr190-[mut.C]*  
8 strain, different mutant versions of snR190 bearing either multiple mutations in box A (*snr190-*  
9 *[mut.A]*) or a single substitution of snR190 guanosine 34 into a cytidine (*snr190-[mut.G34C]*), to  
10 mimic the mutation on the 25S rRNA (C2392U) isolated in our suppressor screen (Fig. 1). In both  
11 cases, the growth defect of the *dbp7Δ* strain was partially alleviated (Supplementary Table 2 and  
12 Supplementary Fig. 15).

13 Analysis of pre-60S r-particle maturation in these strains showed rescue effects consistent  
14 with the growth data. As previously described<sup>30</sup>, the *dbp7Δ* strain showed an increase in the  
15 steady-state levels of the 35S and the 27SA<sub>2</sub> precursors and a marked decrease of the 27SB pre-  
16 rRNAs (Fig. 7b, c). We observed a partial restoration of 27SB precursor levels in the double *dbp7Δ*  
17 *snr190-[mut.C]* mutants and upon mutagenesis of box A. In particular, the single G34C  
18 substitution in snR190 (*snr190-[mut.G34C]*) partially restored production of the 27SB  
19 intermediates when introduced in the *dbp7Δ* strain (Fig. 7b, c). These data indicated that the loss  
20 of snR190 directly alleviates the 27SB pre-rRNA production defects arising in the absence of  
21 Dbp7. Interestingly, however, 35S pre-rRNA accumulation was not restored to the wild-type level  
22 in these strains, which could reflect additional snR190-independent functions of Dbp7 (see  
23 Discussion).

24 Altogether, these data show that the lack of snR190, or mutations weakening the base-  
25 pairing between its box A and pre-rRNA, partially suppress the growth and pre-rRNA processing  
26 defects of a *dbp7Δ* strain. Thus, the function of Dbp7 becomes less limiting in these conditions,  
27 strongly suggesting that the snR190-pre-rRNA duplex is a cellular substrate of Dbp7.

28

29 **Stable association of the Npa1 complex with pre-ribosomes requires snR190**

1 snR190 is the snoRNA most efficiently cross-linked to Npa1<sup>25</sup>. To understand further this  
2 relationship, we next studied the impact of the lack of snR190 and Dbp7 on the association of the  
3 Npa1 complex with nascent pre-ribosomes. To specifically purify early 90S and pre-60S r-particles  
4 containing the Npa1 complex, we fused Noc1, another known component of these early r-  
5 particles<sup>42</sup>, to the Tandem-Affinity Purification (TAP) tag in wild-type (BY4741), *snr190-[mut.C]*  
6 and *dbp7Δ* strains. The RNAs and proteins co-purified with Noc1-TAP in each condition were  
7 analyzed by northern and western blotting respectively (Fig. 8). In the absence of snR190, all  
8 tested members of the Npa1 complex, namely Npa1, Dbp6, Nop8 and Rsa3, were less efficiently  
9 co-purified with Noc1-TAP compared to the wild-type conditions. This effect was not due to a  
10 lesser immunoprecipitation efficiency of early pre-ribosomes as the levels of the 35S, 33S/32S  
11 and 27SA<sub>2</sub> precursors were slightly higher in the Noc1-TAP-purified sample obtained from the  
12 *snr190-[mut.C]* strain, as were the levels of the box H/ACA snoRNP protein Nhp2 and the RNA  
13 helicase Prp43. We conclude that snR190 is required for efficient recruitment of the Npa1  
14 complex into nascent pre-ribosomes or for its stable association. In contrast, we observed  
15 opposite effects in the absence of Dbp7, namely that members of the Npa1 complex were more  
16 efficiently co-purified with Noc1-TAP compared to the wild-type control. Altogether, these  
17 results suggest that snR190 facilitates recruitment of the Npa1 complex into early pre-ribosomal  
18 particles. Once the functions of snR190 and the Npa1 complex have been fulfilled, the RNA  
19 helicase Dbp7 promotes removal of the snR190 snoRNP from its target site(s) in pre-60S r-  
20 particles, which in turn induces or facilitates the dissociation of the Npa1 complex and other  
21 snoRNPs.

22

## 23 **Discussion**

24 Eukaryotic ribosome synthesis relies on the function of numerous DExD/H-box ATPases. In yeast,  
25 most of these enzymes are essential for cell viability, indicating that each fulfills a specific, non-  
26 redundant function in r-subunit maturation. Yeast genetics proved highly valuable in revealing  
27 functionally relevant links between several DExD/H-box ATPases and their substrates<sup>43–46</sup>. The  
28 data presented herein strongly suggest that Dbp7 is the enzyme responsible for the dissociation  
29 of snR190 from the pre-rRNA to facilitate maturation of early pre-60S r-particles. Our genetic

1 screen shows that a single C-to-U transition in the 25S rRNA sequence predicted to base-pair with  
2 snR190 partially alleviates the growth defect of the *dbp7Δ* strain. This mutation may impact  
3 ribosome synthesis and function in two ways. On the one hand, it creates an additional U-A base-  
4 pair within helix H73 of the 25S rRNA (Supplementary Fig. 1) that therefore likely stabilizes this  
5 helix, with potential consequences on pre-60S r-particle maturation and/or translation. On the  
6 other hand, it weakens the base-pairing between snR190 box A and the 25S rRNA sequence by  
7 replacing a canonical C-G base-pair by a wobble U•G base-pair. It is difficult to determine which  
8 of these two aspects, or whether both simultaneously, are responsible for the suppression effect.  
9 Although the EMY65 strain used in our genetic screen displays a severe growth defect compared  
10 to conventional strains as ribosome synthesis is impaired, we still analyzed the sedimentation  
11 profile of snR190 in presence or absence of the 25S rRNA C2392U suppressor mutation  
12 (Supplementary Fig. 13a, b). We observed a slight but reproducible decrease in the retention of  
13 snR190 into pre-ribosomes in this strain grown on a glucose-containing medium (Dbp7 depletion)  
14 in the presence of the C2392U mutation. This phenotype is in line with the partial suppression of  
15 the pre-rRNA processing (Supplementary Fig. 14a, b) and growth (Fig. 1a) defects of the strain in  
16 these conditions. This result suggests that the C2392U mutation weakens the snR190/pre-rRNA  
17 base-pairing. This hypothesis is reinforced by the fact that lack of snR190 or mutations that  
18 weaken its base-pairing with the pre-rRNA also suppress the growth and pre-rRNA processing  
19 defects of the *dbp7Δ* strain in a conventional genetic background.

20 Yeast 25S rRNA G2395 ribose 2'-O-methylation has not been detected by several different  
21 high-throughput approaches<sup>26-28</sup>, what we confirmed using directed analyses (Fig. 3). The  
22 molecular rationale behind this remains unclear as snR190 contains a C'/D' motif and antisense  
23 element (box A). The internal stem mobilizing part of box A within snR190 does not seem to be  
24 the reason (Fig. 3). snR190 is efficiently immunoprecipitated with Nop1, the methyltransferase  
25 of C/D-type snoRNPs<sup>47</sup>. Still, as snR190 contains both a C/D and a C'/D' motif and its box A is  
26 linked to the C'/D' motif, it could be that only the C/D motif bound by the core proteins ensures  
27 proper accumulation of the snoRNP and that the core proteins are not positioned properly on  
28 the C'/D' motif to catalyze the G2395 methylation. In line with this, sequence alignment of  
29 snR190 sequences from different yeast species revealed that boxes C' and D' of snR190 diverge

1 from the consensus sequences<sup>39</sup>. Furthermore, in some species, box C' can be interrupted by  
2 several intervening nucleotides and may not be active<sup>39</sup>. Thus, we favor the hypothesis that the  
3 C'/D' motif of snR190 does not allow proper positioning of core proteins and thus precludes  
4 catalysis of the methylation.

5 Our data support the hypothesis that snR190 functions as a snoRNA chaperone during  
6 pre-60S r-subunit maturation. Loss-of-function of snR190 affects the conversion of the 27SA<sub>2</sub> pre-  
7 rRNA into 27SB. This is correlated with reduced large r-subunit production and the formation of  
8 half-mer polysomes. snR190 contains two antisense elements, boxes A and B, with the potential  
9 to base-pair with domains VI and I of the 25S rRNA respectively. Two hypotheses can be  
10 formulated concerning the mode of action of snR190 in chaperoning the pre-rRNA during pre-  
11 60S r-particle maturation. First, in cooperation with the Npa1 complex, snR190 may establish a  
12 physical bridge between the 5' and 3' regions of the 25S rRNA to promote or stabilize their  
13 clustering during compaction of pre-60S r-particles. This clustering is a crucial early event in pre-  
14 60S r-particle maturation<sup>20</sup> that is evolutionarily conserved as in bacteria, the 5' and 3' regions of  
15 large subunit rRNA are brought in close proximity through formation of a stem between flanking  
16 sequences on the RNA precursor<sup>48</sup>. This clustering may implicate a complex interplay between  
17 assembly factors, such as the Npa1 complex and snoRNAs in eukaryotes. In agreement with this  
18 hypothesis, our results show that the absence of snR190 affects the incorporation or stable  
19 association of the Npa1 complex within early pre-ribosomal particles. Second, snR190 shields 25S  
20 rRNA sequences complementary to its antisense boxes A and B to prevent them from establishing  
21 non-functional base-pairing interactions. In line with this, chemical probing experiments  
22 suggested that within the 35S pre-rRNA, the 5' end of the 5.8S rRNA is base-paired with ITS1  
23 sequences<sup>41,49</sup>, although this has been later challenged<sup>21</sup>. Processing events in the ITS1 are  
24 expected to abrogate this base-pairing and release the 5' region of the 5.8S rRNA for base-pairing  
25 with the 25S rRNA. As these conformational changes are expected to occur relatively late during  
26 the maturation pathway, after processing at site B<sub>1S</sub> and B<sub>1L</sub>, we propose that snR190 may  
27 function as a placeholder to shield the 25S rRNA region until the 5' end of the 5.8S rRNA becomes  
28 available for base-pairing. Our data show that inactivation of either box A or box B does not  
29 induce significant growth or processing defects, whereas mutation of both boxes simultaneously

1 is more deleterious. This observation better supports a role of snR190 as a placeholder shielding  
2 its complementary sequences in the 5' and 3' regions of the 25S rRNA. A defect in shielding of  
3 any of the two sequences seems benign in terms of growth and processing, but a cumulative  
4 defect may become more deleterious.

5 Our genetic screen showed that a C-to-U transition in the 25S rRNA predicted to weaken  
6 the base-pairing with snR190 alleviates the growth defect resulting from Dbp7 depletion. We  
7 showed in addition that the absence of snR190 or mutations within its antisense box A also  
8 alleviates the growth and processing defects of the *dbp7Δ* strain. Importantly, a single nucleotide  
9 substitution within snR190 box A, predicted to be synonymous to the mutation identified in the  
10 25S rRNA in the genetic screen, also partially restores the growth of the *dbp7Δ* strain. We  
11 therefore conclude that Dbp7 becomes more dispensable in the presence of mutations  
12 weakening the base-pairing between snR190 and the pre-rRNA, suggesting that Dbp7 may utilize  
13 its catalytic activity to resolve the snR190 box A/pre-rRNA duplex. In line with this model, a CRAC  
14 analysis of Dbp7 binding sites described in a parallel study<sup>50</sup> revealed that Dbp7 binds to both  
15 snR190 and domain V of the 25S rRNA, in the vicinity of the base-pairing site of snR190 box A.  
16 Biochemical evidence also supports the model that Dbp7 dissociates snR190 from pre-60S r-  
17 particles. snR190, but not several other snoRNAs predicted to interact with the pre-rRNA in the  
18 PTC area, such as snR10 or snR42, is retained within pre-ribosomal particles in the absence of  
19 Dbp7 (Fig. 5). However, several canonical modification guide snoRNAs (e.g. snR37, snR38, snR71)  
20 targeting nucleotides of the PTC region are also retained within pre-60S r-particles in the absence  
21 of Dbp7, as are also most members of the Npa1 complex. As our genetic screen revealed a clear  
22 link between snR190 and Dbp7, the accumulation of the other snoRNAs is likely an indirect  
23 consequence of a defect in snR190 release.

24 The phenotypes resulting from lack of snR190 are less severe than those observed in the  
25 absence of Dbp7 (for a direct comparison of the defects, see Supplementary Fig. 6). As the  
26 absence of Dbp7 induces the retention of several snoRNAs other than snR190 within 90S or pre-  
27 60S r-particles (Fig. 5), this cumulative retention could simply be the reason for the more severe  
28 defects observed upon deletion of *DBP7* than upon inactivation of snR190. It is possible that,  
29 without the function of Dbp7, resolving pre-60S r-particles with several trapped snoRNAs might

1 be more challenging for cells than generating spontaneously helix H73 in the absence of snR190.  
2 In any case, whether or not Dbp7 is actively or indirectly involved in the displacement of those  
3 abovementioned snoRNAs from the pre-rRNA remains to be solved. Another hypothesis to  
4 explain the more severe phenotypes of the *dbp7Δ* strain could be that Dbp7 fulfills other  
5 functions in the maturation of 90S and pre-60S particles, such as modulating the stability of intra-  
6 molecular duplexes of the 25S rRNA or displacing protein-RNA interactions. Dbp7 CRAC data  
7 indicated that Dbp7 interacts with domain VI of the 25S rRNA in addition to domain V, suggesting  
8 that it may also intervene in remodeling events in this domain of the 25S rRNA within 90S or pre-  
9 60S r-particles<sup>50</sup>.

10

## 11 **Methods**

### 12 **Yeast strains and media**

13 All yeast strains used in this study were derivatives of either *S. cerevisiae* strains BY4741 (*MATa*,  
14 *his3Δ1*, *leu2Δ0*, *met15Δ0*, *ura3Δ0*) or W303-1A (*MATa*, *leu2-3*, *112 trp1-1*, *can1-100*, *ura3-1*,  
15 *ade2-1*, *his3-11,15*). They are listed in the Supplementary Table 3. Strains were grown either in  
16 YP medium (1% yeast extract, 1% peptone) (Becton-Dickinson) supplemented with 2% glucose as  
17 the carbon source (YPD, rich medium) or in synthetic medium (0.17% yeast nitrogen base (MP  
18 Biomedicals), 0.5% (NH<sub>4</sub>)<sub>2</sub>SO<sub>4</sub>) supplemented with 2% glucose and the required amino acids (SD,  
19 minimal medium). Selection of the kanamycin-resistant transformants was done by addition of  
20 G418 to a final concentration of 0.2 mg/ml.

21 The strain expressing Nop7-HTP (His tag-Tev cleavage site-Z sequence derived from *S.*  
22 *aureus* Protein A) was obtained by transforming BY4741 with a PCR cassette produced using  
23 plasmid pBS1539-HTP and primers listed in Supplementary Table 4. Clones having integrated the  
24 *URA3* gene were selected on SD-Ura medium.

25

### 26 **Genome editing using CRISPR-Cas9**

27 In yeast, snR190 is expressed from a dicistronic precursor transcript (UMO1), also supporting  
28 expression of U14, an essential box C/D snoRNA that functions as an RNA chaperone in the  
29 maturation of the 18S rRNA<sup>32</sup>. Both snoRNAs are co-transcribed by RNA Pol II from the same

1 promoter and then converted to mature snoRNAs by a series of endo- and exo-nucleolytic  
2 processing events<sup>32</sup>. This particular genomic context precluded using conventional genomic  
3 knockout approaches to inactivate snR190 expression without affecting that of U14. To interfere  
4 with snR190 expression post-transcriptionally, we introduced point mutations in the genomic  
5 sequences encoding box C and the terminal stem of the snoRNA (snr190-[mut.C], Supplementary  
6 Fig. 2b) using the CRISPR-Cas9 approach<sup>33</sup>. As previously described, these mutations are  
7 predicted to prevent assembly of C/D-type snoRNP core proteins and result in the exonucleolytic  
8 degradation of snR190 during maturation of the dicistronic precursor, without interfering with  
9 U14 production<sup>51</sup>.

10 To generate the *snr190-[mut.C]* strain, the Cas9 expressing vector PML104 was first  
11 digested with *Swa*I (New England Biolabs) overnight at 25 °C. The enzyme was then inactivated  
12 at 65 °C for 20 min. *Bcl*I (Fermentas) was subsequently added to the reaction for 2 h at 50 °C. In  
13 order to target *SNR190* box C, oligonucleotides OHA494 and OHA495 (Supplementary Table 4)  
14 were designed using the online CRISPR Toolset (<http://wyrickbioinfo2.smb.wsu.edu/crispr.html>)  
15 and were hybridized at a concentration of 3 μM in T4 DNA Ligase Buffer. The hybridization was  
16 performed using a thermocycler: the oligonucleotide mix was heated at 95 °C for 6 min and the  
17 temperature was then gradually decreased to 25 °C at a rate of 1 °C per min. The hybridized  
18 oligonucleotides were then ligated to the digested PML104 plasmid overnight at 16 °C. The  
19 ligated vector was then transformed into competent *E. coli* (Stellar, Clontech). *SNR190* guide  
20 sequence insertion was confirmed by sequencing the resulting plasmids using the OHA497Bis  
21 primer (Supplementary Table 4). Yeast cells were then transformed by a one step-transformation  
22 procedure with the single guide-containing plasmid along with a single stranded donor  
23 oligonucleotide containing the desired *SNR190* Box C mutations as well as mutations in the PAM  
24 sequence (OHA496, Supplementary Table 4). For a better transformation efficiency, carrier DNA  
25 (fish sperm DNA) was added and the transformation reaction was incubated for 45 min at 30 °C.  
26 Transformants were then selected on SD-Ura medium and the Cas9 plasmid was then eliminated  
27 by plating clones on medium containing 5-fluoroorotic acid (5-FOA) before being streaked on YPD  
28 plates. Genomic DNA from the resulting colonies were purified, the *SNR190* locus was amplified  
29 by PCR using (OHA497 and OHA498 primers, Supplementary Table 4) and the resulting PCR

1 fragments sequenced with the same primers to verify the mutations. The same protocol was  
2 applied to generate, in the *dbp7Δ* strain, loss-of-function mutations in *SNR190* (*snr190-[mut.C]*),  
3 and introduce in its box A multiple mutations (*snr190-[mut.A]*) or the G34C mutation (*snr190-*  
4 *[mut.G34C]*) (the corresponding oligonucleotides are listed in Supplementary Table 4). Most of  
5 the conclusions of this study stem from the analysis of two independent mutant clones in two  
6 different genetic backgrounds (BY4741 and W303), and two biological replicates of the  
7 experiments have been performed in each case.

8

### 9 **Plasmid constructions**

10 Ectopic expression of snR190 in the *snr190-[mut.C]* strain was achieved using the pCH32 plasmid<sup>52</sup>  
11 containing the genomic *U14-SNR190* expression cassette. This cassette was amplified by PCR  
12 using primers OMJ122 and OMJ123 (Supplementary Table 4) and inserted into the pCH32 plasmid  
13 previously digested with *EcoRI* and *EcoRV*, using the In-Fusion system (Clontech). The In-Fusion  
14 reaction was transformed into competent *E. coli* cells (Stellar, Clontech) and recombinant clones  
15 were sequenced using the OHA498 primer (Supplementary Table 4).

16 Introduction of mutations in box A (*snr190-[mut.A]*), box B (*snr190-[mut.B]*) or the  
17 internal stem (*snr190-[mut.S]*) of *SNR190* in the pCH32 plasmid containing the *U14-SNR190*  
18 expression cassette was achieved using the PCR-based In-Fusion mutagenesis system and  
19 appropriate primers for each mutation (Supplementary Table 4). The original template plasmid  
20 was then eliminated by the “Cloning Enhancer” treatment (Clontech) and the linear PCR products  
21 were circularized using the In-Fusion system before transformation into competent *E. coli* cells  
22 (Stellar, Clontech). All resulting plasmids were verified by sequencing. To generate a *U14-SNR190*  
23 expression vector bearing mutations in boxes A and B of snR190 (*snr190-[mut.AB]*), mutations in  
24 box B were introduced using the same protocol on the plasmid already harboring the *snr190-*  
25 *[mut.A]* mutation.

26 Introduction of the C2392T substitution in plasmid pNOY373 or reversion of T2392 to the  
27 wild-type cytosine in plasmids Sup. #2 or Sup. #10 was achieved as described above using the  
28 PCR-based In-Fusion mutagenesis system and appropriate primers for each mutation  
29 (Supplementary Table 4).

1  
2  
3  
4  
5  
6  
7  
8  
9  
10  
11  
12  
13  
14  
15  
16  
17  
18  
19  
20  
21  
22  
23  
24  
25  
26  
27  
28  
29

## **Genetic screen for rRNA suppressors of Dbp7 loss-of-function**

To obtain rRNA suppressors able to bypass the growth defect of Dbp7 depletion, we first integrated at the *DBP7* locus, a *GAL::HA-DBP7* construct in the strain NOY891 (*MATa ade2-1 ura3-1 leu2-3 leu2-112 his3-11 can1-100 rdnΔΔ::HIS3*). In this strain (a generous gift from Prof. Nomura's lab), the chromosomal rDNA repeats are completely deleted (*rdnΔΔ*) and the sole source of mature rRNAs is a single rDNA repeat expressed from the 2μ plasmid pNOY353, in which expression of 35S pre-rRNA is under the control of a galactose-inducible *GAL7* promoter (*P<sub>GAL7</sub>-35S rDNA, 5S rDNA, TRP1*)<sup>31</sup>. The chromosomal *DBP7* gene was replaced by a *GAL1::HA-DBP7* construct by transformation, which was generated by the one-step PCR strategy on the pFA6a-KanMX6-*P<sub>GAL1</sub>-3HA* plasmid<sup>53</sup>. This strain was named EMY65. The presence of the *GAL1::HA-DBP7* allele was confirmed by PCR and DNA sequencing. Western blotting also confirmed the presence of a single protein band of the expected molecular mass when candidates are grown in SGal medium (Supplementary Fig. 3).

Then, we performed random mutagenesis of pNOY373, a 2μ *LEU2* plasmid carrying a single rDNA repeat expressing both the 35S and 5S pre-rRNAs from their cognate promoters. For mutagenesis, the *E. coli* mutator strain XL1-Red (Stratagene) was used, following the procedure described by the manufacturer. About 15 independent mutageneses were performed, then, cells were pooled and plasmids purified by a standard midi-prep procedure. As the result of the mutagenesis, it was estimated that ca. 40% of the plasmid clones harbored loss-of-function mutations in the *LEU2* marker. The mutated plasmids were introduced into strain EMY65 and fast-growing transformants were screened on SD-His-Leu medium, where the expression of *GAL1*- and *GAL7*- driven promoters was repressed. The mutated pNOY373 plasmids were rescued from fast-growing candidates and used to re-transform EMY65 strain in order to link the growth suppression to the presence of the mutagenized plasmid.

## **Construction of a double *dbp7Δ snR190-[mut.C]* mutant**

To determine if the severe growth defect linked to the *dbp7* null allele could be partially suppressed by the loss-of-function of snR190, we performed a genetic analysis. To this end, the

1 MCD1-7C strain (a *dbp7::HIS3MX6* strain complemented with a YCplac33-DBP7 plasmid)<sup>30</sup> was  
2 crossed to *snr190-[mut.C]* strain generated in the W303 background. The resulting diploid was  
3 sporulated, and tetrads were dissected. After dissection, as expected, the HIS3MX6 marker that  
4 deleted-disrupted the *DBP7* gene segregated 2<sup>+</sup>:2<sup>-</sup> in complete tetrads. Then, we counter-  
5 selected the *URA3*-marked YCplac33-DBP7 plasmid from several complete tetrads in plates  
6 containing 5-FOA. To identify tetratypes, we obtained total DNA from these tetrads and  
7 sequenced the genomic region containing the coding sequence of the *SNR190* gene. Two  
8 tetratypes were selected for further analyses.

9

### 10 **Detection of ribose-methylated nucleosides**

11 Ribose methylation was tested by reverse transcription at low dNTP concentrations. Briefly, 5 µg  
12 of total yeast RNAs were mixed with 0.2 pmol of a radiolabeled oligonucleotide hybridizing  
13 downstream from the site of ribose methylation (primer #1 or #2). After heat denaturation (95  
14 °C, 1 min), primer extension was carried out in the presence of either 1 mM (high concentration)  
15 or 0.1 mM (low concentration) dNTPs and with 10 units of AMV reverse transcriptase (Promega)  
16 according to the manufacturer's protocol. Sequencing of a plasmid containing the yeast 25S rRNA  
17 sequence (2333-2457) was performed with the USB® Sequenase™ version 2.0 DNA Polymerase  
18 Kit and used as a ladder.

19

### 20 **Sedimentation on sucrose gradients**

21 Yeast cells growing exponentially (500 ml cultures at OD<sub>600</sub> approximately 0.6) were treated for  
22 10 min with 50 µg/ml cycloheximide (Sigma) added directly to the culture medium. Cells were  
23 collected by centrifugation, rinsed with buffer K [20 mM Tris-Cl pH 7.4, 50 mM KCl, 10 mM MgCl<sub>2</sub>]  
24 supplemented with 50 µg/ml cycloheximide and collected again by centrifugation. Dry pellets  
25 were resuspended with approximately one volume of ice-cold buffer K supplemented with 1 mM  
26 dithiothreitol (DTT), 1× Complete EDTA-free protease inhibitor cocktail (Roche), 0.1 U/µl RNasin  
27 (Promega), and 50 µg/ml cycloheximide. About 250 µl of ice-cold glass beads (Sigma) were added  
28 to 500 µl aliquots of the resuspended cells which were broken by vigorous shaking, three times 2  
29 min, separated by 2 min incubations on ice. Extracts were clarified through two successive

1 centrifugations at 16,000 x g and 4 °C for 5 min and quantified by measuring absorbance at 260  
2 nm ( $A_{260}$ ). Equal amounts of extracts were loaded on 10%-50% sucrose gradients in TMK buffer.  
3 Gradients were centrifuged at 260,800 x g for 2.5 h at 4 °C in a SW41 Ti rotor (Optima L-100 XP  
4 ultracentrifuge, Beckman Coulter). The gradient fractions were collected with a Foxy R1 gradient  
5 collector (Teledyne Isco) driven by PeakTrak software (Version 1.10, Isco Inc.). The  $A_{254}$  was  
6 measured during collection with a UA-6 UV/VIS DETECTOR (Teledyne Isco).  
7 For the fractionation experiment shown in Supplementary Fig. 11, we prepared r-subunits exactly  
8 as described previously<sup>54</sup>. Briefly, cell extracts were prepared in a buffer containing 50 mM Tris-  
9 HCl, pH 7.4, 50 mM NaCl, and 1 mM DTT in the absence of cycloheximide. Ten  $A_{260}$  units were  
10 loaded on 7%-50% linear, low-Mg<sup>2+</sup> sucrose gradients prepared in the same buffer and run at  
11 260,800 x g in a SW41 Ti rotor for 4.5 h at 4 °C. After centrifugation, fractions of 0.5 ml were  
12 collected manually; these were then adjusted to a final concentration of 10 mM Tris-HCl, pH 7.5,  
13 10 mM EDTA and 0.5 % SDS. Total RNA was isolated by two consecutive extractions with 10 mM  
14 Tris-HCl, pH 7.5 saturated phenol:chloroform:isoamyl alcohol (25:24:1), followed by a  
15 chloroform:isoamyl alcohol (24:1) extraction. Total RNA was precipitated with ethanol in the  
16 presence of 0.3 M sodium acetate, pH 5.2. Finally, RNA pellets were dissolved in 20 µl of distilled  
17 water and 10 µl were resolved on a 7% polyacrylamide, 8 M urea gel and subjected to northern  
18 blotting using specific [<sup>32</sup>P]-labelled oligonucleotides as probes (Supplementary Table 4).

19

## 20 **RNA extraction and northern blotting experiments**

21 Extraction of yeast total RNAs were performed as follows<sup>12</sup>: dry yeast cell pellets were  
22 resuspended with 0.5 ml water-saturated phenol and 0.5 ml guanidine thiocyanate (GTC) mix (50  
23 mM Tris-HCl, pH 8.0, 10 mM EDTA, pH 8.0, 4 M guanidine thiocyanate, 2% *N*-Lauroylsarcosine,  
24 143 mM β-Mercaptoethanol). Cells were broken by vigorous vortexing three times for 2 min at 4  
25 °C in the presence of glass beads. The resulting samples were mixed with 7.5 ml water-saturated  
26 phenol and 7.5 ml GTC mix and incubated for 5 min at 65 °C. After addition of 7.5 ml chloroform  
27 and 4 ml sodium acetate buffer (10 mM Tris-HCl, pH 8.0, 1 mM EDTA, pH 8.0, 100 mM sodium  
28 acetate), samples were mixed vigorously and centrifuged at 3220 x g for 5 min at 4 °C. Aqueous  
29 phases were recovered and RNAs were re-extracted two additional times with water-saturated

1 phenol:chloroform (1:1). RNAs were then concentrated by ethanol precipitation and ultimately  
2 resuspended in ultrapure H<sub>2</sub>O. In all northern blotting experiments (see below), equal amounts  
3 of these total RNAs (4 µg) were analyzed.

4 For Northern blotting analyses of high-molecular-mass RNA species, RNAs were separated as  
5 described in “Molecular Cloning”, Sambrook and Russell, CSHL Press (“Separation of RNA  
6 According to Size: Electrophoresis of Glyoxylated RNA through Agarose Gels”). RNAs were then  
7 transferred to Hybond N+ membranes (GE Healthcare) by capillarity using 5x SSC as a transfer  
8 buffer. Low-molecular-mass RNA species were separated by electrophoresis through 6%  
9 acrylamide:bisacrylamide (19:1), 8 M urea gels using 1x TBE as a running buffer. RNAs were then  
10 transferred to Hybond N membranes (GE Healthcare) by electro-transfer in 0.5x TBE buffer, 20  
11 V, 4 °C, overnight). In all cases, membranes were hybridized with <sup>32</sup>P-labelled oligonucleotide  
12 probes using Rapid-hyb buffer (GE Healthcare). Radioactive membranes were exposed to  
13 Phosphorimaging screens and revealed using Typhoon TRIO or Typhoon 9400 Variable Mode  
14 Imagers (GE Healthcare) driven by Typhoon Scanner Control software (Version 5.0). Sequences  
15 of the oligonucleotides used as probes in this study are described in the Supplementary Table 4.  
16 Quantifications of the signals were performed using PhosphorImager data and Multi Gauge  
17 software (Version 3.0, FUJIFILM). Statistically significant differences were determined using one-  
18 tailed Student’s t-test (<https://www.socscistatistics.com/tests/studentttest/default2.aspx>).

19

20 **Western blotting experiments**

21 For western blotting experiments, protein samples were separated on 10% SDS-polyacrylamide  
22 gels and transferred to nitrocellulose membranes using a Trans-Blot Turbo apparatus (BioRad).  
23 Membranes were saturated for 1 h with PBST buffer (137 mM NaCl, 2.7 mM KCl, 10 mM Na<sub>2</sub>HPO<sub>4</sub>,  
24 2 mM KH<sub>2</sub>PO<sub>4</sub>, 0.1% Tween-20) containing 5% (w/v) powder milk. Following incubation for 2 h  
25 with the same buffer containing the primary antibodies, membranes were rinsed 3 times for 5  
26 min with PBST buffer, incubated for 1 h with the secondary antibodies diluted in PBST containing  
27 5% (w/v) powder milk and finally washed three times for 10 min with PBST buffer. Luminescent  
28 signals were generated using the Clarity Western ECL Substrate (Bio-Rad), captured using a  
29 ChemiDoc Touch Imaging System (Bio-Rad) and quantified using the Image Lab software (Version

1 5.2.1, Bio-Rad). HA-tagged proteins were detected using HRP-conjugated mouse monoclonal  
2 anti-HA antibodies (Roche Diagnostics, Cat. # 12013819001, 1:1,000 dilution); Pgk1 protein was  
3 detected using mouse monoclonal anti-Pgk1 antibodies (Clone 1086CT10.2.1, Invitrogen, Cat. #  
4 MA5-37712, 1:8,000 dilution). Primary antibodies used to detect Npa1 (1:5,000 dilution), Dbp6  
5 (1:10,000 dilution), Nop8 (1:2,000 dilution), Rsa3 (1:10,000 dilution), Nhp2 (1:5,000 dilution) and  
6 Prp43 (1:4,000 dilution) were generated by custom antibody production services and described  
7 elsewhere<sup>25,55,56</sup>. Secondary antibodies were purchased from Promega (HRP-conjugated anti-  
8 mouse antibodies, Cat. # W402B, 1:10,000 dilution; HRP-conjugated anti-rabbit antibodies, Cat.  
9 # W401B, 1:10,000 dilution).

10

### 11 **Immunoprecipitation experiments**

12 Cell pellets corresponding to 500 ml cultures at OD<sub>600</sub> approximately 0.6 were resuspended with  
13 approximately one volume of ice-cold A200-KCl buffer [20 mM Tris-HCl, pH 8.0, 5 mM magnesium  
14 acetate, 200 mM KCl, 0.2% Triton-X100] supplemented with 1 mM DTT, 1× Complete EDTA-free  
15 protease inhibitor cocktail (Roche), 0.1 U/μl RNasin (Promega). About 400 μl of ice-cold glass  
16 beads (0.5 mm diameter, Sigma) were added to 800 μl aliquots of the resuspended cells which  
17 were broken by vigorous shaking, 2 times 30 sec separated by 1 min incubation on ice using  
18 Precellys (Ozyme). Extracts were clarified through two successive centrifugations at 16,000 x g  
19 and 4 °C for 5 min and quantified by measuring A<sub>260</sub>. Equal amounts of soluble extracts were  
20 incubated for 2 h at 4 °C with 15 μl (bed volume) of immunoglobulin G (IgG)-Sepharose beads (GE  
21 Healthcare) in a total volume of 1 ml (adjusted with A200-KCl buffer supplemented with 1 mM  
22 DTT, 1× Complete EDTA-free protease inhibitor cocktail, 0.1 U/μl RNasin) on a rocking table. For  
23 RNA analyses, beads were washed 7 times with 1 ml of ice-cold A200-KCl buffer supplemented  
24 with 1 mM DTT and 1× Complete EDTA-free protease inhibitor cocktail. RNA was extracted from  
25 bead pellets as follows: 160 μl of 4 M guanidium isothiocyanate solution, 4 μl of glycogen (Roche),  
26 80 μl of [10 mM Tris-HCl, pH 8.0, 1 mM EDTA, pH 8.0, 100 mM sodium acetate], 120 μl of phenol  
27 and 120 μl of chloroform were added. Tubes were shaken vigorously, incubated 5 min at 65 °C  
28 and centrifuged 5 min at 16,000 x g (4 °C). Aqueous phases (240 μl) were mixed vigorously with  
29 120 μl of phenol and 120 μl of chloroform, centrifuged 5 min at 16,000 x g (4 °C) and the resulting

1 aqueous phases were ethanol precipitated. For protein analyses, beads were washed 5 times with  
2 1 ml of ice-cold A200-KCl buffer supplemented with 1 mM DTT and 1× Complete EDTA-free  
3 protease inhibitor cocktail and 2 additional times with 1 ml of A200-NaCl buffer [20 mM Tris-HCl,  
4 pH 8.0, 5 mM magnesium acetate, 200 mM NaCl, 0.2% Triton-X100] supplemented with 1 mM  
5 DTT, 1× Complete EDTA-free protease inhibitor cocktail. Beads were resuspended directly with  
6 2× SDS gel-loading buffer [100 mM Tris-HCl, pH 6.8, 4% SDS, 20% glycerol, 200 mM DTT, 0.2%  
7 bromophenol blue].

8

### 9 **Purification of recombinant proteins from *E. coli***

10 The coding sequence of *DBP7* was cloned into a pQE80-derived plasmid for expression of N-  
11 terminally His<sub>10</sub>-ZZ-tagged recombinant proteins in *E. coli* (His<sub>10</sub>-ZZ-Dbp7<sub>WT</sub>). Site-directed  
12 mutagenesis was used to introduce mutations leading to substitution of lysine 197 for alanine  
13 (His<sub>10</sub>-ZZ-Dbp7<sub>K197A</sub>). Plasmids were used to transform BL21 Codon Plus *E. coli* and protein  
14 expression was induced with 1 mM IPTG overnight at 18 °C. After harvesting, cell pellets were  
15 resuspended in a lysis buffer containing 50 mM Tris-HCl, pH 7, 500 mM NaCl, 1 mM MgCl<sub>2</sub> 10 mM  
16 imidazole, 1 mM PMSF, 10% glycerol. Cells were lysed by sonication and the lysate cleared by  
17 centrifugation. Polyethyleneimine was added to a final concentration of 0.05% and precipitated  
18 nucleic acids were removed. The lysate was incubated with cComplete™ His-Tag purification resin  
19 (Roche) and after binding, the matrix was washed using buffers containing (i) 50 mM Tris-HCl, pH  
20 7.1, 500 mM NaCl, 1 mM MgCl<sub>2</sub>, 30 mM imidazole, 10% glycerol and (ii) 50 mM Tris-HCl, pH 7.1,  
21 1 M NaCl, 1 mM MgCl<sub>2</sub>, 30 mM imidazole, 10% glycerol. Elution of bound proteins were  
22 performed using a buffer containing 50 mM Tris-HCl, pH 7, 500 mM NaCl, 1 mM MgCl<sub>2</sub>, 300 mM  
23 imidazole and 10% glycerol. Purified protein was dialyzed against a buffer containing 50 mM Tris-  
24 HCl, pH 7, 120 mM NaCl, 2 mM MgCl<sub>2</sub>, 20% glycerol. A Bradford assay was used to determine  
25 protein concentration.

26

### 27 **In vitro NADH-coupled ATPase assay**

28 In vitro NADH-coupled ATPase assays<sup>17,19</sup> were performed to monitor ATP hydrolysis by purified  
29 His<sub>10</sub>-ZZ-Dbp7<sub>WT/K197A</sub>. Each reaction contained 50 mM Tris-HCl, pH 7.4, 25 mM NaCl, 2 mM MgCl<sub>2</sub>,



## 1 **Data availability**

2 All the source data used for this study (raw images, graphs and quantifications) are provided in  
3 the “Source Data file” available in the supplementary material. Other data are available from the  
4 corresponding author upon request.

5

## 6 **References**

- 7 1. Wimberly, B. T. *et al.* Structure of the 30S ribosomal subunit. *Nature* **407**, 327–339 (2000).
- 8 2. Ban, N., Nissen, P., Hansen, J., Moore, P. B. & Steitz, T. A. The complete atomic structure of  
9 the large ribosomal subunit at 2.4 Å resolution. *Science* **289**, 905–920 (2000).
- 10 3. Cech, T. R. Structural biology. The ribosome is a ribozyme. *Science* **289**, 878–879 (2000).
- 11 4. Woolford, J. L. & Baserga, S. J. Ribosome biogenesis in the yeast *Saccharomyces cerevisiae*.  
12 *Genetics* **195**, 643–681 (2013).
- 13 5. Henras, A. K., Plisson-Chastang, C., O’Donohue, M.-F., Chakraborty, A. & Gleizes, P.-E. An  
14 overview of pre-ribosomal RNA processing in eukaryotes. *Wiley Interdiscip Rev RNA* **6**, 225–  
15 242 (2015).
- 16 6. de la Cruz, J., Karbstein, K. & Woolford, J. L. Functions of ribosomal proteins in assembly of  
17 eukaryotic ribosomes in vivo. *Annu. Rev. Biochem.* **84**, 93–129 (2015).
- 18 7. Dez, C. *et al.* Npa1p, a component of very early pre-60S ribosomal particles, associates with  
19 a subset of small nucleolar RNPs required for peptidyl transferase center modification. *Mol.*  
20 *Cell. Biol.* **24**, 6324–6337 (2004).
- 21 8. Massenet, S., Bertrand, E. & Verheggen, C. Assembly and trafficking of box C/D and H/ACA  
22 snoRNPs. *RNA Biol.* **14**, 680–692 (2017).
- 23 9. Watkins, N. J. & Bohnsack, M. T. The box C/D and H/ACA snoRNPs: key players in the  
24 modification, processing and the dynamic folding of ribosomal RNA. *Wiley Interdiscip Rev*  
25 *RNA* **3**, 397–414 (2012).
- 26 10. Beltrame, M. & Tollervey, D. Base pairing between U3 and the pre-ribosomal RNA is required  
27 for 18S rRNA synthesis. *EMBO J.* **14**, 4350–4356 (1995).
- 28 11. Liang, W. Q. & Fournier, M. J. U14 base-pairs with 18S rRNA: a novel snoRNA interaction  
29 required for rRNA processing. *Genes Dev.* **9**, 2433–2443 (1995).
- 30 12. Tollervey, D. A yeast small nuclear RNA is required for normal processing of pre-ribosomal  
31 RNA. *EMBO J.* **6**, 4169–4175 (1987).

- 1 13. Morrissey, J. P. & Tollervey, D. Yeast snR30 is a small nucleolar RNA required for 18S rRNA  
2 synthesis. *Mol. Cell. Biol.* **13**, 2469–2477 (1993).
- 3 14. Martin, R., Straub, A. U., Doebele, C. & Bohnsack, M. T. DExD/H-box RNA helicases in  
4 ribosome biogenesis. *RNA Biol.* **10**, 4–18 (2013).
- 5 15. Rodríguez-Galán, O., García-Gómez, J. J. & de la Cruz, J. Yeast and human RNA helicases  
6 involved in ribosome biogenesis: current status and perspectives. *Biochim. Biophys. Acta*  
7 **1829**, 775–790 (2013).
- 8 16. Dembowski, J. A., Kuo, B. & Woolford, J. L. Has1 regulates consecutive maturation and  
9 processing steps for assembly of 60S ribosomal subunits. *Nucleic Acids Res.* **41**, 7889–7904  
10 (2013).
- 11 17. Brüning, L. *et al.* RNA helicases mediate structural transitions and compositional changes in  
12 pre-ribosomal complexes. *Nat. Commun.* **9**, 5383 (2018).
- 13 18. Bohnsack, M. T. *et al.* Prp43 bound at different sites on the pre-rRNA performs distinct  
14 functions in ribosome synthesis. *Mol. Cell* **36**, 583–592 (2009).
- 15 19. Aquino, G. R. R. *et al.* RNA helicase-mediated regulation of snoRNP dynamics on pre-  
16 ribosomes and rRNA 2'-O-methylation. *Nucleic Acids Res.* (2021). doi:10.1093/nar/gkab159
- 17 20. Gamalinda, M. *et al.* A hierarchical model for assembly of eukaryotic 60S ribosomal subunit  
18 domains. *Genes Dev.* **28**, 198–210 (2014).
- 19 21. Burlacu, E. *et al.* High-throughput RNA structure probing reveals critical folding events during  
20 early 60S ribosome assembly in yeast. *Nat. Commun.* **8**, 714 (2017).
- 21 22. Kater, L. *et al.* Visualizing the Assembly Pathway of Nucleolar Pre-60S Ribosomes. *Cell* **171**,  
22 1599–1610.e14 (2017).
- 23 23. Rosado, I. V. & de la Cruz, J. Npa1p is an essential trans-acting factor required for an early  
24 step in the assembly of 60S ribosomal subunits in *Saccharomyces cerevisiae*. *RNA* **10**, 1073–  
25 1083 (2004).
- 26 24. Rosado, I. V. *et al.* Characterization of *Saccharomyces cerevisiae* Npa2p (Urb2p) reveals a  
27 low-molecular-mass complex containing Dbp6p, Npa1p (Urb1p), Nop8p, and Rsa3p involved  
28 in early steps of 60S ribosomal subunit biogenesis. *Mol. Cell. Biol.* **27**, 1207–1221 (2007).
- 29 25. Joret, C. *et al.* The Npa1p complex chaperones the assembly of the earliest eukaryotic large  
30 ribosomal subunit precursor. *PLoS Genet.* **14**, e1007597 (2018).
- 31 26. Birkedal, U. *et al.* Profiling of ribose methylations in RNA by high-throughput sequencing.  
32 *Angew. Chem. Int. Ed. Engl.* **54**, 451–455 (2015).

- 1 27. Marchand, V., Blanloeil-Oillo, F., Helm, M. & Motorin, Y. Illumina-based RiboMethSeq  
2 approach for mapping of 2'-O-Me residues in RNA. *Nucleic Acids Res.* **44**, e135 (2016).
- 3 28. Taoka, M. *et al.* The complete chemical structure of *Saccharomyces cerevisiae* rRNA: partial  
4 pseudouridylation of U2345 in 25S rRNA by snoRNA snR9. *Nucleic Acids Res.* **44**, 8951–8961  
5 (2016).
- 6 29. Bernstein, K. A., Granneman, S., Lee, A. V., Manickam, S. & Baserga, S. J. Comprehensive  
7 mutational analysis of yeast DEXD/H box RNA helicases involved in large ribosomal subunit  
8 biogenesis. *Mol. Cell. Biol.* **26**, 1195–1208 (2006).
- 9 30. Daugeron, M. C. & Linder, P. Dbp7p, a putative ATP-dependent RNA helicase from  
10 *Saccharomyces cerevisiae*, is required for 60S ribosomal subunit assembly. *RNA* **4**, 566–581  
11 (1998).
- 12 31. Wai, H. H., Vu, L., Oakes, M. & Nomura, M. Complete deletion of yeast chromosomal rDNA  
13 repeats and integration of a new rDNA repeat: use of rDNA deletion strains for functional  
14 analysis of rDNA promoter elements in vivo. *Nucleic Acids Res.* **28**, 3524–3534 (2000).
- 15 32. Chanfreau, G., Rotondo, G., Legrain, P. & Jacquier, A. Processing of a dicistronic small  
16 nucleolar RNA precursor by the RNA endonuclease Rnt1. *EMBO J.* **17**, 3726–3737 (1998).
- 17 33. Laughery, M. F. *et al.* New vectors for simple and streamlined CRISPR-Cas9 genome editing  
18 in *Saccharomyces cerevisiae*. *Yeast* **32**, 711–720 (2015).
- 19 34. Foiani, M., Cigan, A. M., Paddon, C. J., Harashima, S. & Hinnebusch, A. G. GCD2, a  
20 translational repressor of the GCN4 gene, has a general function in the initiation of protein  
21 synthesis in *Saccharomyces cerevisiae*. *Mol. Cell. Biol.* **11**, 3203–3216 (1991).
- 22 35. Helser, T. L., Baan, R. A. & Dahlberg, A. E. Characterization of a 40S ribosomal subunit  
23 complex in polyribosomes of *Saccharomyces cerevisiae* treated with cycloheximide. *Mol.*  
24 *Cell. Biol.* **1**, 51–57 (1981).
- 25 36. Cavallé, J., Nicoloso, M. & Bachellerie, J. P. Targeted ribose methylation of RNA in vivo  
26 directed by tailored antisense RNA guides. *Nature* **383**, 732–735 (1996).
- 27 37. Kiss-László, Z., Henry, Y., Bachellerie, J. P., Caizergues-Ferrer, M. & Kiss, T. Site-specific ribose  
28 methylation of preribosomal RNA: a novel function for small nucleolar RNAs. *Cell* **85**, 1077–  
29 1088 (1996).
- 30 38. Maden, B. E. Mapping 2'-O-methyl groups in ribosomal RNA. *Methods* **25**, 374–382 (2001).
- 31 39. van Nues, R. W. *et al.* Box C/D snoRNP catalysed methylation is aided by additional pre-rRNA  
32 base-pairing. *EMBO J.* **30**, 2420–2430 (2011).

- 1 40. Miles, T. D. *et al.* Ytm1, Nop7, and Erb1 form a complex necessary for maturation of yeast  
2 66S preribosomes. *Mol. Cell. Biol.* **25**, 10419–10432 (2005).
- 3 41. Granneman, S., Petfalski, E. & Tollervey, D. A cluster of ribosome synthesis factors regulate  
4 pre-rRNA folding and 5.8S rRNA maturation by the Rat1 exonuclease. *EMBO J.* **30**, 4006–  
5 4019 (2011).
- 6 42. Milkereit, P. *et al.* Maturation and intranuclear transport of pre-ribosomes requires Noc  
7 proteins. *Cell* **105**, 499–509 (2001).
- 8 43. Liang, W. Q., Clark, J. A. & Fournier, M. J. The rRNA-processing function of the yeast U14  
9 small nucleolar RNA can be rescued by a conserved RNA helicase-like protein. *Mol. Cell. Biol.*  
10 **17**, 4124–4132 (1997).
- 11 44. Kos, M. & Tollervey, D. The Putative RNA Helicase Dbp4p Is Required for Release of the U14  
12 snoRNA from Preribosomes in *Saccharomyces cerevisiae*. *Mol. Cell* **20**, 53–64 (2005).
- 13 45. Soltanieh, S. *et al.* DEAD-box RNA helicase Dbp4 is required for small-subunit processome  
14 formation and function. *Mol. Cell. Biol.* **35**, 816–830 (2015).
- 15 46. Sardana, R. *et al.* The DEAH-box helicase Dhr1 dissociates U3 from the pre-rRNA to promote  
16 formation of the central pseudoknot. *PLoS Biol.* **13**, e1002083 (2015).
- 17 47. Balakin, A. G., Smith, L. & Fournier, M. J. The RNA world of the nucleolus: two major families  
18 of small RNAs defined by different box elements with related functions. *Cell* **86**, 823–834  
19 (1996).
- 20 48. Deutscher, M. P. in *Molecular biology of RNA processing and decay in prokaryotes* **85**, 369–  
21 391 (Elsevier, 2009).
- 22 49. Yeh, L. C., Thweatt, R. & Lee, J. C. Internal transcribed spacer 1 of the yeast precursor  
23 ribosomal RNA. Higher order structure and common structural motifs. *Biochemistry* **29**,  
24 5911–5918 (1990).
- 25 50. Aquino, G. R. R. *et al.* The RNA helicase Dbp7 promotes domain V/VI compaction and  
26 stabilization of inter-domain interactions during early 60S assembly. *Nat. Commun.* (2021).
- 27 51. Huang, G. M., Jarmolowski, A., Struck, J. C. & Fournier, M. J. Accumulation of U14 small  
28 nuclear RNA in *Saccharomyces cerevisiae* requires box C, box D, and a 5', 3' terminal stem.  
29 *Mol. Cell. Biol.* **12**, 4456–4463 (1992).
- 30 52. Hoareau-Aveilla, C., Bonoli, M., Caizergues-Ferrer, M. & Henry, Y. hNaf1 is required for  
31 accumulation of human box H/ACA snoRNPs, scaRNPs, and telomerase. *RNA* **12**, 832–840  
32 (2006).

- 1 53. Longtine, M. S. *et al.* Additional modules for versatile and economical PCR-based gene  
2 deletion and modification in *Saccharomyces cerevisiae*. *Yeast* **14**, 953–961 (1998).
- 3 54. de la Cruz, J., Kressler, D., Rojo, M., Tollervey, D. & Linder, P. Spb4p, an essential putative  
4 RNA helicase, is required for a late step in the assembly of 60S ribosomal subunits in  
5 *Saccharomyces cerevisiae*. *RNA* **4**, 1268–1281 (1998).
- 6 55. Henras, A., Dez, C., Noaillac-Depeyre, J., Henry, Y. & Caizergues-Ferrer, M. Accumulation of  
7 H/ACA snoRNPs depends on the integrity of the conserved central domain of the RNA-  
8 binding protein Nhp2p. *Nucleic Acids Res.* **29**, 2733–2746 (2001).
- 9 56. Lebaron, S. *et al.* The splicing ATPase prp43p is a component of multiple preribosomal  
10 particles. *Mol. Cell. Biol.* **25**, 9269–9282 (2005).

11

## 12 **Acknowledgements**

13 Our work has benefited from fruitful technical and scientific contacts with the neighboring groups  
14 of Jérôme Cavallé (J.C., Jade Hebras), Olivier Gadad (O.G., Christophe Dez, Frédéric Beckouët),  
15 Pierre-Emmanuel Gleizes (Simon Lebaron) and Tamás Kiss at the LBME/CBI. We thank Jade  
16 Hebras for technical help with the detection of ribose-methylated nucleosides. We thank Hussein  
17 Hamze for experiments related to the study not presented in this manuscript. We thank all  
18 members of the Henry/Henras team for helpful discussions. The Henry/Henras group is  
19 supported by grants from ANR (ANR-20-CE12-0026) and funding from CNRS and University of  
20 Toulouse. R.A.M. is supported by grants from the *Rectorat* of Lebanese University. M.J. is  
21 supported by a Ph.D. fellowship from the Lebanese University and CIOES Organization. The group  
22 of J.d.I.C. is supported by the Spanish Ministry of Science and Innovation [PID2019-103859-GB-  
23 I00 AEI/ 10.13039/501100011033], and the Andalusian Regional Government (JA; BIO-271). J.C.  
24 was supported by Ph.D. fellowship (PIF) from the University of Seville, and S.M.-V. is an academic  
25 research staff of the JA (PAIDI2020). M.T.B. and K.E.B. are supported by funding from the  
26 Deutsche Forschungsgemeinschaft (SFB860) and the University Medical Centre Göttingen. We  
27 thank F. Espinar-Marchena and H. Domínguez-Martín for assistance during the initial design of  
28 the rRNA suppressor screen.

29

## 30 **Author contributions**

1 M.J., J.C., P.V., O.H., N.J.W., E.V., M.T.B., K.E.B., Y.H, R.A.M., J.d.I.C. and A.H. designed the  
2 experiments. Experiments were performed by M.J., J.C., C.D., S.M.-V., R.C., P.V., O. R.-G., C.V.,  
3 Y.H., E.V., M.T.B., K.E.B., J.d.I.C. and A.H. All authors interpreted the data. M.J., J.d.I.C and A.H  
4 wrote the manuscript with strong contributions from Y.H.

5

### 6 **Competing interest statement**

7 The authors declare no competing interests.

8

9

### 10 **Figure legends**

#### 11 **Fig. 1 rRNA suppressors of the Dbp7 depletion**

12 **a** Serial dilution growth test of control (pNOY373) and suppressor (Sup. #2 and Sup. #10) strains  
13 isolated in the genetic screen for rRNA suppressors of Dbp7 depletion. Growth of strain EMY65  
14 transformed with plasmid pNOY373 bearing the specific C2392T mutation, or with plasmids Sup.  
15 #2 and Sup. #10 in which mutation T2392 has been reverted to the original C2392 is also tested.  
16 All strains grow similarly on selective SGal medium, which allows expression of Dbp7. On selective  
17 SD medium, the control strain shows a strong growth defect resulting from Dbp7 depletion,  
18 which is alleviated in all the strains expressing the mutant 25S rRNA with the C2392U  
19 substitution. Plates were incubated at 30 °C for 4 days. **b** Serial dilution growth test of strain  
20 NOY891 (original Nomura's lab strain, *DBP7*) and strain EMY65 (*GAL::HA-DBP7*) transformed with  
21 either the control pNOY373 plasmid or the suppressor Sup. #10 plasmid. All strains grow similarly  
22 on selective SGal medium. On selective SD medium, strain EMY65 transformed with the pNOY373  
23 plasmid showed a strong growth defect, which is only partially rescued, with respect to the  
24 reference NOY891 strain, by the Sup. #10 plasmid. Plates were incubated at 30 °C for 4 days. **c**  
25 Schematic representation of the secondary structure of the 25S rRNA in the PTC region (domain  
26 V). The sequence complementary to snR190 box A is highlighted in pink. The predicted  
27 methylation site of snR190 (G2395) and the nucleotide found mutated in the genetic screen  
28 (C2392U) are indicated in red.

29

#### 30 **Fig. 2 snR190 functions in pre-60S r-particle maturation**

1 **a** Accumulation levels of rRNA precursors in W303 wild-type (WT) and *snr190-[mut.C]* strains.  
2 Total RNA extracted from two independent clones (#1 and #2) for each strain was analyzed by  
3 northern blotting. The RNA molecules detected using radiolabeled oligonucleotide probes  
4 (Supplementary Table 4) are indicated on the left. **b** Accumulation levels of rRNA precursors in  
5 W303 *snr190-[mut.C]* strain and upon ectopic re-expression of snR190. Total RNA extracted from  
6 two independent clones (#1 and #2) of strain W303 *snr190-[mut.C]* transformed with a vector  
7 rescuing snR190 expression (*SNR190-U14*) or the corresponding empty vector as control (*E.V.*)  
8 was analyzed by northern blotting. The same probes as in (a) were used. **c** Polysome profiles on  
9 sucrose gradients of wild-type (green) and *snr190-[mut.C]* (red) strains in the W303 background.  
10 Total cellular extracts prepared from these strains were centrifuged through 10% to 50% sucrose  
11 gradients.  $A_{254}$  was measured during gradient fractionation. The identity of the different peaks is  
12 indicated and half-mers are marked with arrows. **d** Polysome profiles on sucrose gradients of  
13 W303 *snr190-[mut.C]* strain transformed with an empty vector (*E.V.*, red) or upon ectopic re-  
14 expression of snR190 (*SNR190-U14*, purple). Total cellular extract preparation and analysis were  
15 carried out as in (c).

16

17 **Fig. 3 snR190 does not function as a methylation guide**

18 Reverse transcription experiment at normal or low dNTP concentration (black triangles) using  
19 total RNA extracted from strain BY4741 *snr190-[mut.C]* transformed with plasmids expressing  
20 the wild-type or *snr190-[mut.S]* versions of snR190 or the empty vector (*E.V.*) as control. Two  
21 different primers were used to initiate reverse transcription: primer #2 (proximal, green) and  
22 primer #1 (distal, blue). A sequencing ladder was loaded in parallel to identify the nucleotides  
23 inducing reverse transcription stops. Note: a weak reverse transcription stop was observed at  
24 position G2395 with the proximal primer, but this signal was detected both in presence or  
25 absence of snR190, suggesting that it may correspond to a non-specific signal rather than a bona  
26 fide methylation-induced reverse transcription stop. The question mark (?) indicates a strong  
27 reverse transcription stop that is not associated to currently known nucleoside methylation.  
28 These experiments were repeated two times independently with each primer and similar results  
29 were obtained.

1  
2  
3  
4  
5  
6  
7  
8  
9  
10  
11  
12  
13  
14  
15  
16  
17

**Fig. 4 snR190 boxes A and B are required for its function in LSU synthesis**

**a** Polysome profiles on sucrose gradients of W303 *snr190-[mut.C]* strain transformed with vectors supporting expression of wild-type snR190 (WT, green) or bearing mutations in its antisense elements box A (*snr190-[mut.A]*, dark blue), box B (*snr190-[mut.B]*, grey) or both (*snr190-[mut.AB]*, pink), or with the empty vector as control (*E.V.*, red). Cell extracts were prepared and analyzed as in Fig. 2c. **b** Steady-state levels of distinct pre-rRNAs and U14 and snR190 snoRNAs in isogenic wild-type and *snr190-[mut.C]* strains in the W303 background; cells were transformed with plasmids supporting expression of wild-type snR190 (WT) or bearing mutations in its antisense elements box A (*snr190-[mut.A]*), box B (*snr190-[mut.B]*) or both (*snr190-[mut.AB]*), or with the empty vector as control (*E.V.*). Experiments were performed as explained in the legend of Fig. 2b. Note: the first five lanes of this figure are identical to those presented in Fig. 2b, where they were used to support the conclusion that ectopic re-expression of snR190 restores pre-rRNA processing in the *snr190-[mut.C]* strain. This experiment was performed once with each independent clone for the W303 background and twice with each independent clone for the BY4741 background (see also supplementary Fig. 8).

18 **Fig. 5 snR190 is retained into pre-ribosomal particles in the absence of Dbp7**

19 **a** Immuno-precipitation of Nop7-HTP-containing pre-ribosomal particles in the presence or  
20 absence of Dbp7. Particles were immuno-precipitated from total cell extracts prepared from  
21 wild-type or *dbp7Δ* strains expressing an HTP-tagged version of Nop7. As a background control,  
22 the wild-type strain expressing untagged Nop7 was similarly processed. Some rRNA precursors  
23 and snoRNAs (indicated on the left) present in the total extracts (Inputs) or in the immuno-  
24 precipitate (IPs) were analyzed by northern blotting using selected radiolabeled probes  
25 (Supplementary Table 4). **b** Quantification of the northern blot signals obtained for the  
26 hybridizations shown in (a) using PhosphorImager data and the MultiGauge software. The  
27 histogram represents the co-immunoprecipitation efficiencies (IPs over Inputs) of the indicated  
28 RNA species with Nop7-HTP in the presence (*DBP7*, black) or absence (*dbp7Δ*, red) of Dbp7. **c**  
29 Sedimentation profile of snR190, snR37, snR42 and snR5 snoRNAs in the presence or absence of

1 Dbp7. Total cellular extracts prepared from the wild-type (green) or *dbp7Δ* (red) strains were  
2 centrifuged through 10% to 50% sucrose gradients.  $A_{254}$  was measured during gradient  
3 fractionation and the profiles are represented. RNAs extracted from the first 18 fractions were  
4 analyzed by northern blotting to detect the indicated snoRNAs. Note: the RNA samples  
5 corresponding to each gradient were processed separately (electrophoresis, transfer,  
6 hybridization, exposure, data acquisition). Therefore, the exposures presented for each snoRNA  
7 in the two strains have been chosen arbitrarily. Please refer to the intra-series quantifications  
8 (pre-ribosome-bound versus free ratios) presented in Supplementary Fig. 10 for the  
9 interpretation of these data. This experiment has been performed once with the *dbp7Δ* strain  
10 and once with the strain expressing the Dbp7<sub>K197A</sub> catalytic mutant (Fig. 6c) with similar results  
11 for the snoRNAs tested.

12

13 **Fig. 6 The ATPase activity of Dbp7 is required for snR190 release from pre-ribosomal particles**

14 **a** His<sub>10</sub>-ZZ-tagged Dbp7<sub>WT</sub> and Dbp7<sub>K197A</sub> were recombinantly expressed in *E. coli* and purified by  
15 nickel-affinity chromatography. Purified proteins were separated by denaturing SDS-PAGE and  
16 visualized by Coomassie staining. **b** The rate of ATP hydrolysis by purified His<sub>10</sub>-ZZ-Dbp7<sub>WT</sub> (black)  
17 Dbp7<sub>K197A</sub> (red) was monitored using an in vitro NADH-coupled ATPase assay in the presence of  
18 increasing amounts of RNA. Data from three independent experiments are presented as mean  
19 +/- standard deviation. Statistically significant differences determined using one-tailed Student's  
20 t-test are indicated by asterisks (0 μM RNA: \*\* = p<0.01 (0,008696); 0.5 μM RNA: \*\*\* = p<0.001  
21 (0,000217); 1 μM RNA: \*\*\*\* = p<0.0001 (0,000061); 1.5 μM RNA: \*\*\*\* = p<0.0001 (0,000106); 2  
22 μM RNA: \*\*\* = p<0.001 (0,000139); 4 μM RNA: \*\* = p<0.01 (0,002657). **c** Sedimentation profile of  
23 Dbp7-3HA, snR190, snR42 and snR10 snoRNAs in cells expressing Dbp7<sub>K197A</sub>. Total cellular  
24 extracts prepared from the *dbp7Δ* strain transformed with vectors encoding 3HA-tagged versions  
25 of Dbp7<sub>WT</sub> (green) or Dbp7<sub>K197A</sub> (red) were centrifuged through 10% to 50% sucrose gradients.  
26  $A_{254}$  was measured during gradient fractionation and the profiles are represented. Proteins and  
27 RNAs extracted from the first 13 fractions were analyzed by western blotting and northern  
28 blotting, respectively, to detect wild-type or mutant Dbp7-3HA proteins and snoRNAs. This

1 experiment has been performed once with the strain expressing the Dbp7<sub>K197A</sub> catalytic mutant  
2 and once with the *dbp7Δ* strain (Fig. 5c) with similar results for the snoRNAs tested.

3

4 **Fig. 7 Mutations in *SNR190* alleviate the phenotypes of the *dbp7Δ* strain**

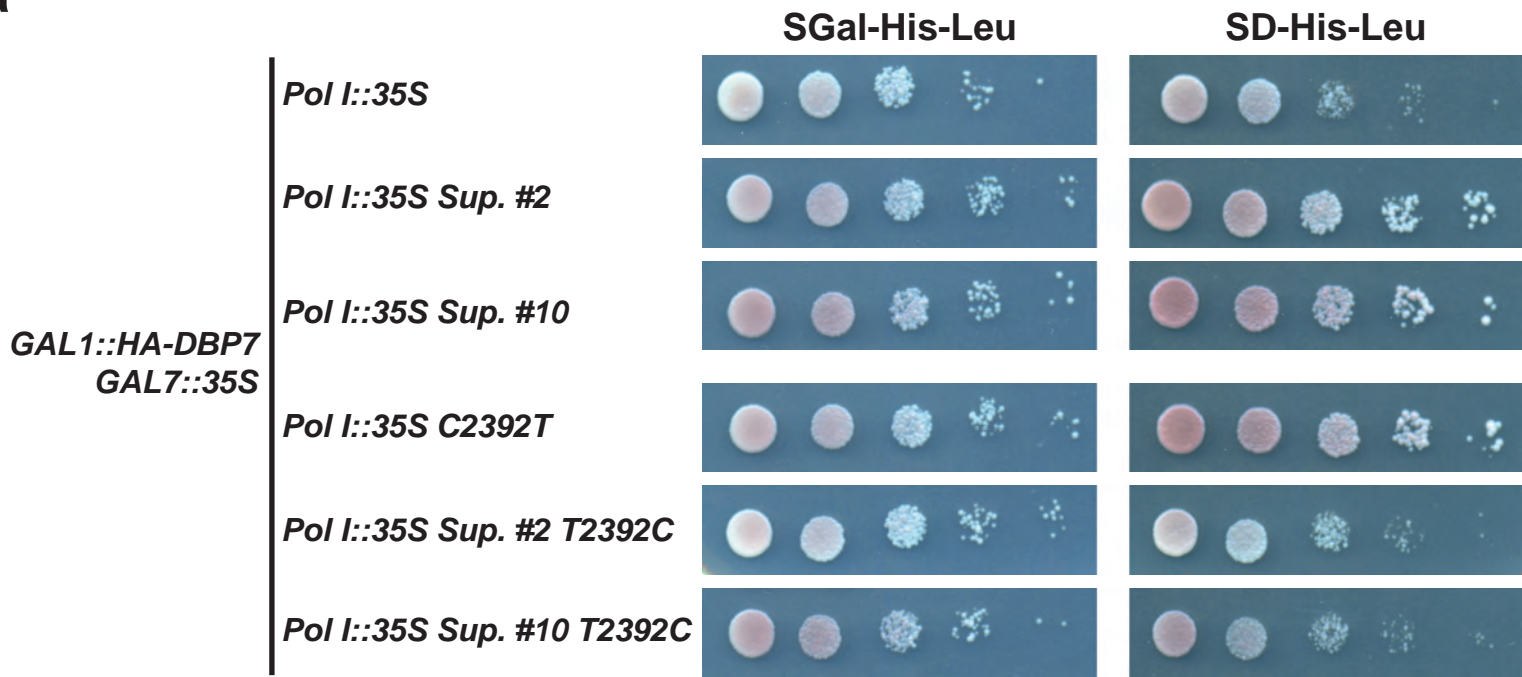
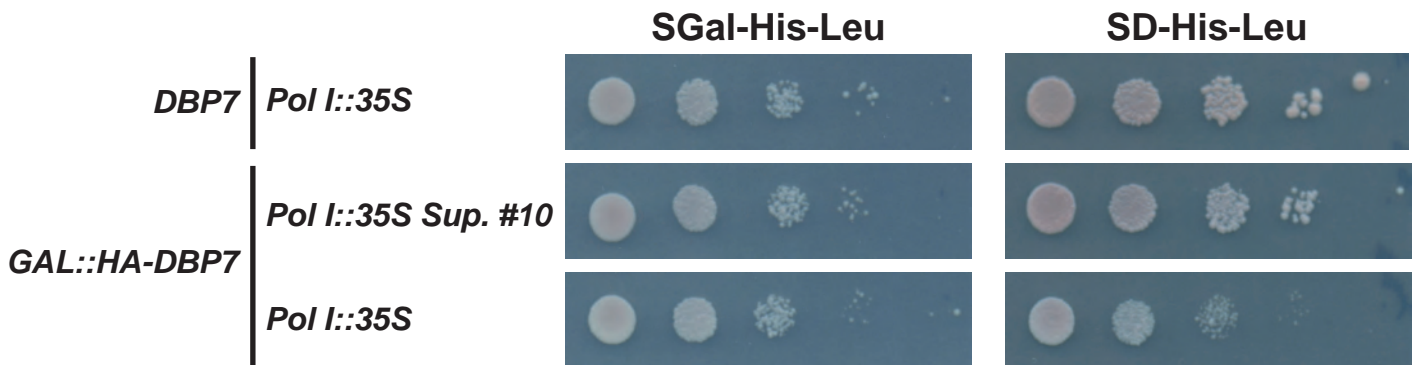
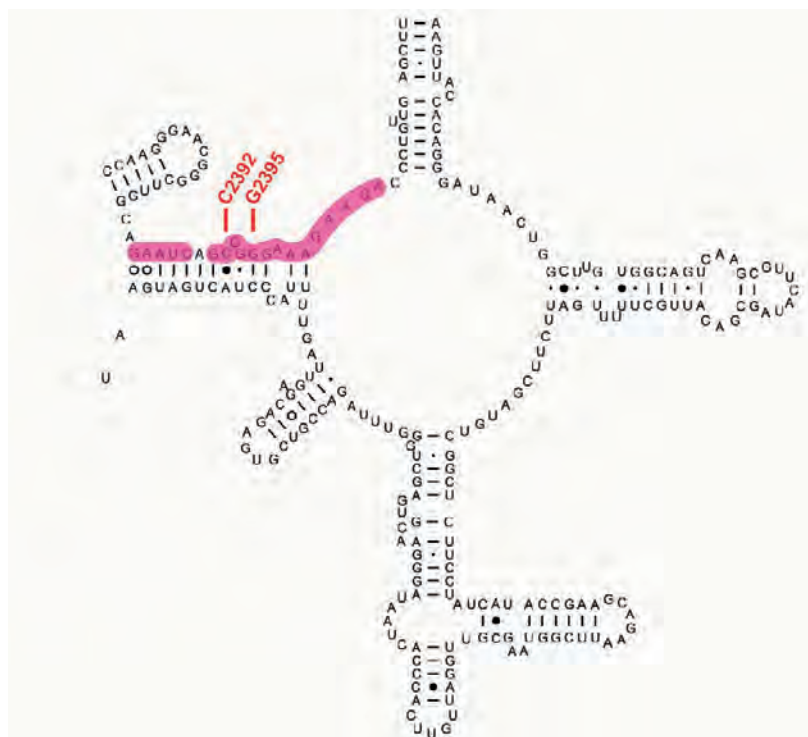
5 **a** Growth assay of isogenic wild-type, single *snr190-[mut.C]*, single *dbp7Δ* and the double *dbp7Δ*,  
6 *snr190-[mut.C]* mutants in the W303 background. Serial dilutions of these strains were grown on  
7 YPD plates at the indicated temperatures for 3-5 days. **b** Accumulation levels of rRNA precursors  
8 in the wild-type BY4741 strain or in two independent clones (#1 and #2) of the *dbp7Δ* strain and  
9 the *dbp7Δ* strain further manipulated using the CRISPR-Cas9 approach to deplete snR190  
10 (*snr190-[mut.C]*) or to express *snr190-[mut.A]* and *snr190-[mut.G34C]*. Experiments were  
11 performed as explained in the legend of Fig. 2b. **c** Quantification of the 27SB/27SA<sub>2</sub> ratios for the  
12 indicated strains from the precursor levels measured in (**b**) using PhosphorImager data and the  
13 MultiGauge software. Data correspond to two biological replicates. Histograms represent the  
14 mean values. The individual data points are shown.

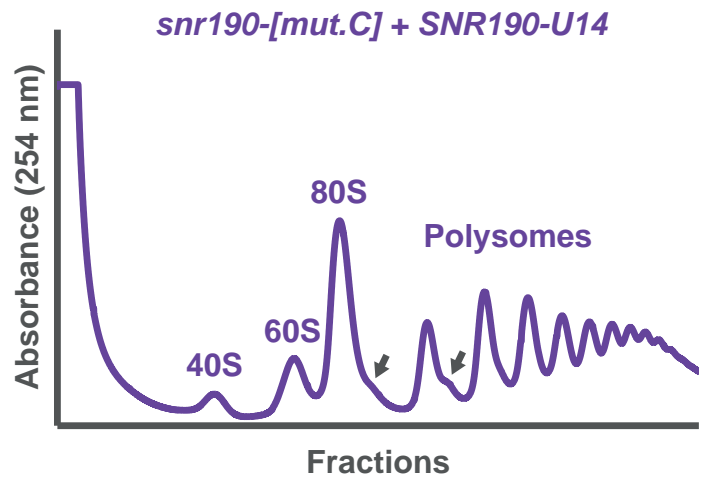
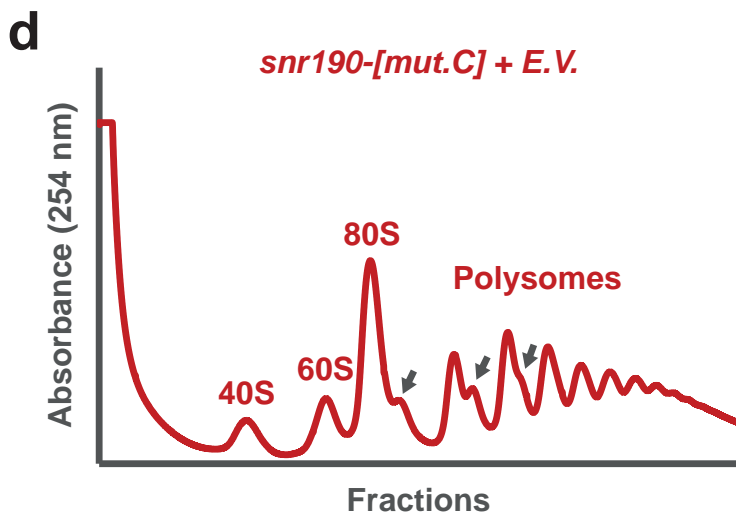
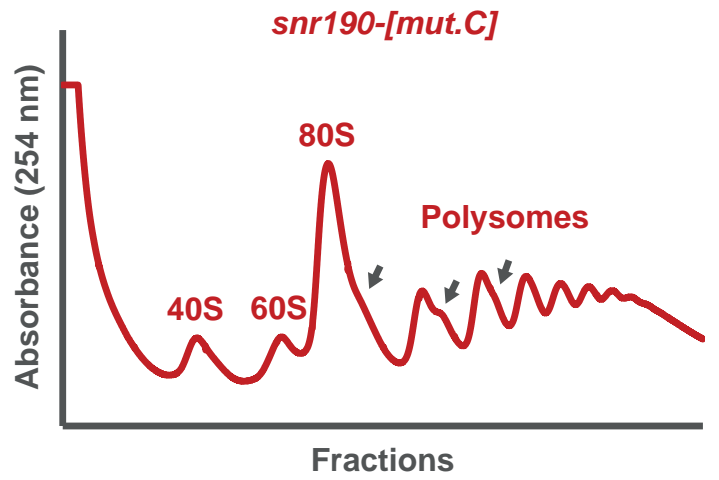
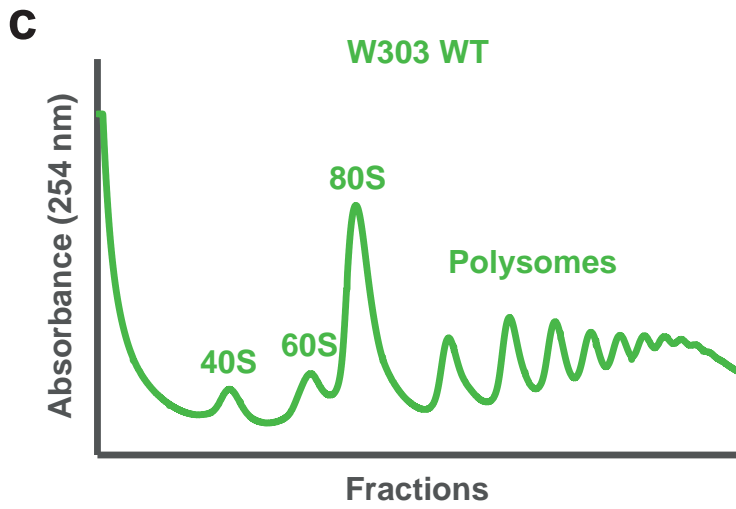
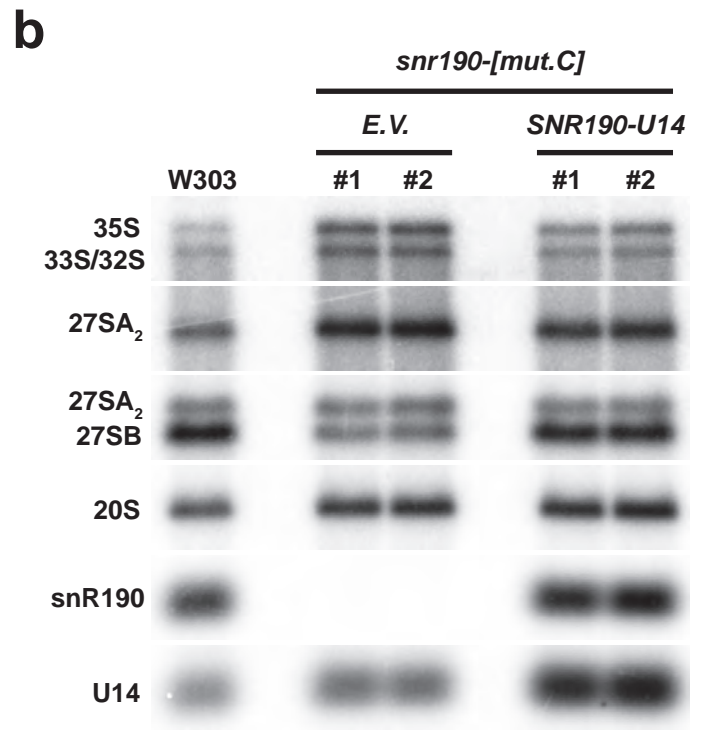
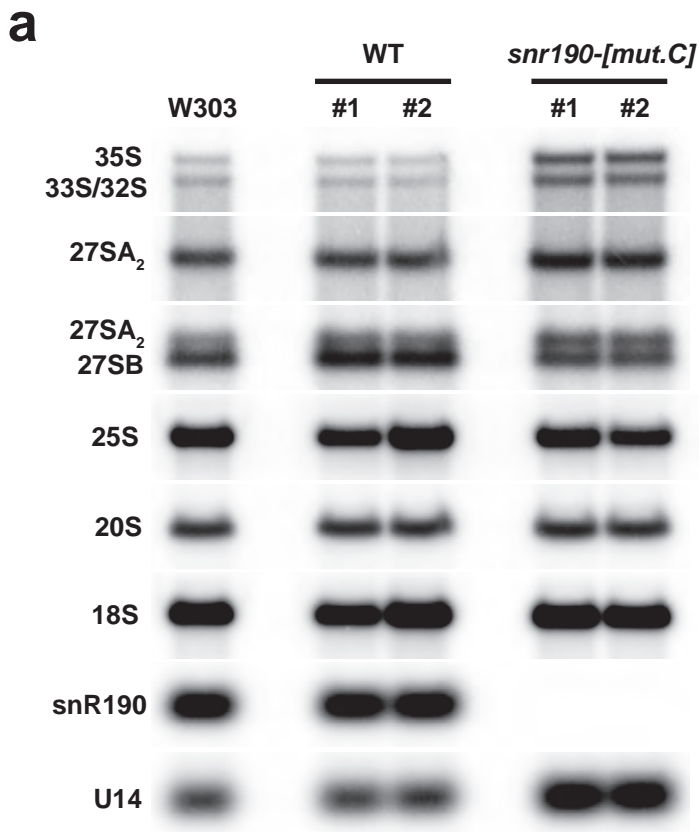
15

16 **Fig. 8 snR190 is required for stable incorporation of the Npa1 complex into pre-ribosomes**

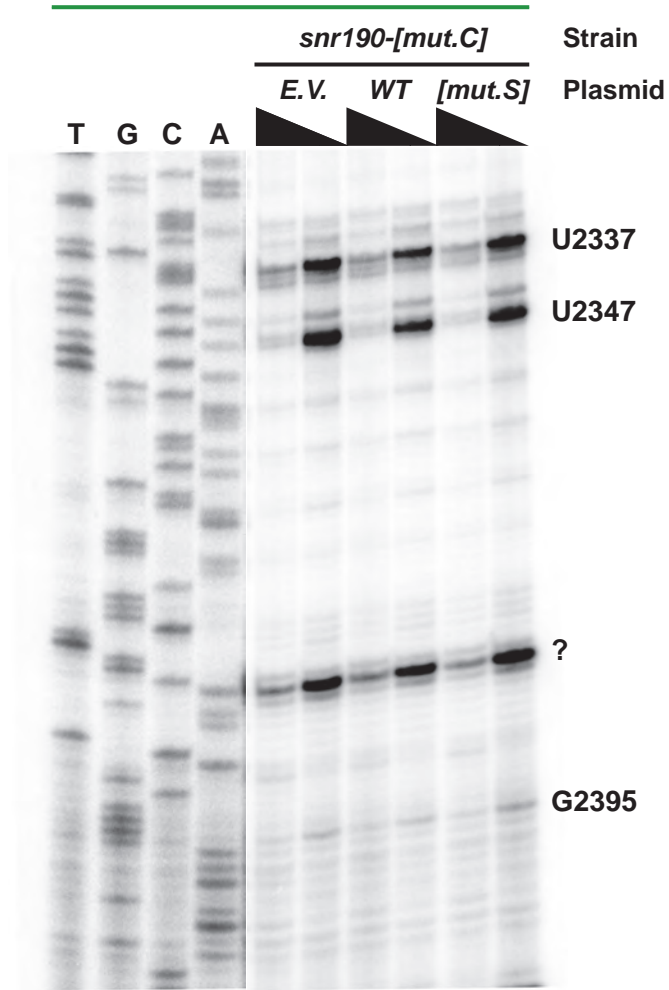
17 **a** Immuno-precipitation of Noc1-TAP-containing pre-ribosomal particles from wild-type, *snr190-*  
18 *[mut.C]* and *dbp7Δ* mutant strains, and analysis of their RNA and protein contents by northern  
19 and western blotting, respectively. Particles were immuno-precipitated from total cell extracts  
20 prepared from wild-type, *snr190-[mut.C]* and *dbp7Δ* strains expressing a TAP-tagged version of  
21 Noc1. Pre-rRNA components of 90S and early pre-60S r-particles (indicated on the left) present  
22 in the total extracts (Inputs) or in the immuno-precipitates (IPs) were analyzed by northern  
23 blotting (upper panel) using a radiolabeled probe (Supplementary Table 4). Protein levels of  
24 components of the Npa1 complex (indicated in grey) or other proteins present in early pre-  
25 ribosomal particles (labeled in black) were analyzed by western blotting on the Input or IP  
26 samples (lower panel) using specific antibodies. \*: non-specific signal detected with the anti-  
27 Nop8 antibodies. \*\*: Prp43 signal resulting from incubation of the membrane with anti-Prp43  
28 antibodies (see above panel) prior to incubation with anti-Dbp6 antibodies. **b** Quantification of  
29 the western blot signals obtained in (**a**). Western blot signals were quantified from ChemiDoc

1 images (Biorad) using the Image Lab software (Biorad). The histogram represents the co-  
2 immunoprecipitation efficiencies (IPs over Inputs) of the indicated proteins with Noc1-TAP in the  
3 wild-type (*WT*, grey), *snr190-[mut.C]* (black) and *dbp7Δ* (red) strains, normalized with respect to  
4 the ratios in the wild-type strain. Note: the Dbp6 signal obtained in (a) could not be quantified  
5 accurately due to the proximity of the Prp43 signal.

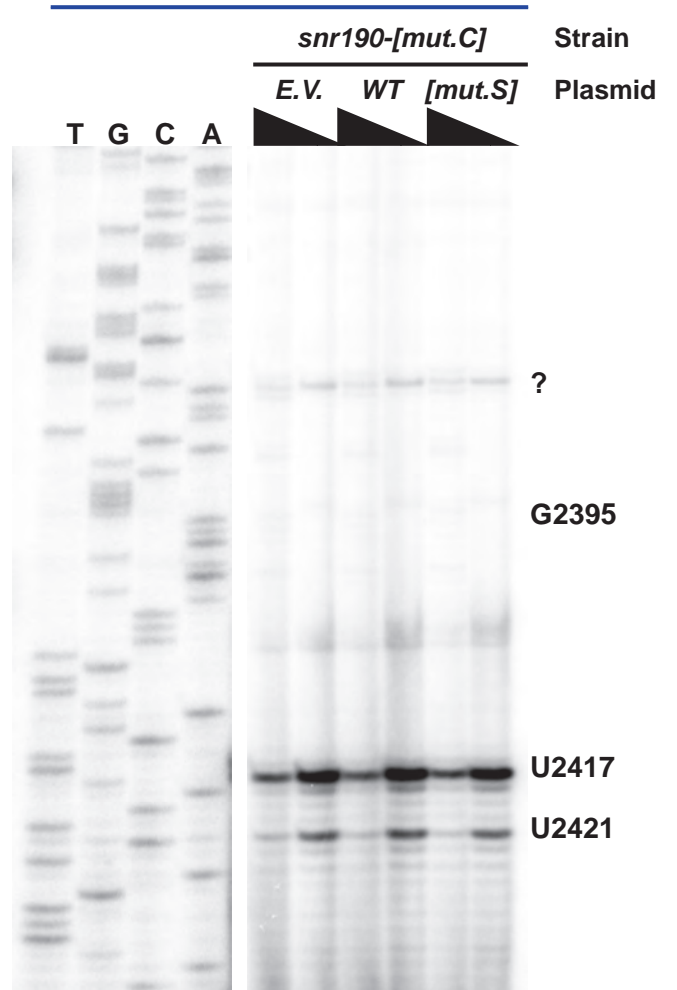
**a****b****c**

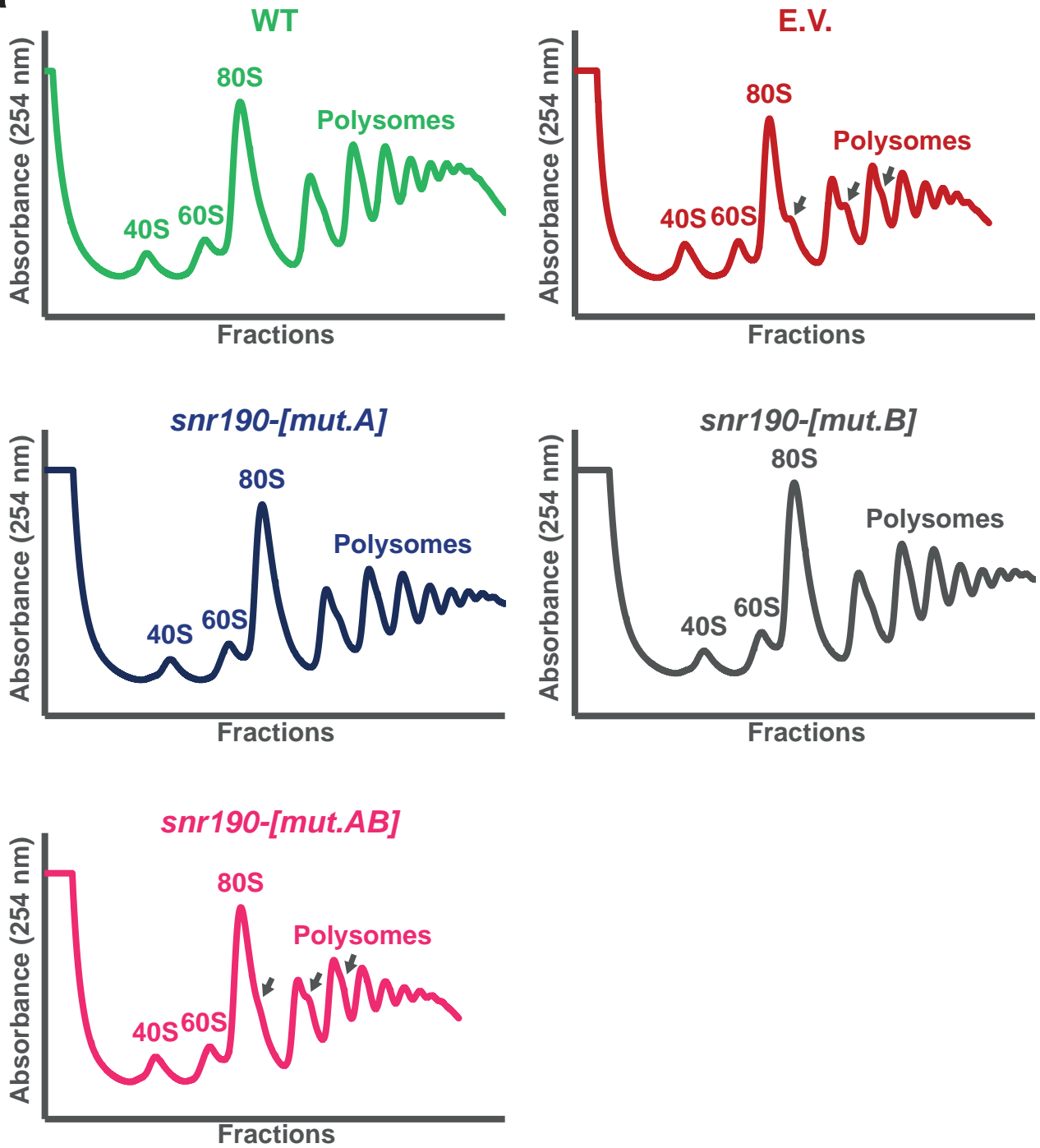
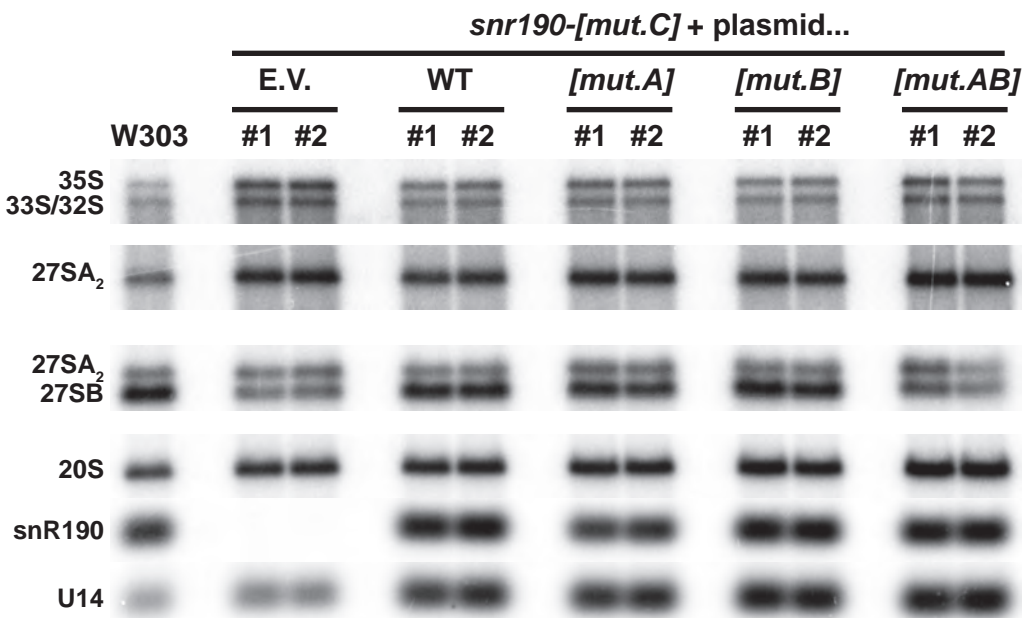


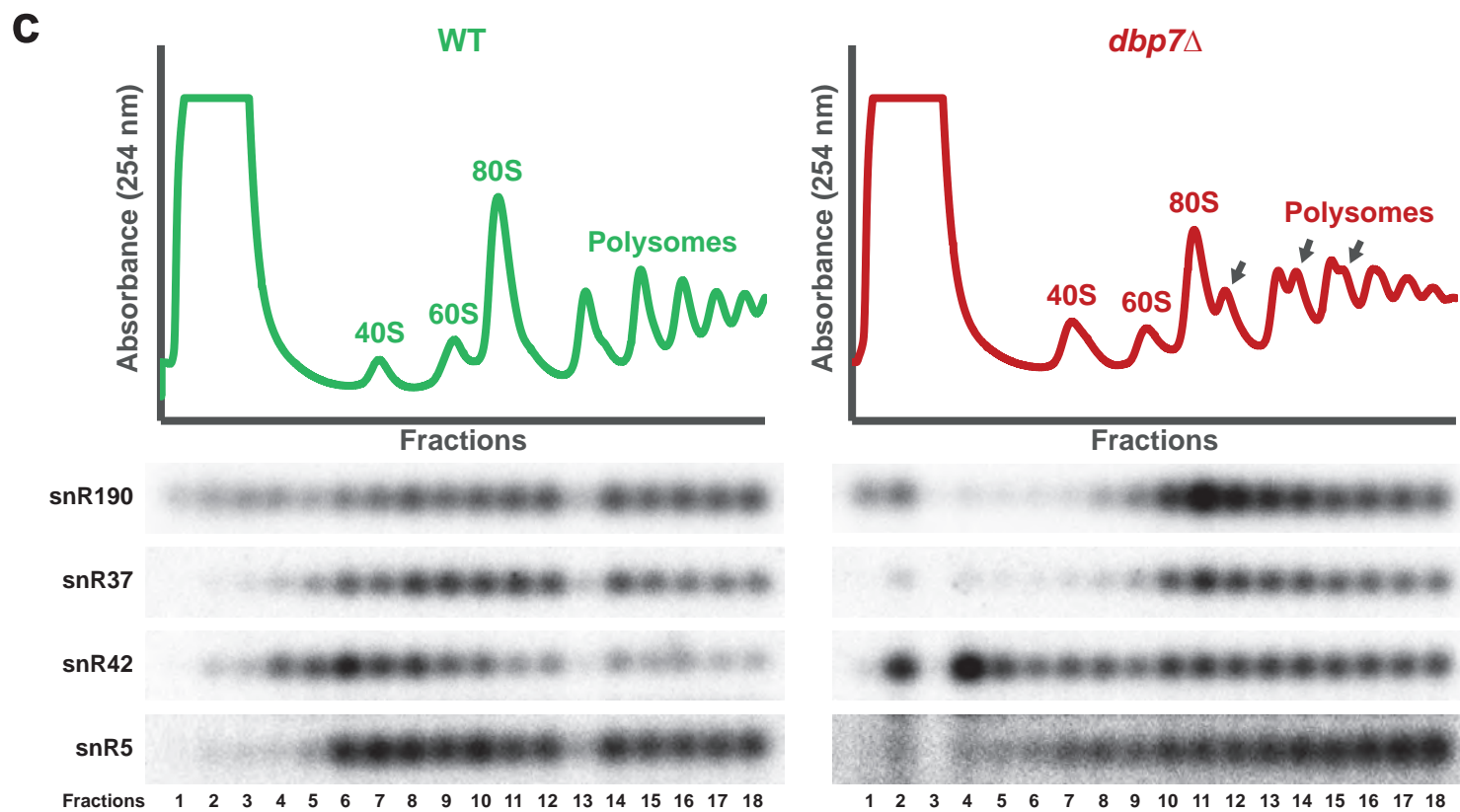
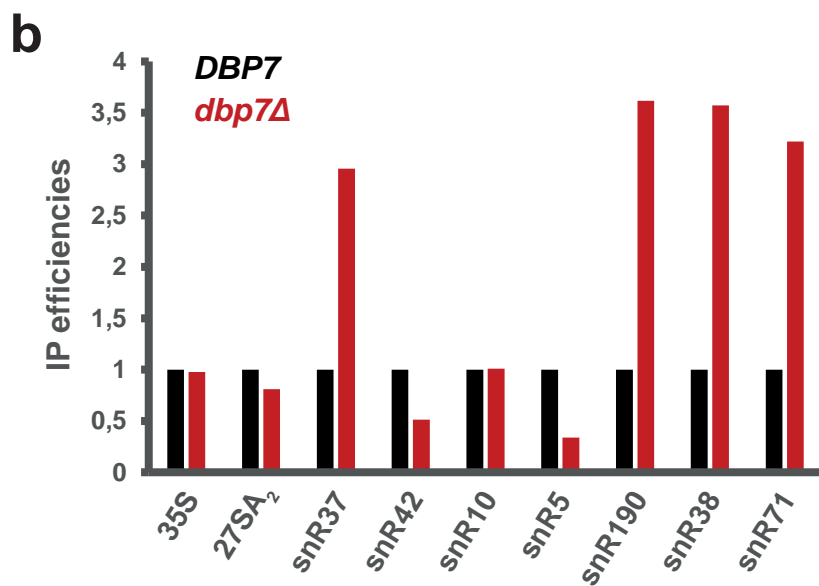
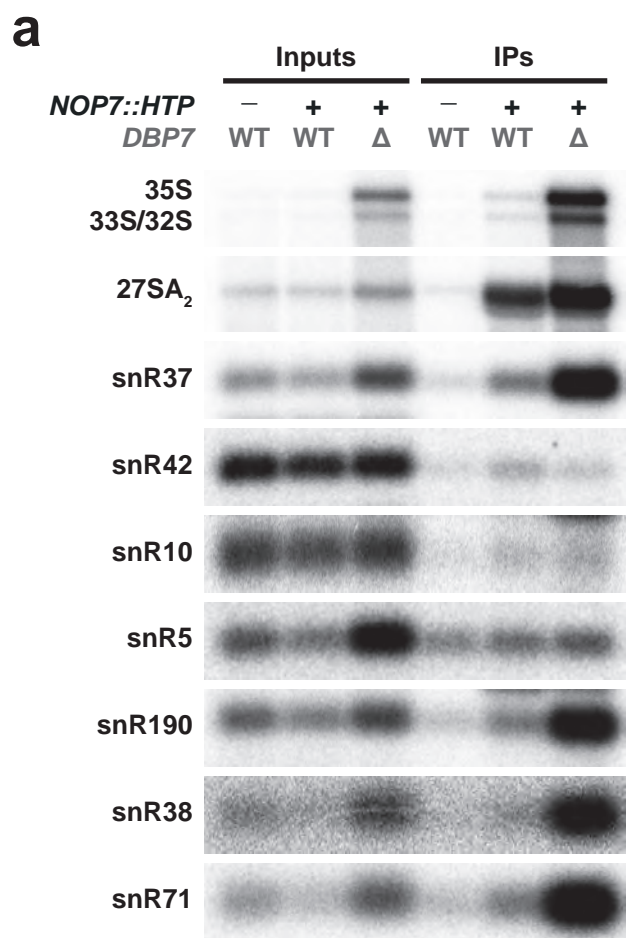
**Primer #2**

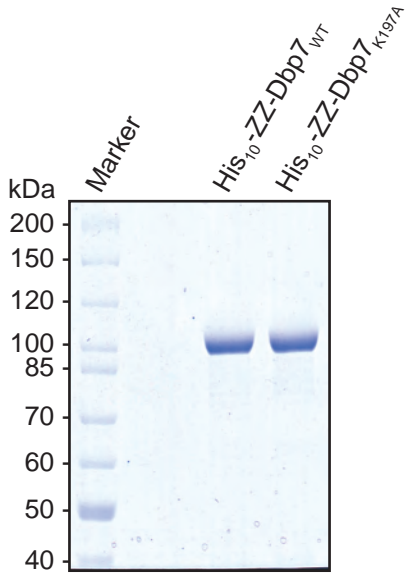
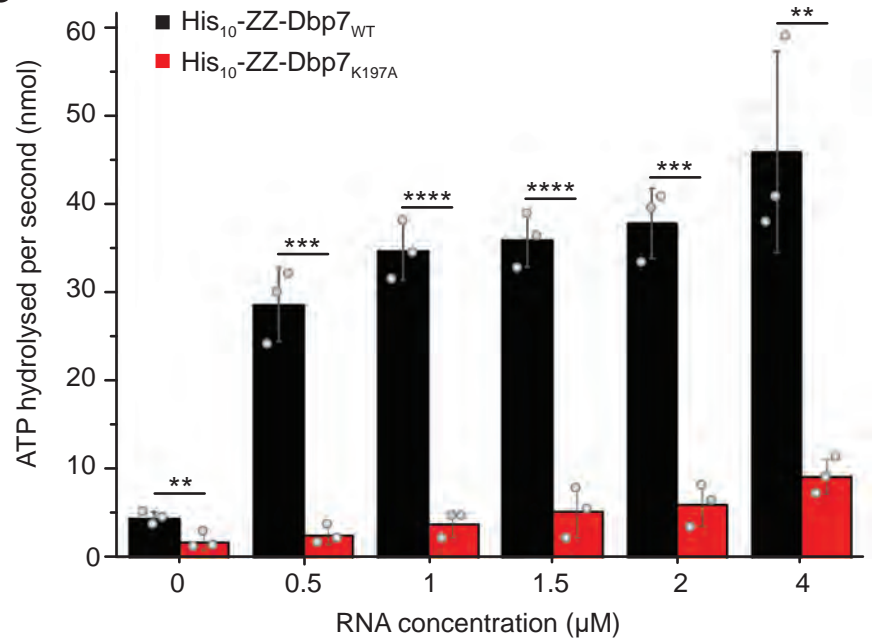
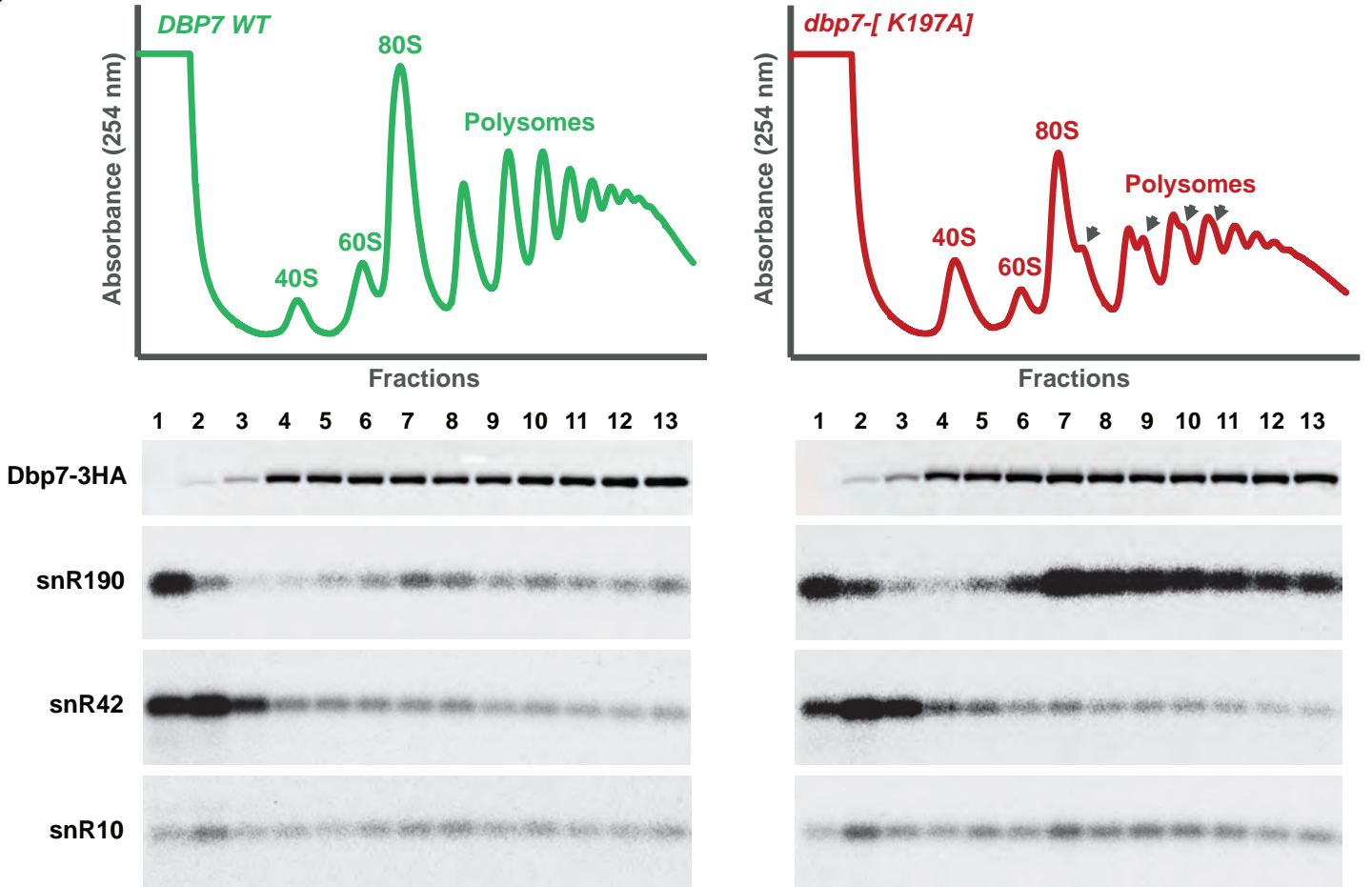


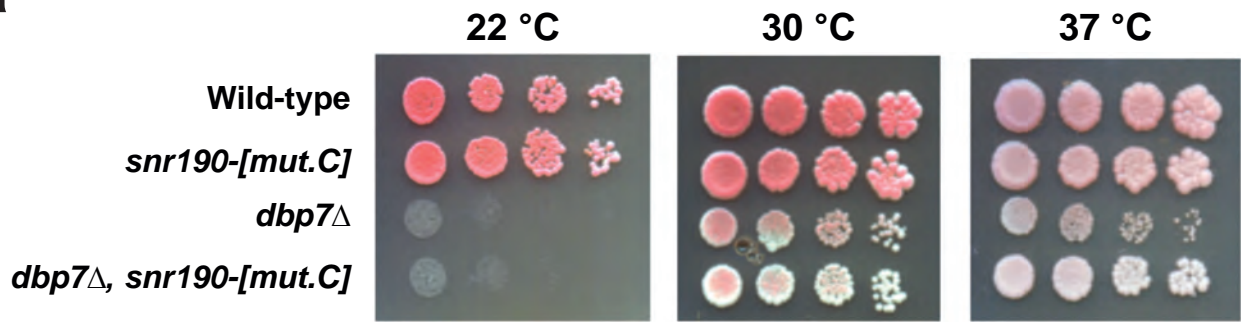
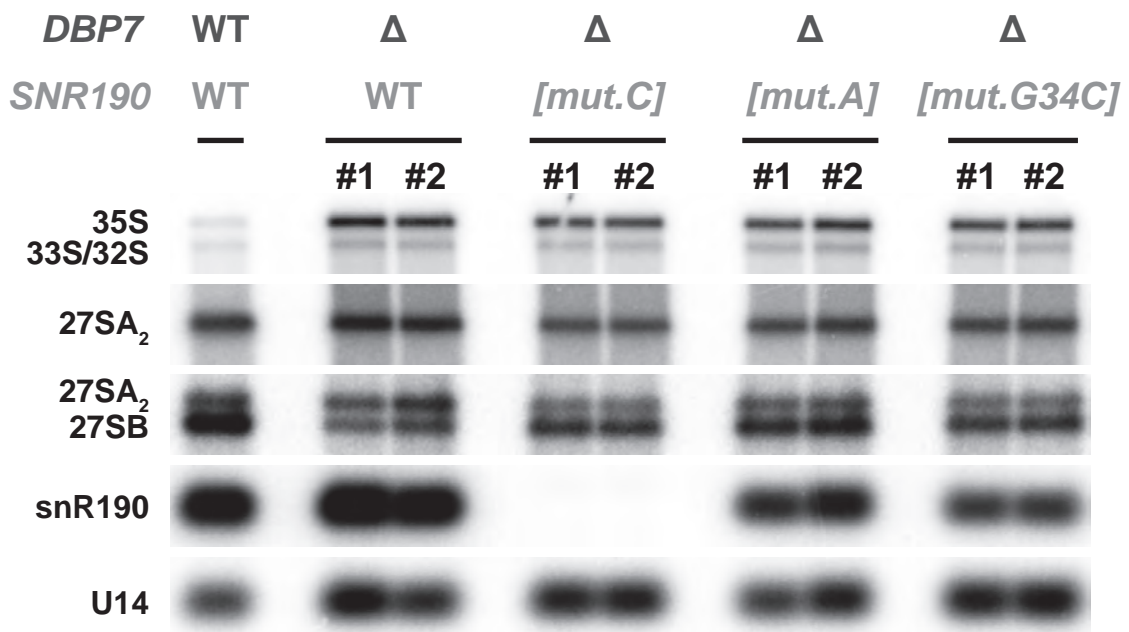
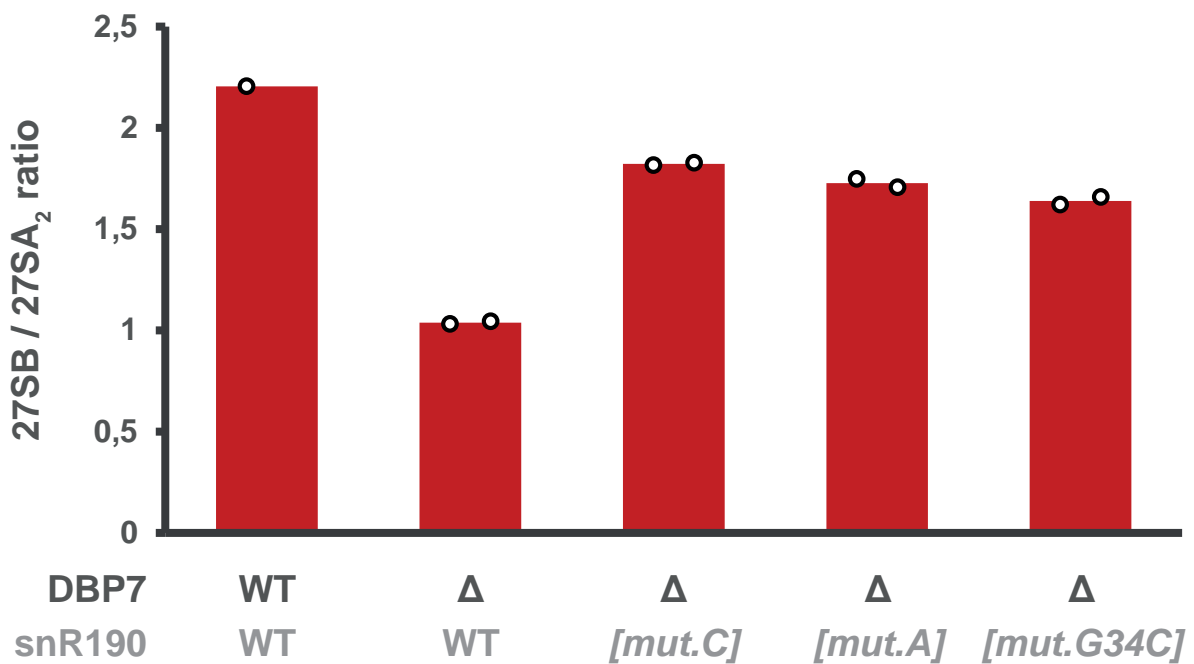
**Primer #1**

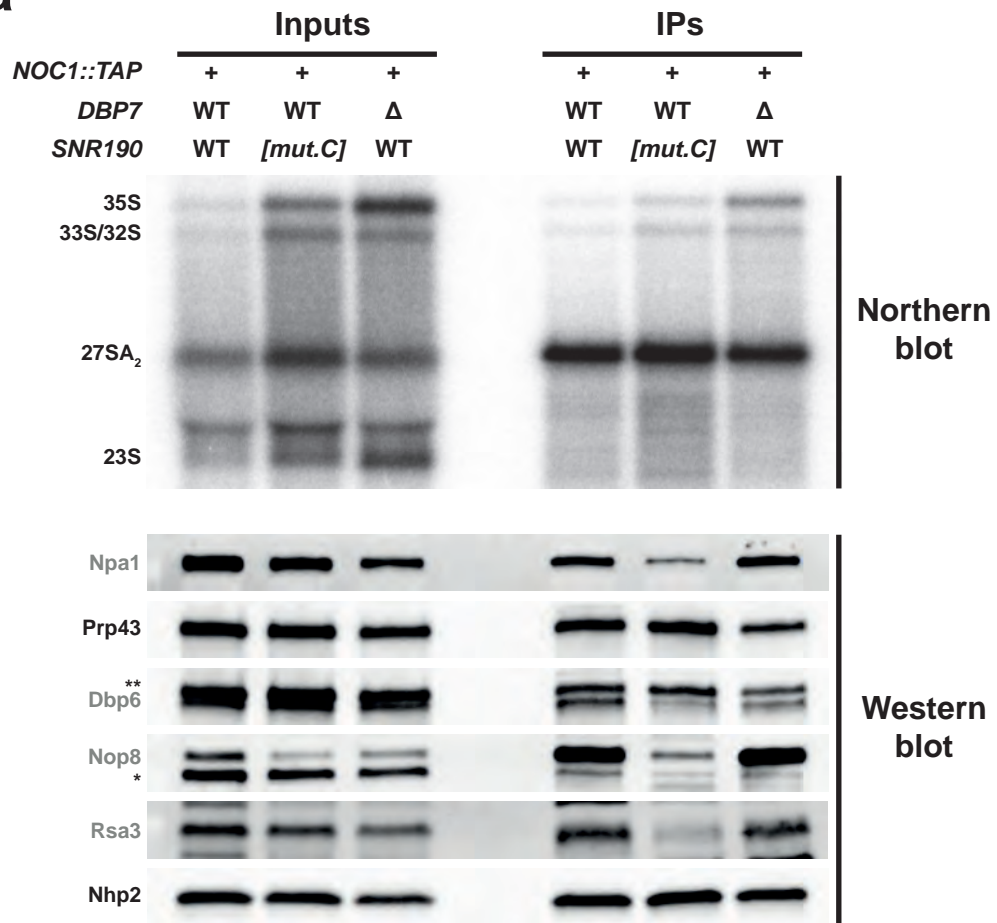
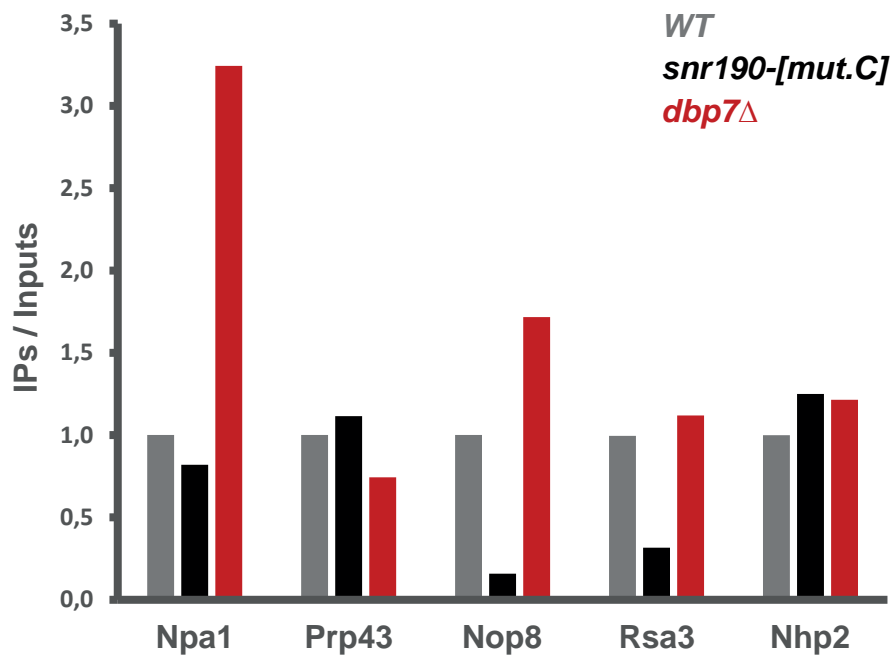


**a****b**



**a****b****c**

**a****b****c**

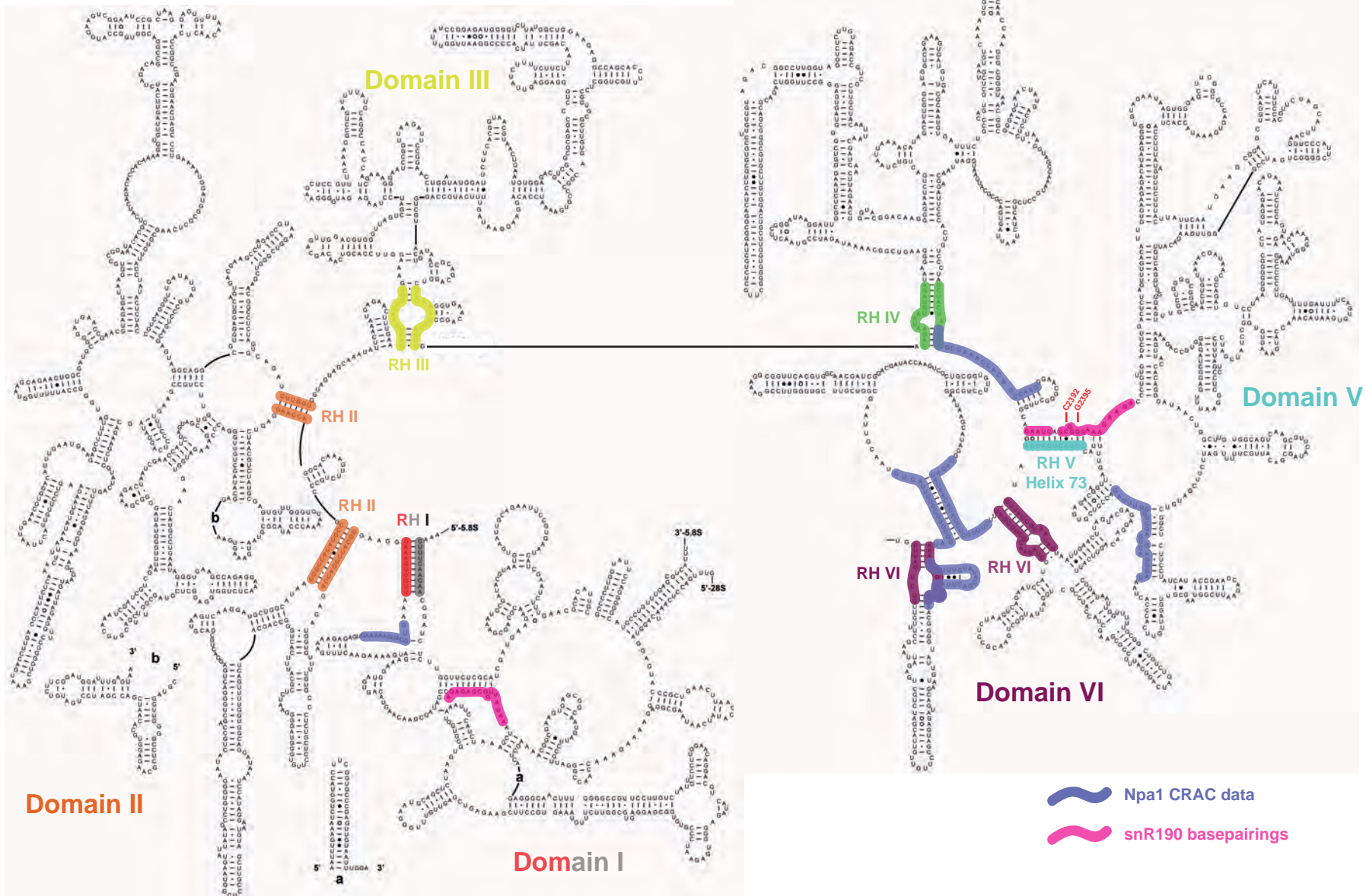
**a****b**

## **SUPPLEMENTARY INFORMATION**

### **Association of snR190 snoRNA chaperone with early pre-60S particles is regulated by the RNA helicase Dbp7 in yeast**

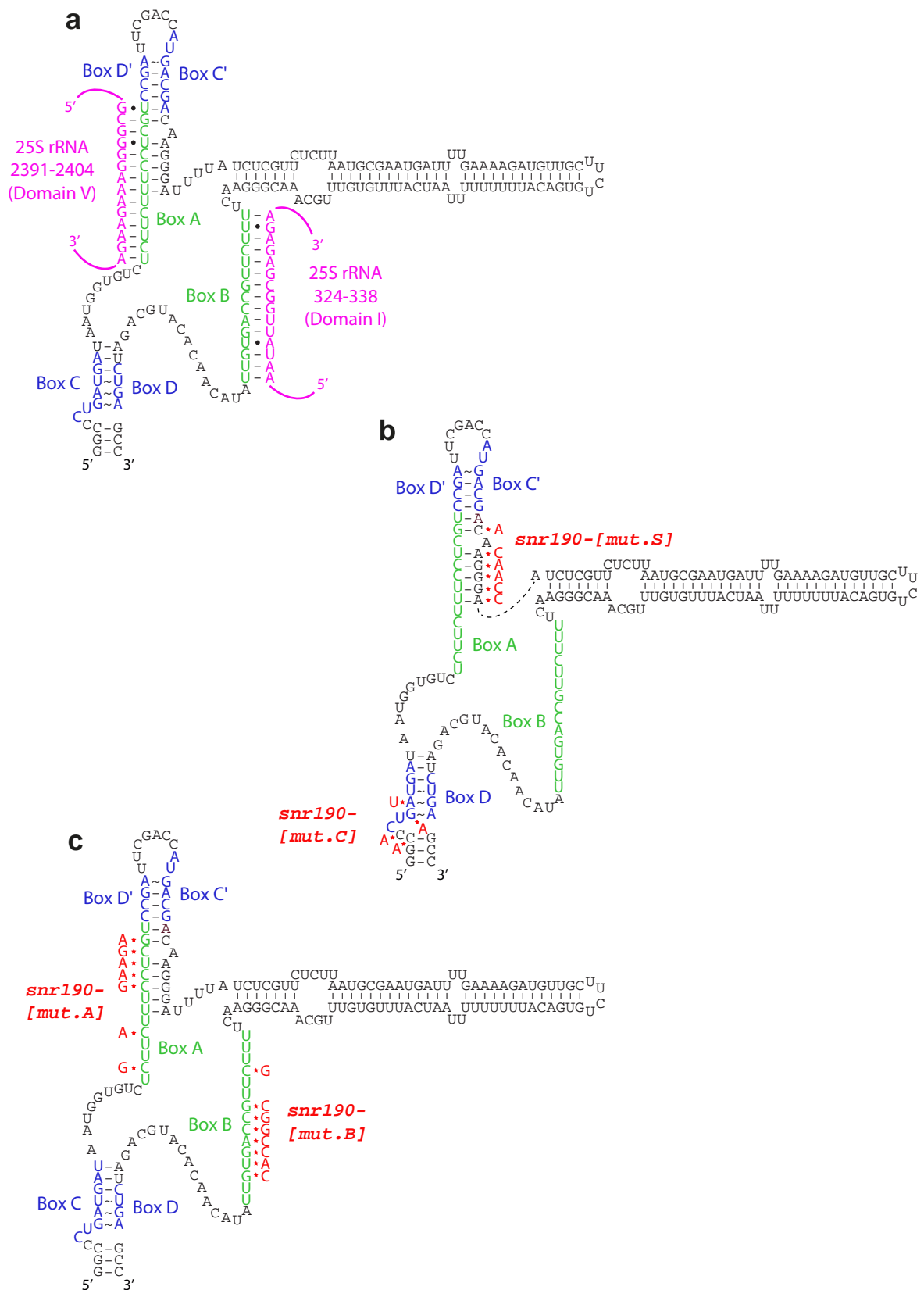
Mariam Jaafar, Julia Contreras, Carine Dominique, Sara Martin Villanueva, Régine Capeyrou, Patrice Vitali, Olga Rodríguez-Galán, Carmen Velasco, Odile Humbert, Nicholas J. Watkins, Eduardo Villalobo, Katherine E. Bohnsack, Markus T. Bohnsack, Yves Henry, Raghida Abou Merhi, Jesús de la Cruz and Anthony K. Henras

## SUPPLEMENTARY FIGURES AND TABLES



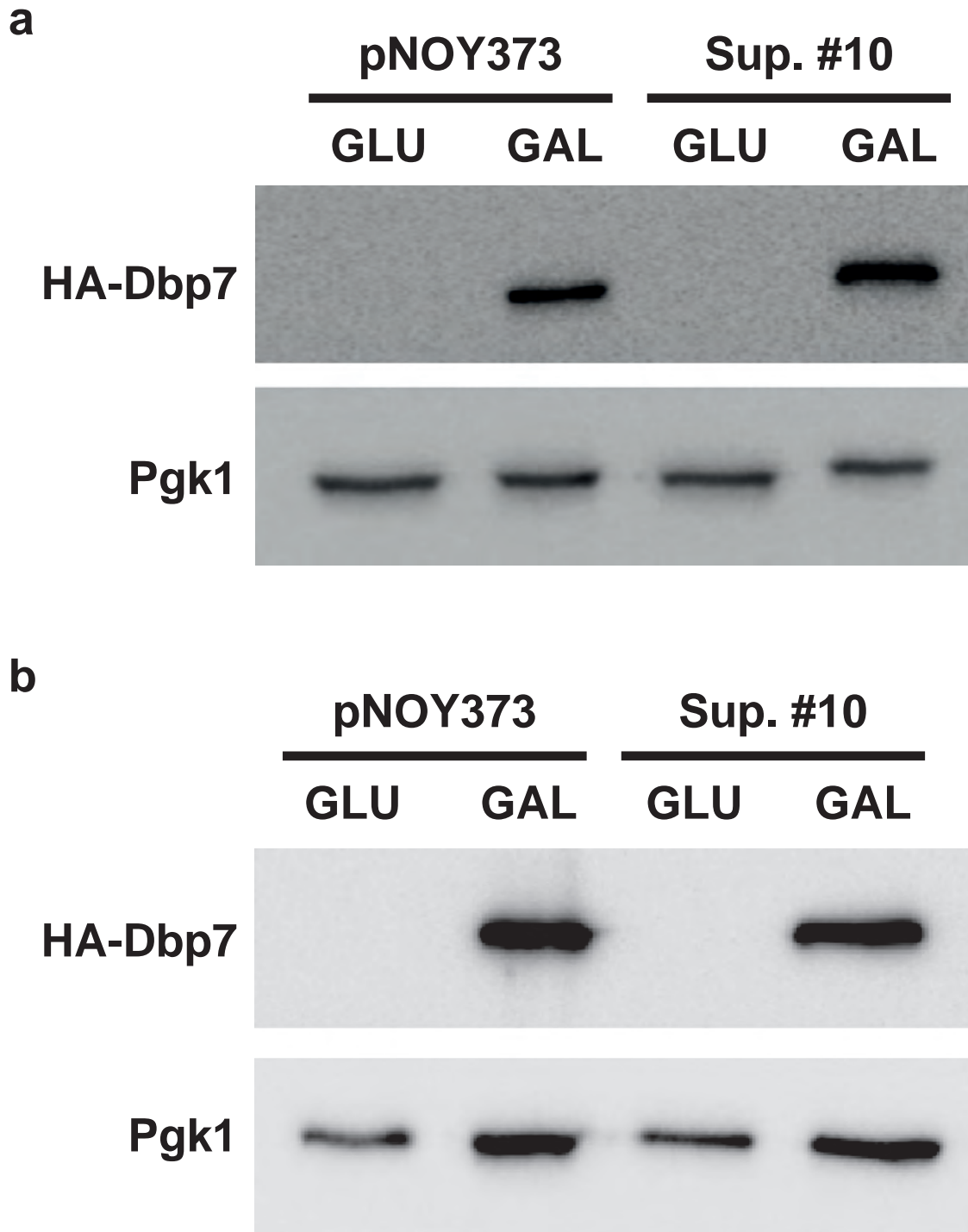
### Supplementary Fig. 1 Secondary structure of the 25S rRNA

Secondary structure of the 25S rRNA obtained from (<http://www.rna.ccbb.utexas.edu>)<sup>1</sup>. Root helices (RH) of the six structural domains of the 25S rRNA (I to VI) are colored (RH I, red/grey; RH II, orange; RH III, yellow; RH IV, green; RH V, light blue/pink; RH VI, purple). Npa1 binding sites in domains I, V and VI are highlighted in blue. 25S rRNA sequences complementary to the antisense boxes A and B of snR190 are highlighted in pink. Position of the predicted methylation site guided by snR190 (G2395) is indicated in red as well as the nucleotide (C2392) found mutated in the rRNA suppressors of the slow-growth of a *dbp7* null mutant described in Fig. 1.



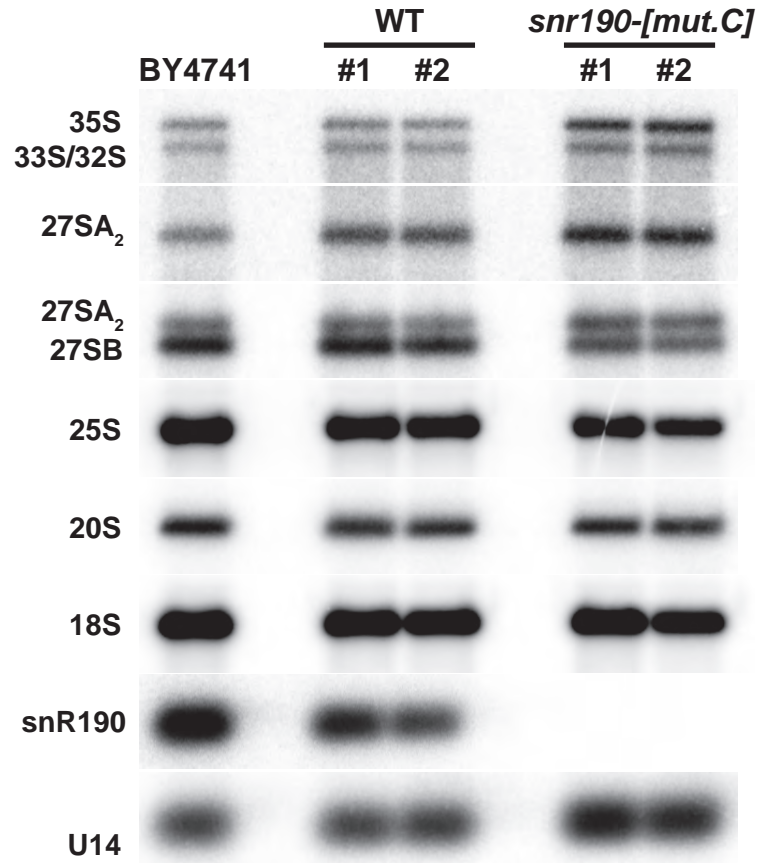
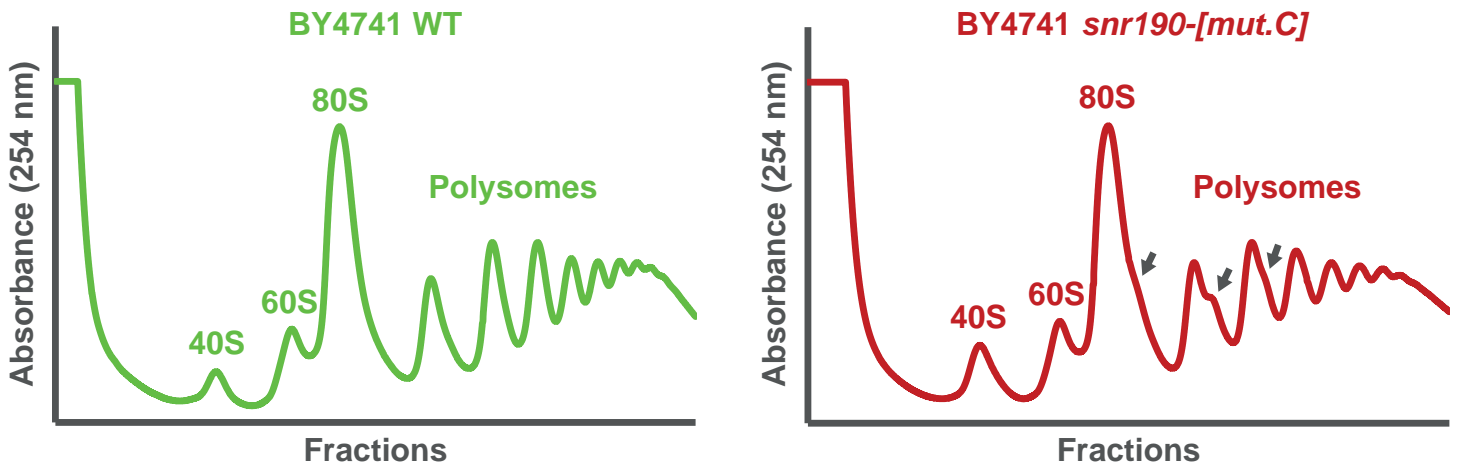
## Supplementary Fig. 2 Secondary structure of snR190 snoRNA

**a** Wild-type snR190 with the regions of interest to this study highlighted in colors: C/D and C'/D' motifs in blue, antisense boxes A and B in green. The 25S rRNA sequences complementary to antisense boxes A and B of snR190 are colored in pink (these sequences are also highlighted in pink on the 2D structure of the 25S rRNA presented in Supplementary Fig. 1). **b** Secondary structure of snR190 with mutations (in red) introduced by CRISPR-Cas9 in box C and terminal stem to abrogate expression of the snoRNA (*snr190-[mut.C]*) as well as the mutations introduced independently to disrupt the internal base-pairing involving part of the antisense box A (*snr190-[mut.S]*). **c** Secondary structure of snR190 with mutations (in pink) introduced in box A (*snr190-[mut.A]*), box B (*snr190-[mut.B]*) or both (*snr190-[mut.AB]*) to disrupt their base-pairing with 25S rRNA sequences.



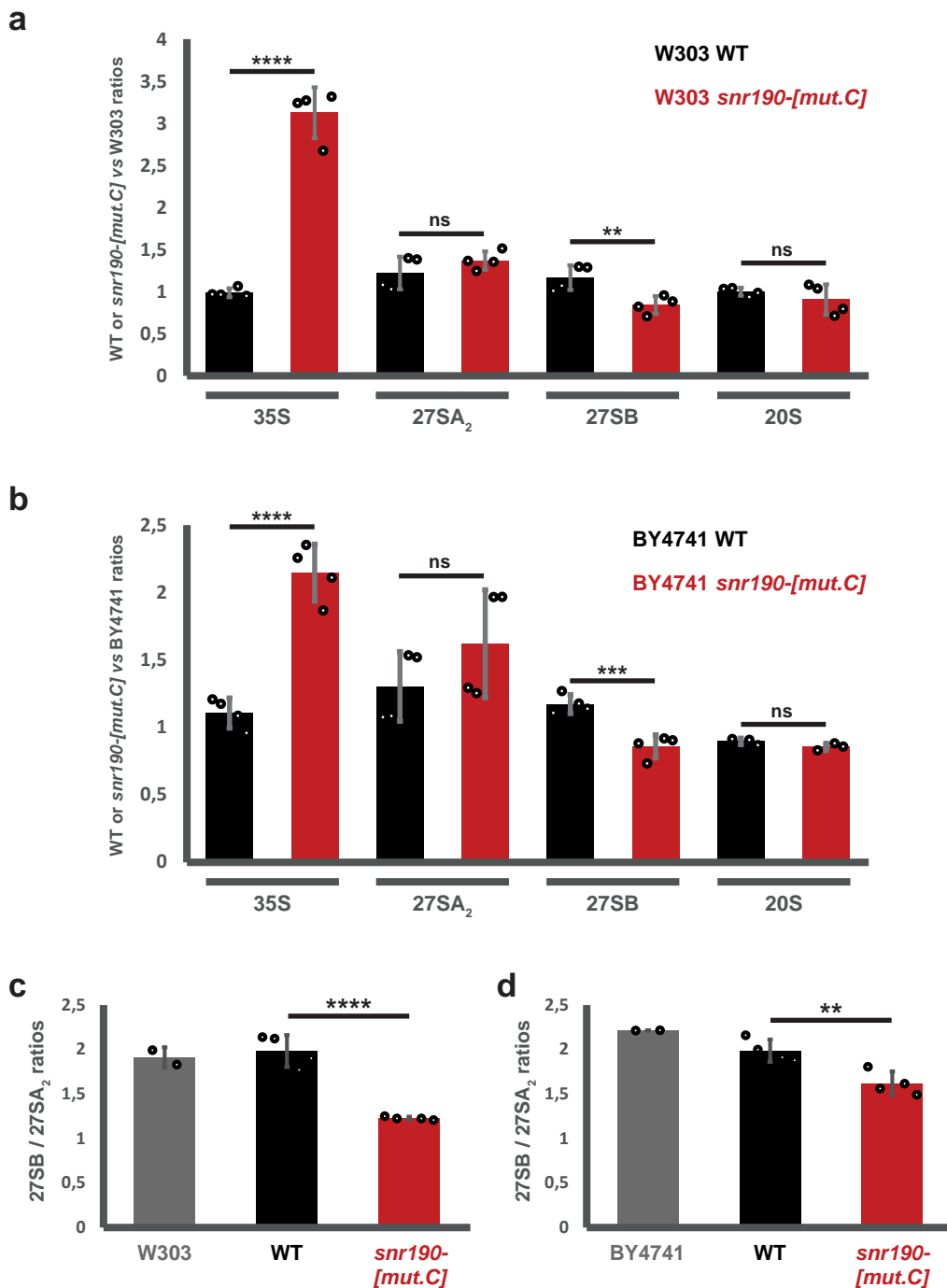
**Supplementary Fig. 3 Expression levels of HA-Dbp7 in the control and Sup. #10 strains**

**a, b** The EMY65 strain transformed with either the control pNOY373 plasmid or the suppressor Sup. #10 plasmid were grown in SGal (GAL) or SD (GLU) liquid media. Cell extracts were prepared and assayed by western blotting. Equal amount of total protein (40  $\mu$ g) were loaded in each lane. HA-Dbp7 and Pgk1 were revealed using anti-HA and anti-Pgk1 antibodies, respectively. Two biological replicates are presented (**a, b**).

**a****b**

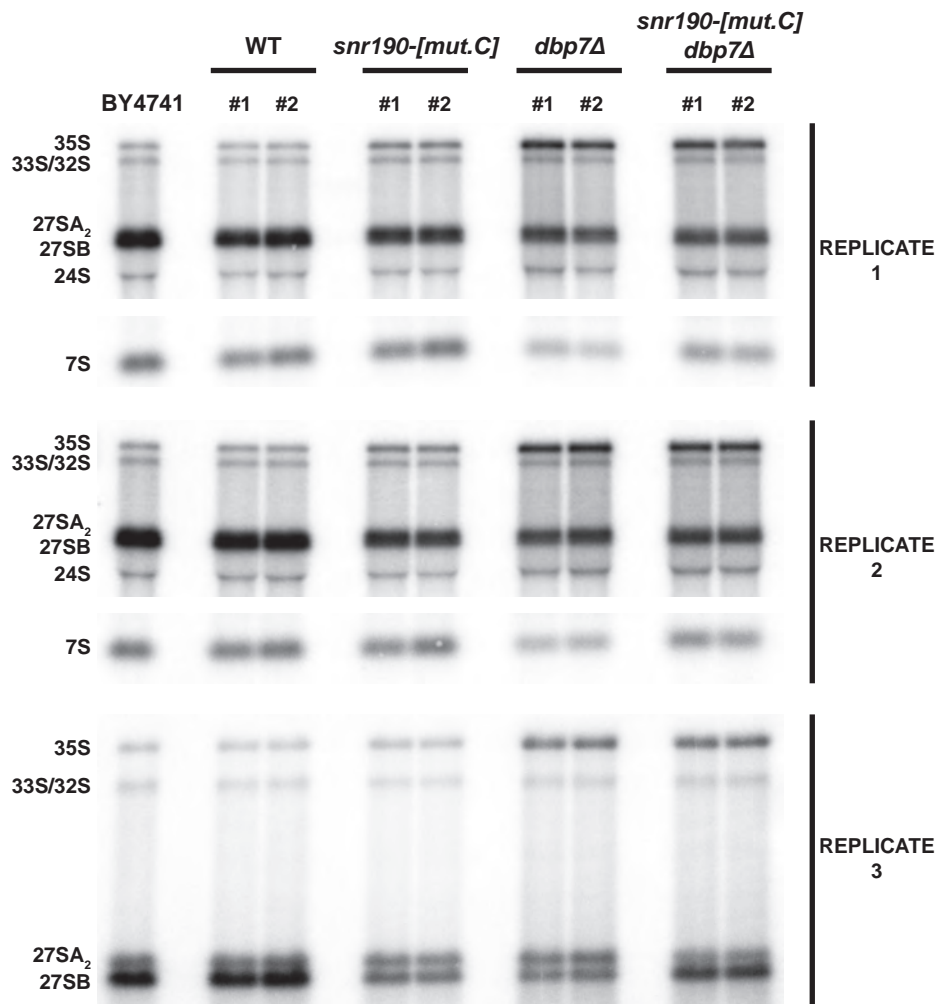
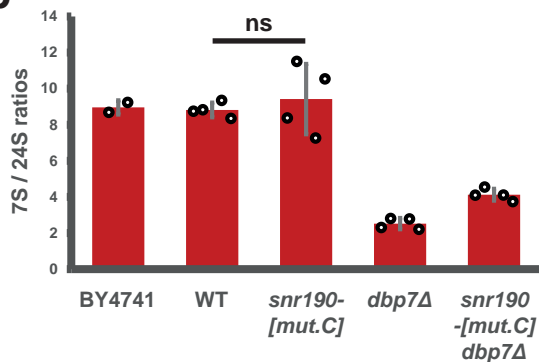
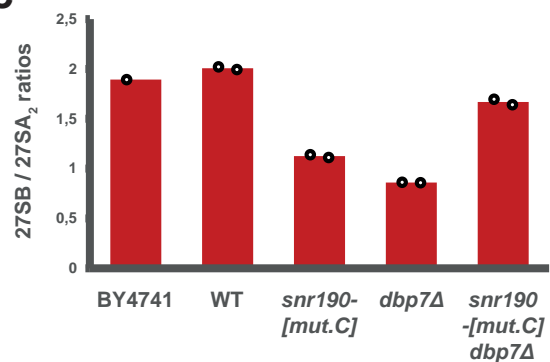
#### Supplementary Fig. 4 snR190 is required for optimal maturation of pre-60S r-particles

**a** Accumulation levels of rRNA precursors in isogenic wild-type and *snr190*-[mut.C] strains in the BY4741 background. Total RNA extracted from two independent clones (#1 and #2) for each strain was analyzed by northern blotting. The different RNA molecules, indicated on the left of each panel, were detected using specific radiolabeled probes (Supplementary Table 4). **b** Polysome profiles of BY4741 wild-type (green) and *snr190*-[mut.C] (red) strains. Total cellular extracts prepared from these strains were centrifuged through 10% to 50% sucrose gradients.  $A_{254}$  was measured during gradient fractionation. The identity of the different peaks is indicated above and half-mers are marked with arrows.



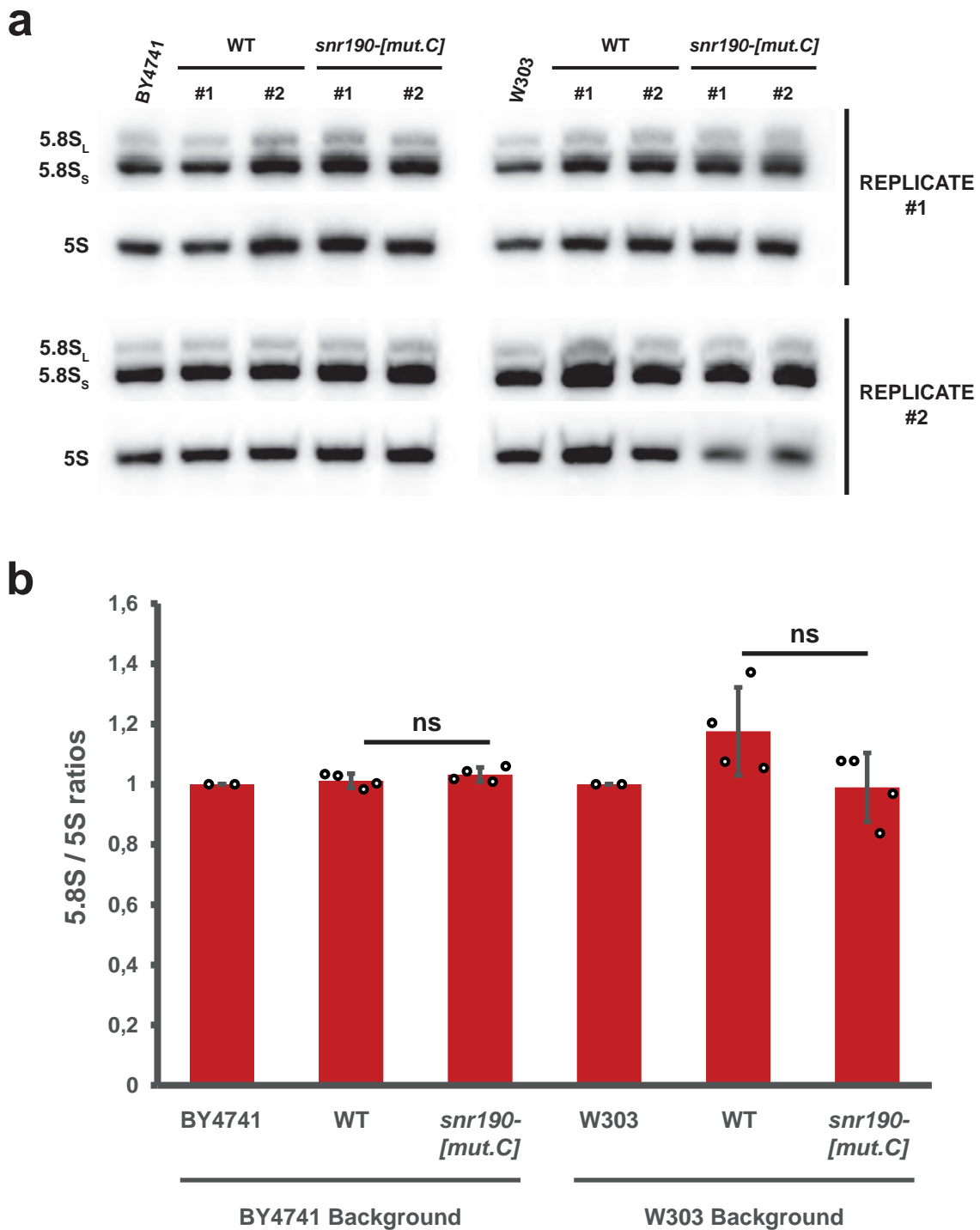
### Supplementary Fig. 5 Quantification of the pre-rRNA processing defects in the absence of snR190

**a** Quantification of rRNA precursor levels in the wild-type (WT) or *snr190-[mut.C]* strains in the W303 background. Radioactive signals presented in Fig. 2a were quantified from PhosphorImager images using MultiGauge software. The histogram represents the ratios of the indicated precursor levels in the wild-type (WT, black) or *snr190-[mut.C]* (red) strains with respect to the levels of the same precursors in the isogenic W303 strain. Data correspond to two biological replicates analyzed as two technical replicates. Histograms represent the mean values  $\pm$  standard deviation. The individual data points are shown. Statistically significant differences determined using one-tailed Student's t-test are indicated by asterisks (35S: \*\*\*\*=  $p < 0.0001$  (0.00001); 27SA<sub>2</sub>: ns= not significant; 27SB: \*\*=  $p < 0.01$  (0.005827); 20S: ns= not significant). **b** Quantification of rRNA precursor levels in the wild-type (WT) or *snr190-[mut.C]* strains in the BY4741 background. The signals presented in Supplementary Fig. 4a were quantified from PhosphorImager images using MultiGauge software. The histogram represents the ratios of the indicated precursor levels in the wild-type (WT, black) or *snr190-[mut.C]* (red) strains with respect to the levels of the same precursors in the isogenic BY4741 strain. Data correspond to two biological replicates analyzed as two technical replicates. Histograms represent the mean values  $\pm$  standard deviation. The individual data points are shown. Statistically significant differences determined using one-tailed Student's t-test are indicated by asterisks (35S: \*\*\*\*=  $p < 0.0001$  (0.000063); 27SA<sub>2</sub>: ns= not significant; 27SB: \*\*\*=  $p < 0.001$  (0.000656); 20S: ns= not significant). **c** Quantification of the 27SB/27SA<sub>2</sub> ratios in the W303 (grey), WT (black) and *snr190-[mut.C]* (red) strains, from the precursor levels measured in (a), corresponding to the northern blot presented in Fig. 2a. Data correspond to one (W303) or two biological replicates (WT, *snr190-[mut.C]*) analyzed as two technical replicates. Histograms represent the mean values  $\pm$  standard deviation. The individual data points are shown. Statistically significant differences determined using one-tailed Student's t-test are indicated by asterisks (\*\*\*\*=  $p < 0.0001$  (0.000078)). **d** Quantification of the 27SB/27SA<sub>2</sub> ratios in the BY4741 (grey), WT (black) and *snr190-[mut.C]* (red) strains, from the precursor levels measured in (b), corresponding to the northern blot presented in Supplementary Fig. 4a. Data correspond to two biological replicates analyzed as two technical replicates. Histograms represent the mean values  $\pm$  standard deviation. The individual data points are shown. Statistically significant differences determined using one-tailed Student's t-test are indicated by asterisks (\*\*=  $p < 0.01$  (0.003581)).

**a****b****c**

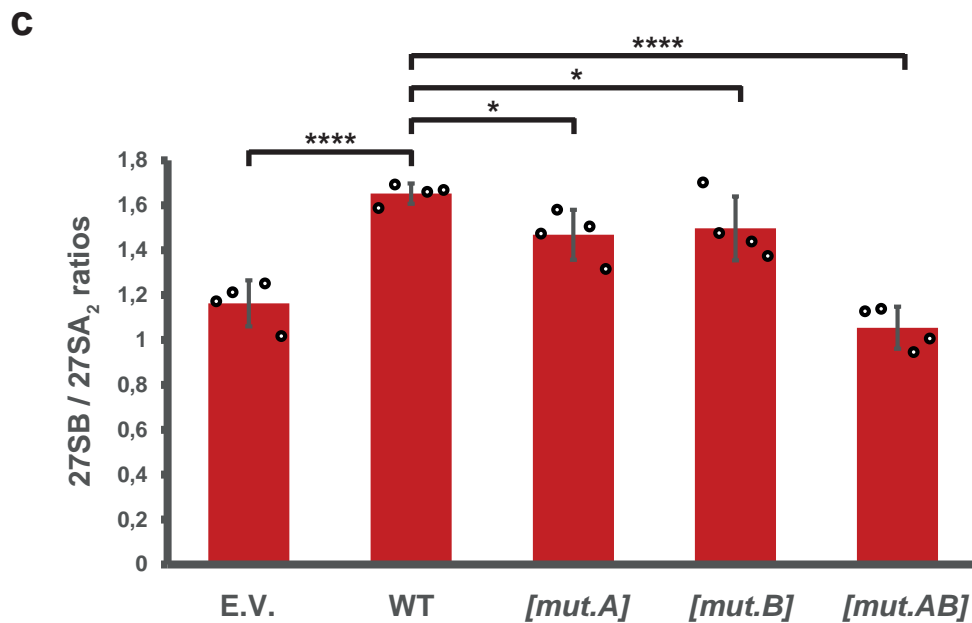
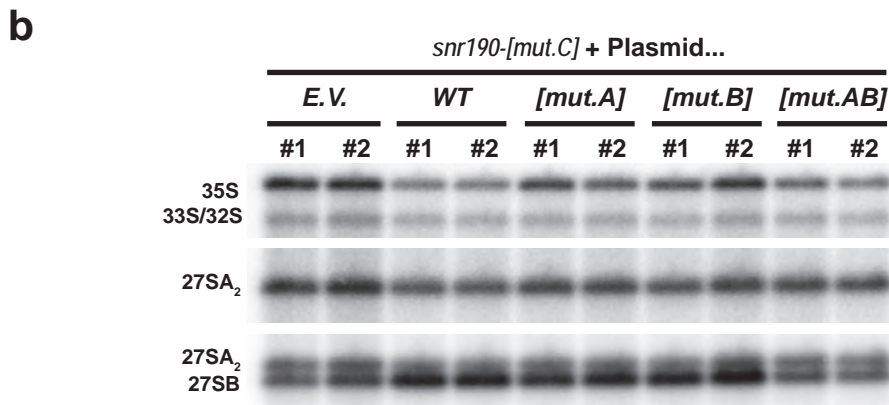
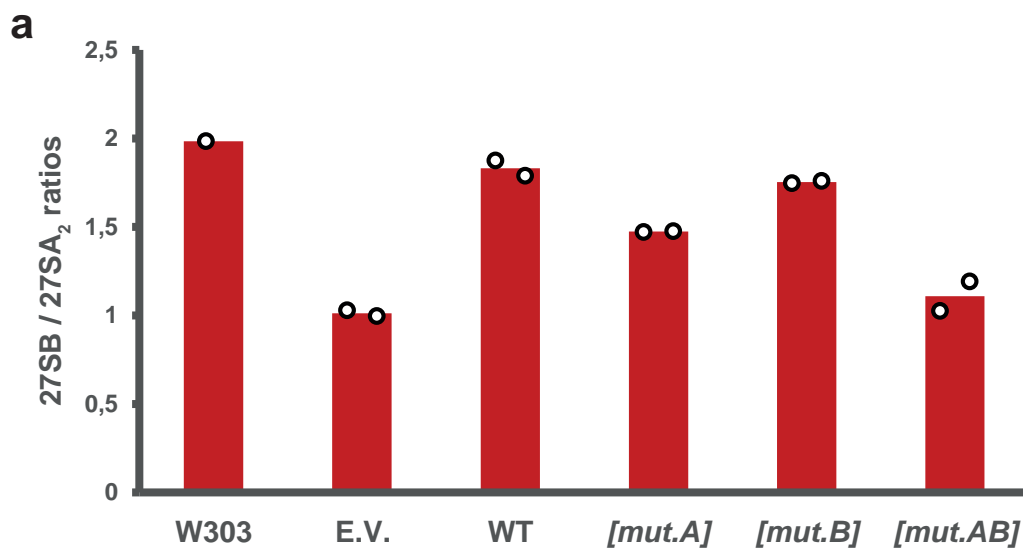
### Supplementary Fig. 6 Comparative analysis of pre-rRNA processing in wild-type and mutant strains

**a** Accumulation levels of rRNA precursors in isogenic wild-type (WT), *snr190-[mut.C]*, *dbp7Δ*, and *snr190-[mut.C] dbp7Δ* strains in the BY4741 background. Total RNA extracted from two independent clones (#1 and #2) for each strain was analyzed by northern blotting. The different RNA molecules, indicated on the left of each panel, were detected using specific radiolabeled probes (Supplementary Table 4). Three technical replicates are shown. Replicates 1 and 2 differ from replicate 3 in term of electrophoresis time. Electrophoresis time was short in replicates 1 and 2 to allow detection of the 7S precursor to the 5.8S rRNA. Electrophoresis time was longer in replicate 3 to separate the 27SA<sub>2</sub> and 27SB intermediates to allow accurate quantifications. **b** Quantification of the 7S/24S ratios for the indicated strains from replicates 1 and 2 in (a). The 24S pre-rRNA<sup>2</sup> was chosen as an invariant species for unbiased quantification. Data correspond to one (BY4741) or two (all the other strains) biological replicates analyzed as two technical replicates (replicates 1 and 2 in a). Histograms represent the mean values +/- standard deviation. The individual data points are shown. Statistically significant differences determined using one-tailed Student's t-test (ns= not significant). **c** Quantification of the 27SB/27SA<sub>2</sub> ratios for the indicated strains from replicate 3 in (a). The individual data points are shown.



**Supplementary Fig. 7 Loss-of-function of snR190 does not affect mature 5.8S levels**

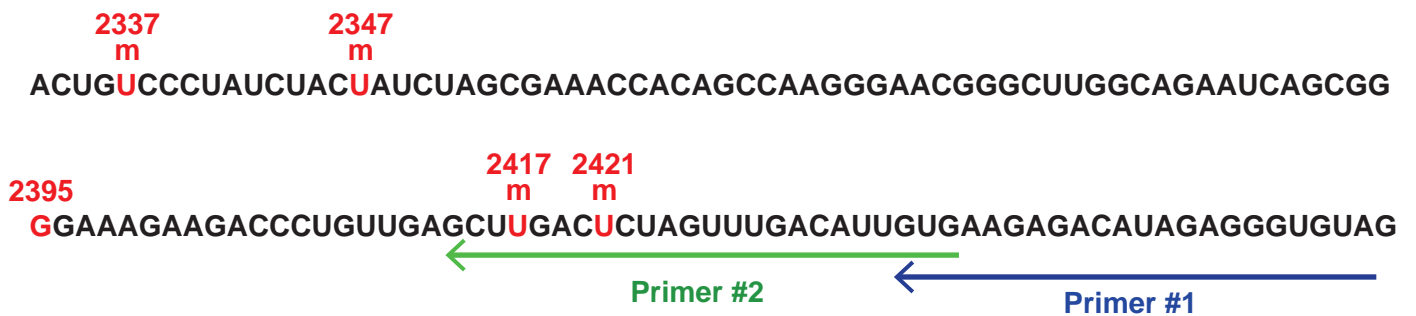
**a** Accumulation levels of 5.8S and 5S rRNAs in isogenic wild-type (WT) and *snr190-[mut.C]* in the BY4741 and W303 backgrounds. Total RNA extracted from two independent clones (#1 and #2) for each strain was analyzed by northern blotting. The 5.8S and 5S rRNAs were detected using specific radiolabeled probes (Supplementary Table 4). Two technical replicates are shown. **b** Quantification of the 5.8S/5S ratios for the indicated strains. Data correspond to one (BY4741 and W303) or two (WT and *snr190-[mut.C]*) biological replicates analyzed as two technical replicates (replicates 1 and 2 in **a**). Histograms represent the mean values +/- standard deviation. The individual data points are shown. Statistically significant differences determined using one-tailed Student's t-test are indicated (ns= not significant).



### Supplementary Fig. 8 Antisense boxes A and B of snR190 are required for its function in LSU synthesis

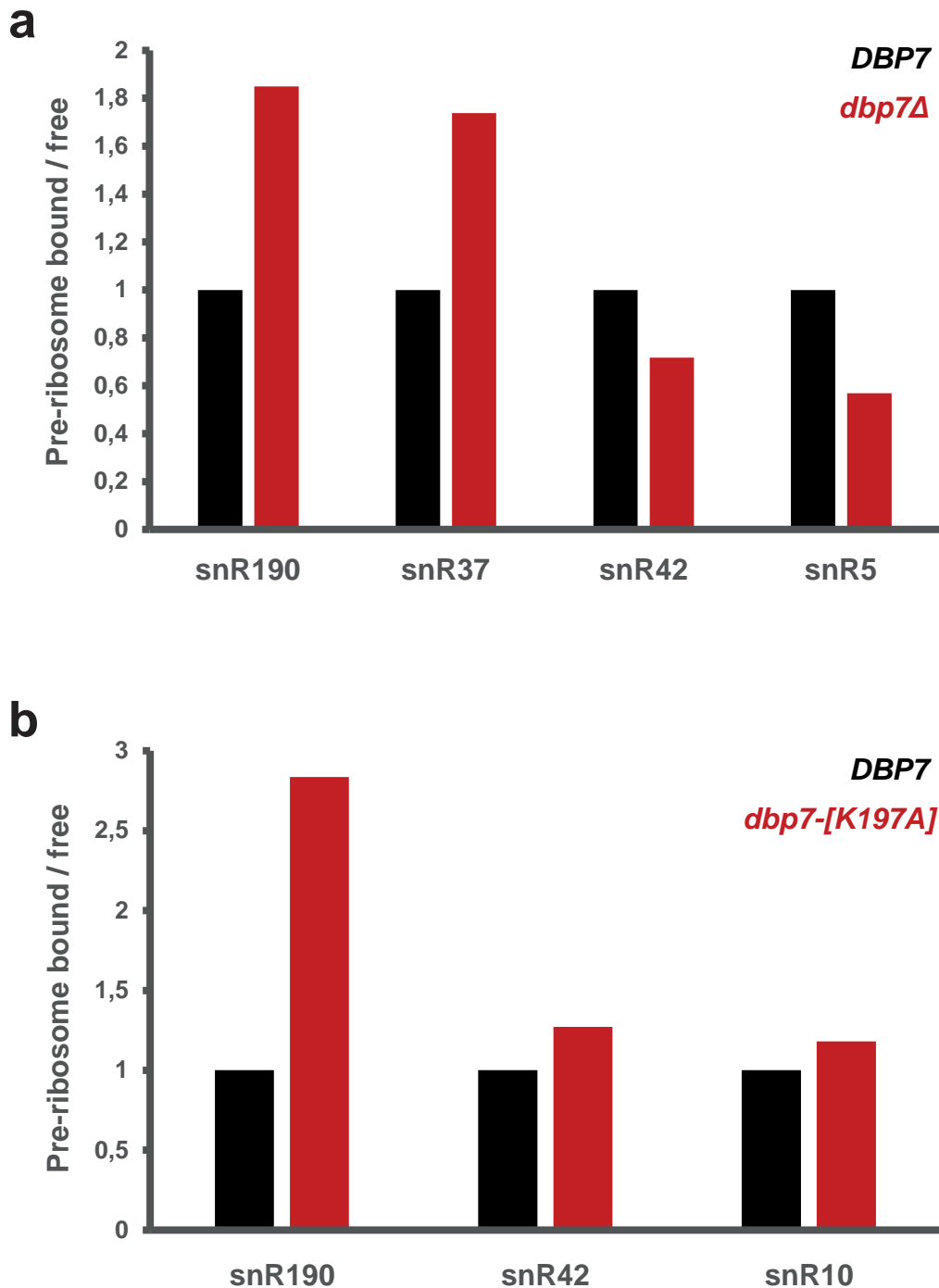
**a** Quantification of the northern blot signals obtained in Fig. 4b using PhosphorImager data and Multi-Gauge software. The histogram represents the mean ratios of the 27SA<sub>2</sub> over 27SB signals for the indicated strains. Individual data points are shown. **b** Accumulation levels of rRNA precursors in the wild-type BY4741 strain or in the *snr190-[mut.C]* strain transformed with plasmids supporting expression of wild-type snR190 (WT) or bearing mutations in its antisense elements box A (*snr190-[mut.A]*), box B (*snr190-[mut.B]*) or both (*snr190-[mut.AB]*), or with the empty vector as control (E.V.). Experiments were performed as explained in the legend of Fig. 2b. **c** Quantification of the 27SB/27SA<sub>2</sub> ratios for the indicated strains from the precursor levels measured in (b). Data correspond to two biological replicates analyzed as two technical replicates. Histograms represent the mean values +/- standard deviation. The individual data points are shown. Statistically significant differences determined using one-tailed Student's t-test are indicated by asterisks (E.V. vs WT: \*\*\*\*= p<0.0001 (0.000063); WT vs [mut.A]: \*= p<0.05 (0.011137); WT vs [mut.B]: \*= p<0.05 (0.04189); WT vs [mut.AB]: \*\*\*\*= p<0.0001 (0.000013)).

### 25S rRNA sequence (2333-2457)



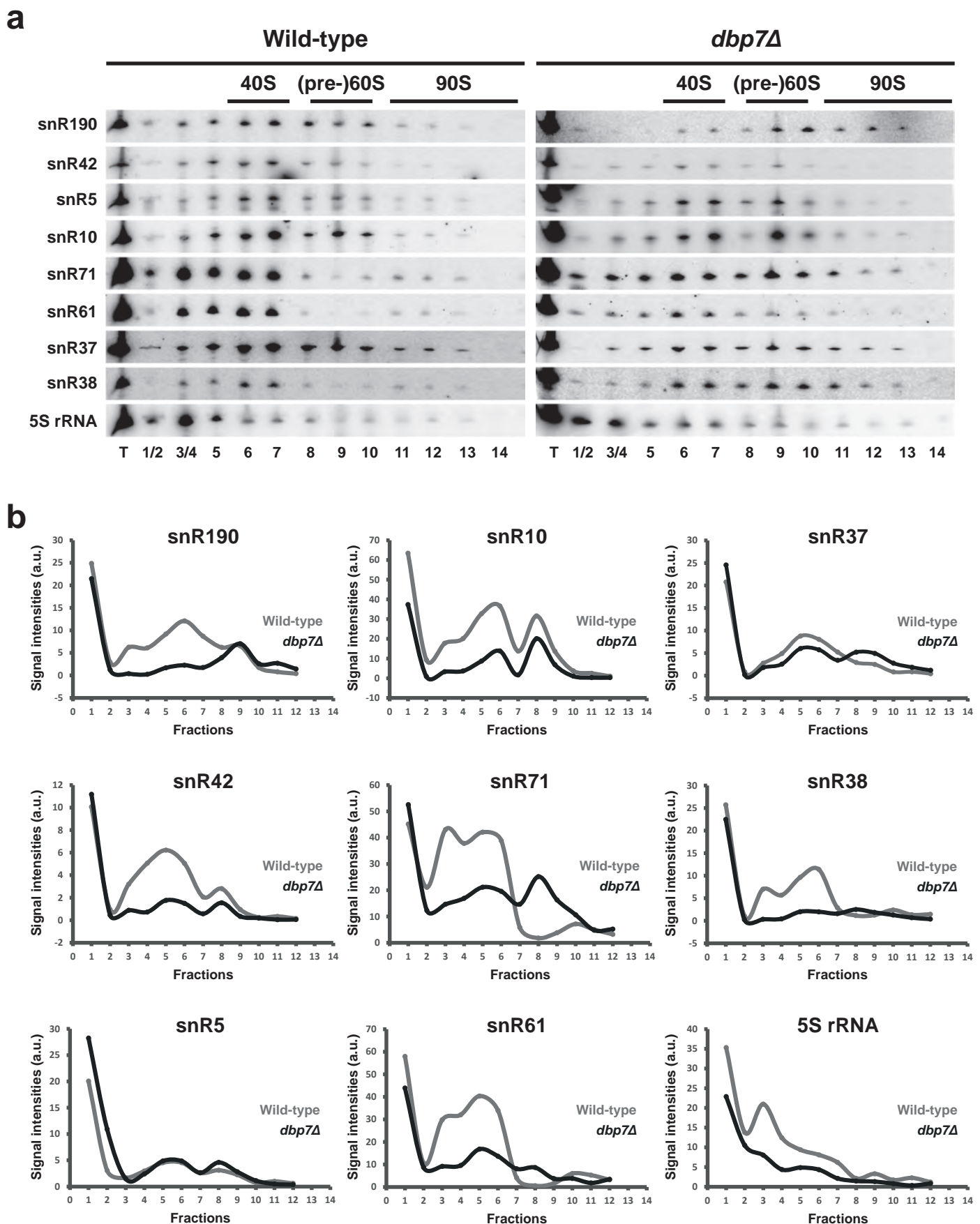
#### Supplementary Fig. 9 Position of primers used to map 25S rRNA G2395 putative methylation

Sequence of the 25S rRNA surrounding guanosine G2395 predicted to be methylated by snR190. The neighboring methylated nucleosides, experimentally identified in Fig. 3 are indicated in red. Position of the two primers (Primer #1, distal, blue; Primer #2, proximal, green) used in reverse transcription experiments in Fig. 3 are also indicated.



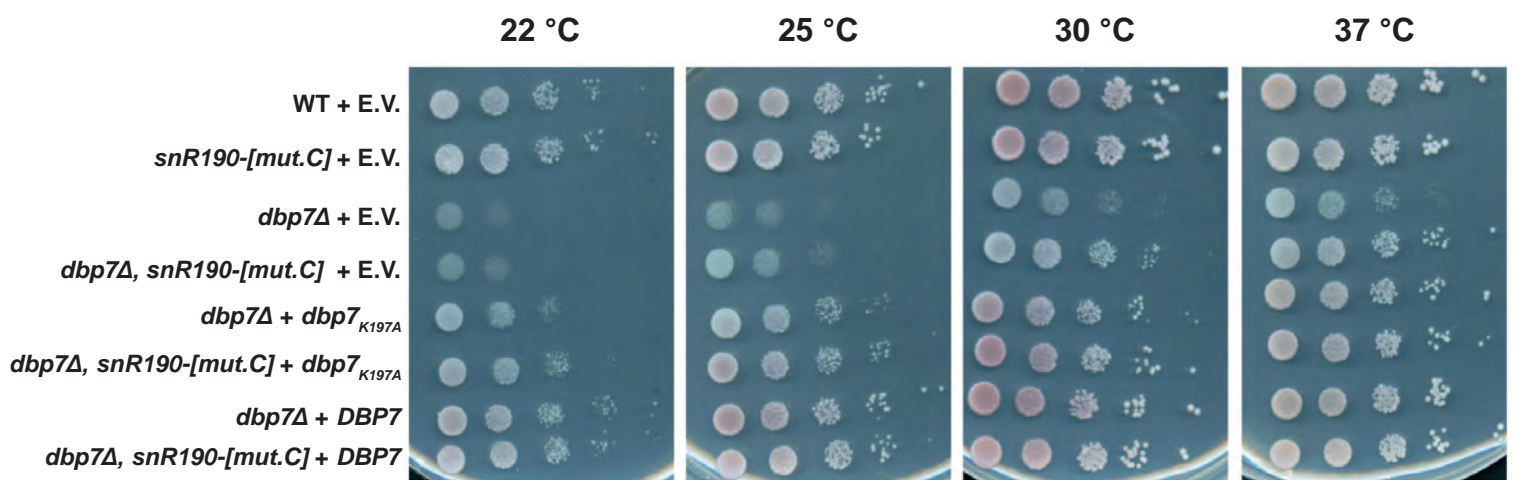
**Supplementary Fig. 10 The ATPase activity of Dbp7 is required for snR190 release from pre-ribosomal particles**

**a** Quantification of the sedimentation profiles of different snoRNAs in wild-type or *dbp7Δ* strains (Fig. 5c). For each snoRNA, the radioactive signals detected in the free fractions (1-5) of the gradients or in the fractions containing pre-ribosomes (7-18) were quantified using PhosphorImager data and MultiGauge software. The histogram represents pre-ribosome-bound versus free signal ratios for the indicated snoRNA in the wild-type (*DBP7*, black) or *dbp7Δ* (red) strains. **b** Quantification of the sedimentation profiles of different snoRNAs in cells expressing *Dbp7<sub>WT</sub>* or *Dbp7<sub>K197A</sub>* (Fig. 6c). For each snoRNA, the radioactive signals detected in the free fractions (1-3) of the gradients or in the fractions containing pre-ribosomes (7-13) were quantified using PhosphorImager data and MultiGauge software. The histogram represents pre-ribosome-bound versus free signal ratios for the indicated snoRNAs in cells expressing *Dbp7<sub>WT</sub>* (*DBP7*, black) or *Dbp7<sub>K197A</sub>* (red).



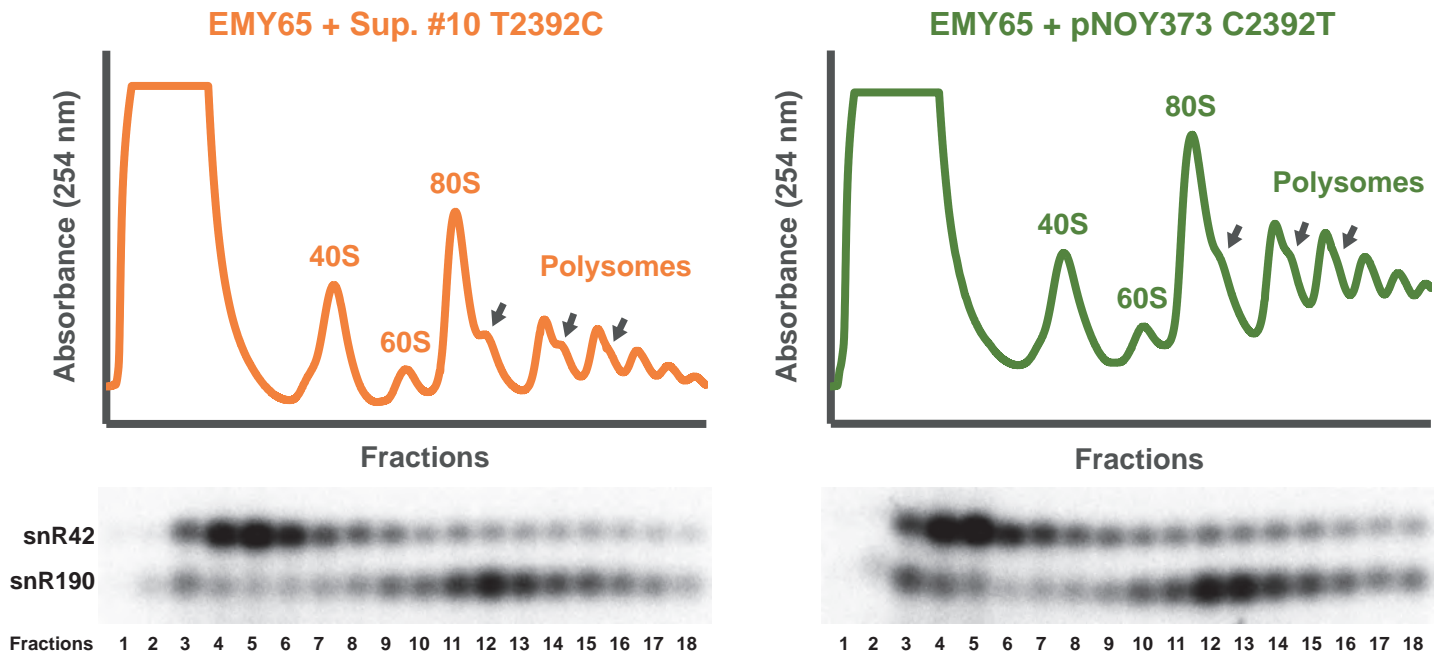
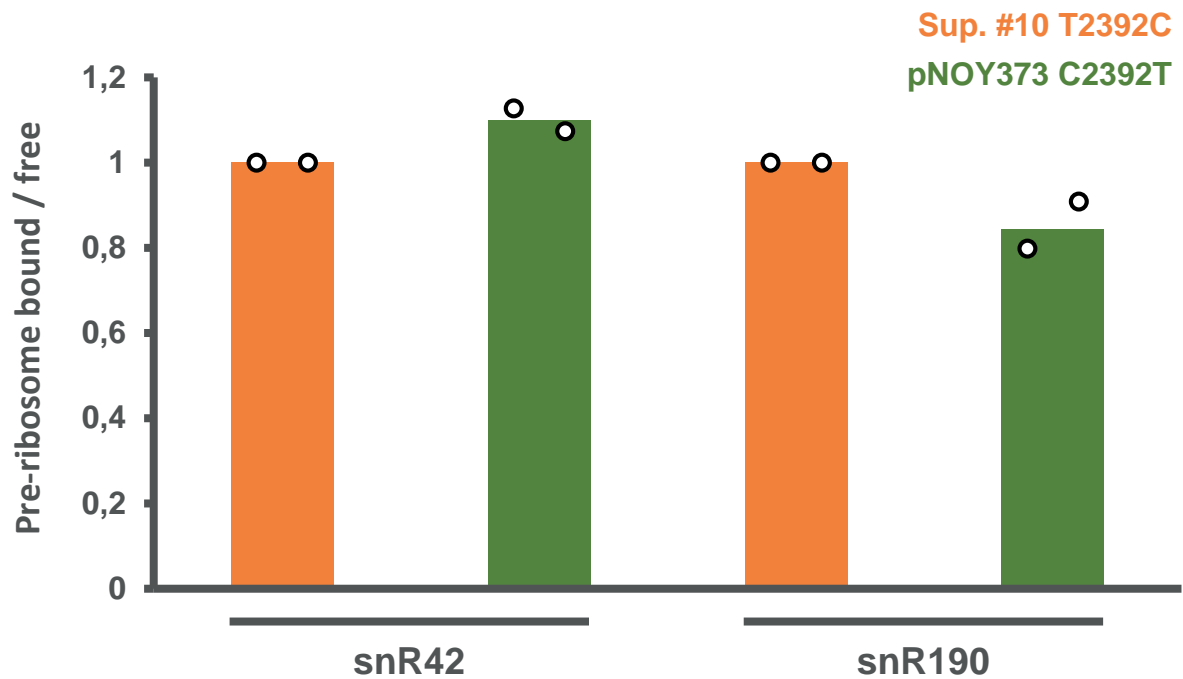
**Supplementary Fig. 11 Dbp7 is required for snR190 release from pre-ribosomal particles**

**a** Sedimentation profile of snoRNAs in wild-type or *dbp7Δ* strains. Total cellular extracts were centrifuged through 7 % to 50 % low-Mg<sup>2+</sup> sucrose gradients. Absorbance profiles at A<sub>254</sub> were measured during gradient fractionation. The approximate positions of the peaks corresponding to the 40S, (pre)-60S and 90S particles are indicated on the basis of previous experiments<sup>3,4</sup>. RNAs extracted from the first 14 fractions were analyzed by northern blotting to detect the indicated snoRNAs. **b** Quantification of the snoRNA sedimentation profiles observed in (a). For each snoRNA, the radioactive signals detected in each fraction was plotted against fraction numbers.



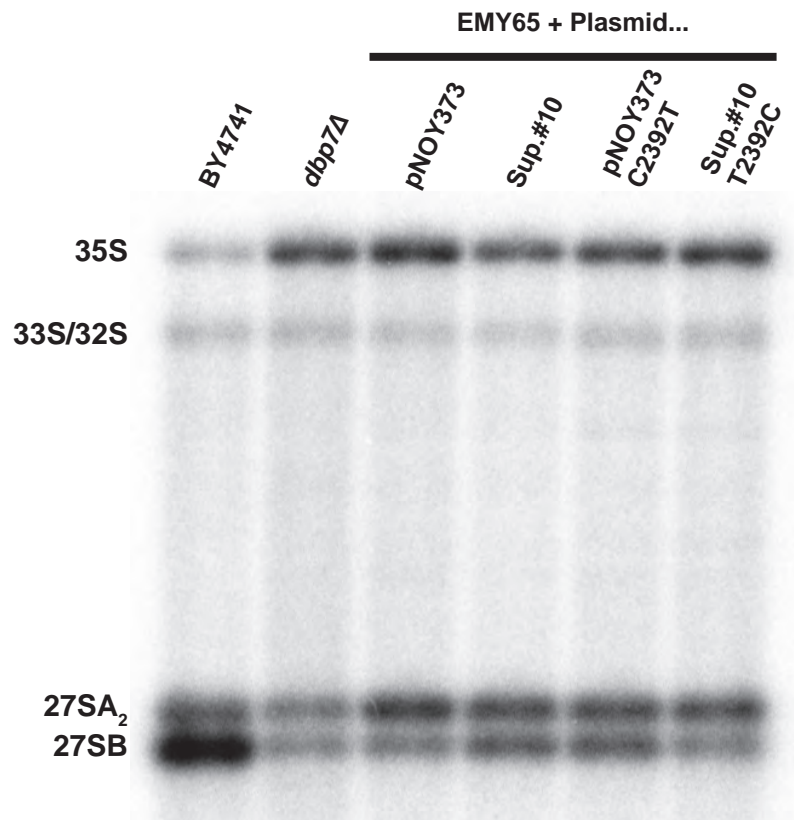
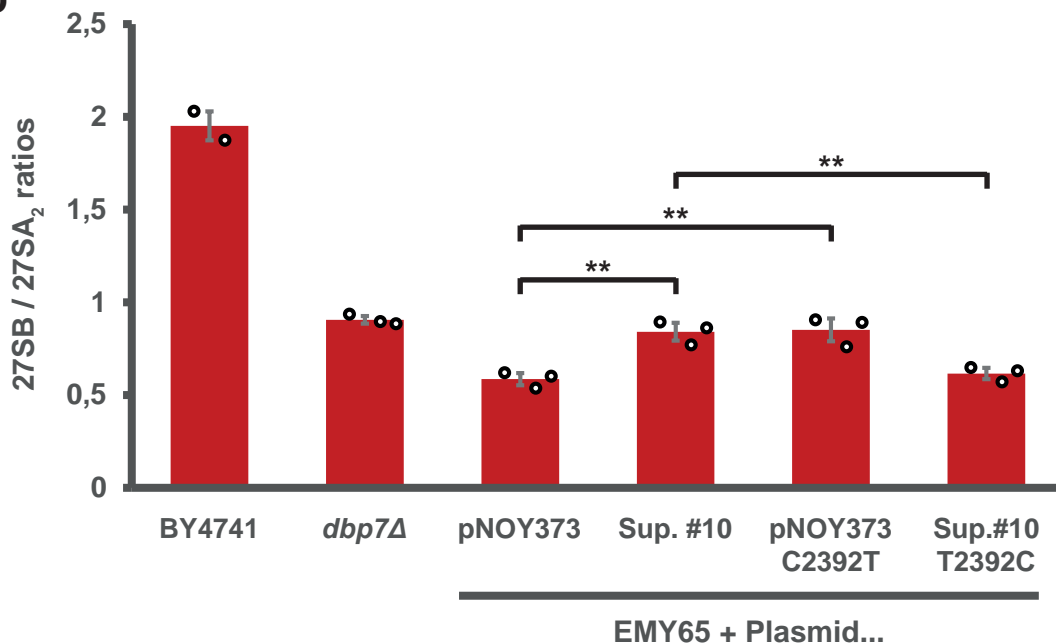
**Supplementary Fig. 12 Loss-of-function of snR190 alleviates the growth defect of cells expressing *Dbp7*<sub>K197A</sub>**

The wild-type W303 strain (WT) and the *snR190-[mut.C]*, *dbp7Δ* and *dbp7Δ snR190-[mut.C]* mutant strains were transformed with plasmids expressing *Dbp7*<sub>WT</sub> or *Dbp7*<sub>K197A</sub>, or the empty vector (E.V.) as control, as indicated on the figure. Serial dilutions of the transformants were spotted on SD medium and plates were incubated for 3 days at the indicated temperatures.

**a****b**

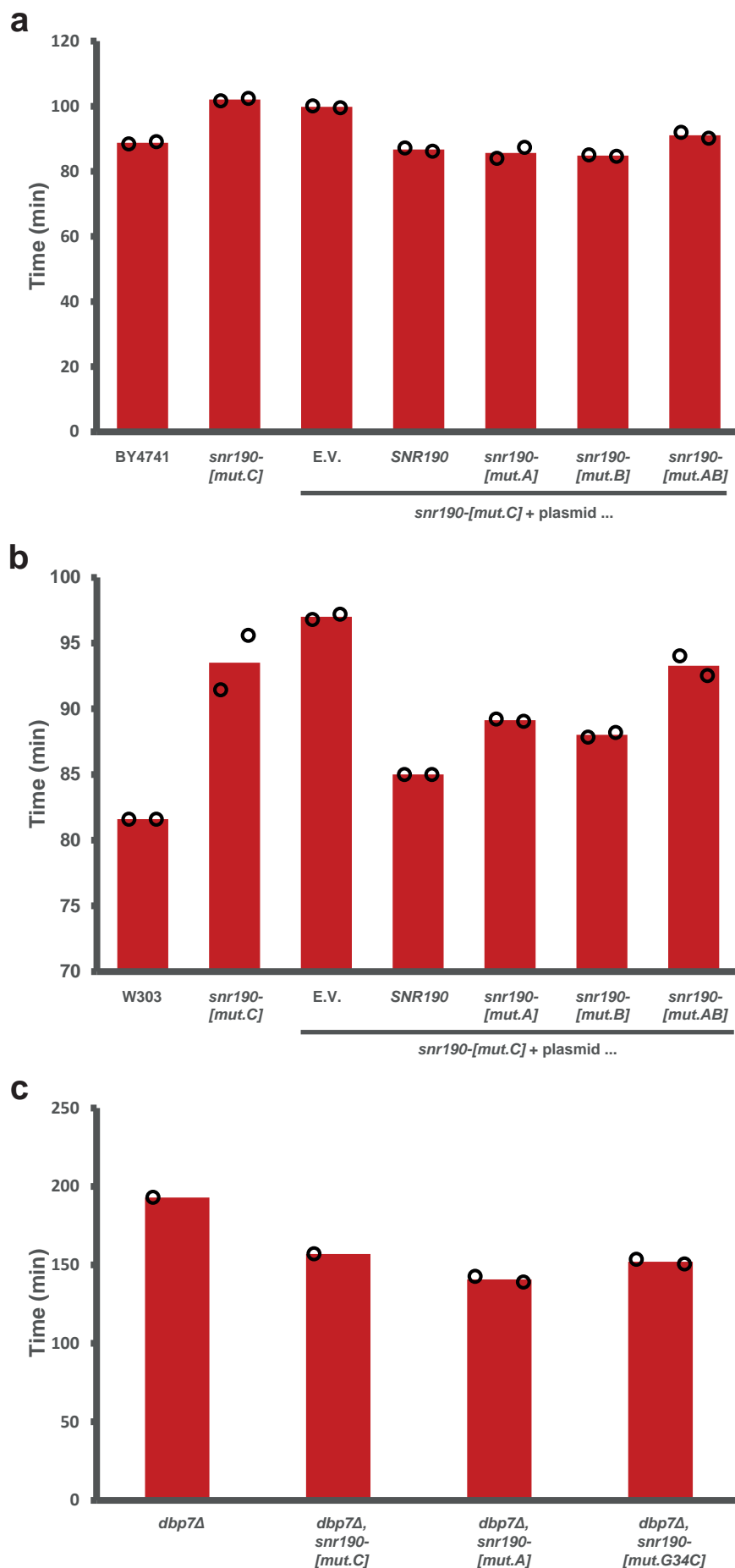
### Supplementary Fig. 13 25S rRNA mutation C2392U partially alleviates retention of snR190 in pre-ribosomal particles

**a** Strain EMY65 was transformed with either the Sup. #10 plasmid in which the suppressor mutation (T2392) has been reverted to the wild-type cytosine (T2392C, orange) or with the pNOY373 plasmid in which the suppressor C2392T mutation has been specifically introduced (C2392T, green). Strains were grown in SD medium and total cellular extracts prepared from these strains were centrifuged through 10% to 50% sucrose gradients.  $A_{254}$  was measured during gradient fractionation. The identity of the different peaks is indicated above and half-mers are marked with arrows. RNAs extracted from the first 18 fractions were analyzed by Northern blotting to detect snR190 and snR42 snoRNAs. **b** Quantification of the sedimentation profiles of snR190 and snR42 snoRNAs in the strains described in (a). For each snoRNA, the radioactive signals detected in the free fractions (1-5) of the gradients or in the fractions containing pre-ribosomes (7-18) were quantified using PhosphorImager data and MultiGauge software. The histogram represents the mean pre-ribosome-bound versus free signal ratios for the indicated snoRNAs in strain EMY65 containing plasmid Sup. #10 T2392C (orange) or pNOY373 C2392T (green). The individual data points are shown.

**a****b**

### Supplementary Fig. 14 Impact of 25S rRNA mutation C2392U on pre-rRNA processing

**a** Accumulation levels of rRNA precursors in isogenic wild-type (WT) and *dbp7*  $\Delta$  strains in the BY4741 background, as well as in EMY65 strain transformed with the indicated plasmids and grown on SD medium. Total RNA extracted from these strains was analyzed by northern blotting. The different RNA molecules, indicated on the left of each panel, were detected using specific radio-labeled probes (Supplementary Table 4). **b** Quantification of the 27SB/27SA<sub>2</sub> ratios for the indicated strain using PhosphorImager data (**a**) and MultiGauge software. Data correspond to two (BY4741) or three (all the other strains) technical replicates. Histograms represent the mean values +/- standard deviation. The individual data points are shown. Statistically significant differences determined using one-tailed Student's t-test are indicated by asterisks (pNOY373 vs Sup. #10: \*\*=  $p < 0.01$  (0.002335); pNOY373 vs pNOY373 C2392T: \*\*=  $p < 0.01$  (0.003574); Sup. #10 vs Sup. #10 T2392C: \*\*=  $p < 0.01$  (0.003384)).



**Supplementary Fig. 15 Doubling time of yeast strain analyzed in this study displayed as bar charts**

**a, b, c** The indicated strains were grown under exponential conditions in YPD medium supplemented or not with G418 depending on the presence of pCH32 plasmid derivatives (G418 resistance marker). Turbidity at 600 nm was measured every two hours and the values were plotted over time in Excel (2016) with a logarithmic scale on the y axis. Doubling times were calculated according to the slopes of the curves. Histograms represent the mean values calculated out of two independent experiments for all strains except the *dbp7Δ*, and *dbp7Δ snr190-[mut.C]* strains (one replicate). See Supplementary Table 2 for a summary.

Suppressor #2 mutations		
Position	Domain	Mutation
912	II (ES10)	Transition (G→A)
1078-1079	II (ES12)	Insertion (A)
1101-1102	II (ES12)	Insertion (A)
1112-1113	II (ES12)	Insertion (GA)
1907-1908	V (H62)	Insertion (A)
2367	V (H72)	Deletion (A→Δ)
<b>2392</b>	<b>V (H73)</b>	<b>Transition (C→U)</b>

Suppressor #10 mutations		
Position	Domain	Mutation
444	I (H25)	Transition (U→C)
985	I (H24)	Transition (U→C)
<b>2392</b>	<b>V (H73)</b>	<b>Transition (C→U)</b>

### Supplementary Table 1 Mutations identified in the suppressor clones

The rDNA inserts of the plasmids recovered from two independent suppressor clones selected in the genetic screen (Sup. #2 and Sup. #10) were sequenced. The mutations identified in each case are detailed in the table: type of mutation, nucleotide position in the 25S rRNA sequence and corresponding structural domain. A C-to-U transition at position C2392 in helix H73 of the 25S rRNA (red on yellow background) has been identified in the two independent clones.

Strain	Doubling time (Minutes)
BY4741 (wild-type)	89 ± 0.3
BY4741 <i>snr190-[mut.C]</i>	102 ± 0.3
W303 (wild-type)	82
W303 <i>snr190-[mut.C]</i>	93 ± 2
<b>BY4741 <i>snr190-[mut.C]</i> + ...</b>	102 ± 0.3
<i>E.V.</i>	100.8
<i>SNR190-U14</i> (wild-type)	87 ± 0.3
<i>snr190-[mut.A]</i>	86 ± 1
<i>snr190-[mut.B]</i>	85 ± 0.3
<i>snr190-[mut.AB]</i>	92 ± 0.3
<b>W303 <i>snr190-[mut.C]</i> + ...</b>	93 ± 2
<i>E.V.</i>	97
<i>SNR190-U14</i> (wild-type)	85
<i>snr190-[mut.A]</i>	89.1
<i>snr190-[mut.B]</i>	88
<i>snr190-[mut.AB]</i>	93.3 ± 1
<b><i>dbp7Δ</i></b>	193
<b><i>dbp7Δ , snr190-[mut.C]</i></b>	157
<b><i>dbp7Δ , snr190-[mut.A]</i></b>	141 ± 2
<b><i>dbp7Δ , snr190-[mut.G34C]</i></b>	152 ± 2

**Supplementary Table 2 Doubling time of yeast strain analyzed in this study**

The indicated strains were grown under exponential conditions in YPD medium supplemented or not with G418 depending on the presence of pCH32 plasmid derivatives (G418 resistance marker). Turbidity at 600 nm was measured every two hours and the values were plotted over time in Excel with a logarithmic scale on the y axis. Doubling times were calculated according to the slopes of the curves.

STRAIN	BACKGROUND	PLASMID	GENOTYPE
BY4741	∅	∅	<i>MATa; his3Δ1; leu2Δ0; met15Δ0; ura3Δ0</i>
W303	∅	∅	<i>MATa; leu2-3,112; trp1-1; can1-100; ura3-1; ade2-1; his3-11,15; [phi<sup>+</sup>]</i>
<i>NOP7::HTP</i>	BY4741	∅	<i>MATa; his3Δ1; leu2Δ0; met15Δ0; ura3Δ0; NOP7::HTP (URA3)</i>
<i>NOP7::HTP, dbp7Δ</i>	BY4741	∅	<i>MATa; his3Δ1; leu2Δ0; met15Δ0; ura3Δ0; dbp7::Kan<sup>R</sup> MX6; NOP7::HTP (URA3)</i>
<i>NOC1::TAP</i>	BY4741	∅	<i>MATa; his3Δ1; leu2Δ0; met15Δ0; ura3Δ0; NOC1::TAP (HIS3)</i>
<i>NOC1::TAP, snr190-[mut.C]</i>	BY4741	∅	<i>MATa; his3Δ1; leu2Δ0; met15Δ0; ura3Δ0; snr190-[mut.C] (CRISPR-Cas9); NOC1::TAP (HIS3)</i>
<i>NOC1::TAP, dbp7Δ</i>	BY4741	∅	<i>MATa; his3Δ1; leu2Δ0; met15Δ0; ura3Δ0; dbp7::Kan<sup>R</sup> MX6; NOC1::TAP (HIS3)</i>
NOY891	NOY505	pNOY353	<i>MATa; ade2-1; ura3-1; leu2-3; his3-11; trp1; can1-100; rdnΔΔ::HIS3; pNOY353 [PGAL7-35S rDNA, 5S rDNA (TRP1)]</i>
EMY65	NOY891	pNOY353	<i>MATa; ade2-1; ura3-1; leu2-3; his3-11; trp1; can1-100; rdnΔΔ::HIS3; GAL1::HA-DBP7 pNOY353 [PGAL7-35S rDNA, 5S rDNA (TRP1)]</i>
EMY65 + pNOY373	NOY891	pNOY353, pNOY373	<i>MATa; ade2-1; ura3-1; leu2-3; his3-11; trp1; can1-100; rdnΔΔ::HIS3; GAL1::HA-DBP7 pNOY353 [PGAL7-35S rDNA, 5S rDNA (TRP1)]; pNOY373 [35S rDNA, 5S rDNA (LEU2)]</i>
EMY65 + pNOY373 C2392T	NOY891	pNOY353, pNOY373 C2392T	<i>MATa; ade2-1; ura3-1; leu2-3; his3-11; trp1; can1-100; rdnΔΔ::HIS3; GAL1::HA-DBP7 pNOY353 [PGAL7-35S rDNA, 5S rDNA (TRP1)]; pNOY373 [35S rDNA, 5S rDNA (LEU2)]</i>
EMY65 + Sup. #2	NOY891	pNOY353, Sup. #2	<i>MATa; ade2-1; ura3-1; leu2-3; his3-11; trp1; can1-100; rdnΔΔ::HIS3; GAL1::HA-DBP7 pNOY353 [PGAL7-35S rDNA, 5S rDNA (TRP1)]; Sup. #2</i>
EMY65 + Sup. #2 T2392C	NOY891	pNOY353, Sup. #2 T2392C	<i>MATa; ade2-1; ura3-1; leu2-3; his3-11; trp1; can1-100; rdnΔΔ::HIS3; GAL1::HA-DBP7 pNOY353 [PGAL7-35S rDNA, 5S rDNA (TRP1)]; Sup. #2 T2392C</i>
EMY65 + Sup. #10	NOY891	pNOY353, Sup. #10	<i>MATa; ade2-1; ura3-1; leu2-3; his3-11; trp1; can1-100; rdnΔΔ::HIS3; GAL1::HA-DBP7 pNOY353 [PGAL7-35S rDNA, 5S rDNA (TRP1)]; Sup. #10</i>
EMY65 + Sup. #10 T2392C	NOY891	pNOY353, Sup. #10 T2392C	<i>MATa; ade2-1; ura3-1; leu2-3; his3-11; trp1; can1-100; rdnΔΔ::HIS3; GAL1::HA-DBP7 pNOY353 [PGAL7-35S rDNA, 5S rDNA (TRP1)]; Sup. #10 T2392C</i>
<i>dbp7Δ</i>	W303	∅	<i>MATa; ade2-1; ura3-1; leu2-3, 112; his3-11, 15; trp1-1; can1-100; dbp7::HIS3MX6</i>
<i>dbp7Δ + DBP7</i>	W303	YCplac22-DBP7	<i>MATa; ade2-1; ura3-1; leu2-3, 112; his3-11, 15; trp1-1; can1-100; dbp7::HIS3MX6;</i>
<i>dbp7Δ + dbp7<sub>K197A</sub></i>	W303	YCplac22- <i>dbp7</i> -[K197A]	<i>MATa; ade2-1; ura3-1; leu2-3, 112; his3-11, 15; trp1-1; can1-100; dbp7::HIS3MX6;</i>
<i>W303 + E.V.</i>	W303	YCplac22	<i>MATa; leu2-3,112; trp1-1; can1-100; ura3-1; ade2-1; his3-11,15; [phi<sup>+</sup>];</i>
<i>snr190-[mut.C] + E.V.</i>	W303	YCplac22	<i>MATa; ade2-1; ura3-1; leu2-3, 112; his3-11, 15; trp1-1; can1-100; snr190-[mut.C];</i>
<i>dbp7Δ + E.V.</i>	W303	YCplac22	<i>MATa; ade2-1; ura3-1; leu2-3, 112; his3-11, 15; trp1-1; can1-100; dbp7::HIS3MX6;</i>
<i>dbp7Δ snr190-[mut.C] + E.V.</i>	W303	YCplac22	<i>MATa; ade2-1; ura3-1; leu2-3, 112; his3-11, 15; trp1-1; can1-100; dbp7::HIS3MX6 snr190-[mut.C];</i>
<i>dbp7Δ snr190-[mut.C] + dbp7<sub>K197A</sub></i>	W303	YCplac22- <i>dbp7</i> -[K197A]	<i>MATa; ade2-1; ura3-1; leu2-3, 112; his3-11, 15; trp1-1; can1-100; dbp7::HIS3MX6 snr190-[mut.C];</i>
<i>dbp7Δ snr190-[mut.C] + DBP7</i>	W303	YCplac22-DBP7	<i>MATa; ade2-1; ura3-1; leu2-3, 112; his3-11, 15; trp1-1; can1-100; dbp7::HIS3MX6 snr190-[mut.C];</i>
<i>dbp7Δ, snr190-[mut.C]</i>	BY4741	∅	<i>MATa; his3Δ1; leu2Δ0; met15Δ0; ura3Δ0; dbp7::Kan<sup>R</sup> MX6; snr190-[mut.C] (CRISPR-Cas9)</i>
<i>dbp7Δ, snr190-[mut.A]</i>	BY4741	∅	<i>MATa; his3Δ1; leu2Δ0; met15Δ0; ura3Δ0; dbp7::Kan<sup>R</sup> MX6; snr190-[mut.A] (CRISPR-Cas9)</i>
<i>dbp7Δ, snr190-[mut.G34C]</i>	BY4741	∅	<i>MATa; his3Δ1; leu2Δ0; met15Δ0; ura3Δ0; dbp7::Kan<sup>R</sup> MX6; snr190-[mut.G34C] (CRISPR-Cas9)</i>
<i>snr190-[mut.C]</i>	BY4741	∅	<i>MATa; his3Δ1; leu2Δ0; met15Δ0; ura3Δ0; snr190-[mut.C] (CRISPR-Cas9)</i>
<i>snr190-[mut.C] + E.V.</i>	BY4741	pCH32	<i>MATa; his3Δ1; leu2Δ0; met15Δ0; ura3Δ0; snr190-[mut.C] (CRISPR-Cas9)</i>
<i>snr190-[mut.C] + SNR190</i>	BY4741	pCH32 + WT U14-SNR190insert	<i>MATa; his3Δ1; leu2Δ0; met15Δ0; ura3Δ0; snr190-[mut.C] (CRISPR-Cas9)</i>
<i>snr190-[mut.C] + snr190-[mut.A]</i>	BY4741	pCH32 + U14- <i>snr190</i> -[mut.A]	<i>MATa; his3Δ1; leu2Δ0; met15Δ0; ura3Δ0; snr190-[mut.C] (CRISPR-Cas9)</i>
<i>snr190-[mut.C] + snr190-[mut.B]</i>	BY4741	pCH32 + U14- <i>snr190</i> -[mut.B]	<i>MATa; his3Δ1; leu2Δ0; met15Δ0; ura3Δ0; snr190-[mut.C] (CRISPR-Cas9)</i>
<i>snr190-[mut.C] + snr190-[mut.AB]</i>	BY4741	pCH32 + U14- <i>snr190</i> -[mut.AB]	<i>MATa; his3Δ1; leu2Δ0; met15Δ0; ura3Δ0; snr190-[mut.C] (CRISPR-Cas9)</i>
<i>snr190-[mut.C] + snr190-[mut.S]</i>	BY4741	pCH32 + U14- <i>snr190</i> -[mut.S]	<i>MATa; his3Δ1; leu2Δ0; met15Δ0; ura3Δ0; snr190-[mut.C] (CRISPR-Cas9)</i>
<i>snr190-[mut.C]</i>	W303	∅	<i>MATa; leu2-3,112; trp1-1; can1-100; ura3-1; ade2-1; his3-11,15; [phi<sup>+</sup>]; snr190-[mut.C] (CRISPR-Cas9)</i>
<i>snr190-[mut.C] + E.V.</i>	W303	pCH32	<i>MATa; leu2-3,112; trp1-1; can1-100; ura3-1; ade2-1; his3-11,15; [phi<sup>+</sup>]; snr190-[mut.C] (CRISPR-Cas9)</i>
<i>snr190-[mut.C] + SNR190</i>	W303	pCH32 + WT U14-SNR190insert	<i>MATa; leu2-3,112; trp1-1; can1-100; ura3-1; ade2-1; his3-11,15; [phi<sup>+</sup>]; snr190-[mut.C] (CRISPR-Cas9)</i>
<i>snr190-[mut.C] + snr190-[mut.A]</i>	W303	pCH32 + U14- <i>snr190</i> -[mut.A]	<i>MATa; leu2-3,112; trp1-1; can1-100; ura3-1; ade2-1; his3-11,15; [phi<sup>+</sup>]; snr190-[mut.C] (CRISPR-Cas9)</i>
<i>snr190-[mut.C] + snr190-[mut.B]</i>	W303	pCH32 + U14- <i>snr190</i> -[mut.B]	<i>MATa; leu2-3,112; trp1-1; can1-100; ura3-1; ade2-1; his3-11,15; [phi<sup>+</sup>]; snr190-[mut.C] (CRISPR-Cas9)</i>
<i>snr190-[mut.C] + snr190-[mut.AB]</i>	W303	pCH32 + U14- <i>snr190</i> -[mut.AB]	<i>MATa; leu2-3,112; trp1-1; can1-100; ura3-1; ade2-1; his3-11,15; [phi<sup>+</sup>]; snr190-[mut.C] (CRISPR-Cas9)</i>

### Supplementary Table 3 Yeast strains used in this study

Inventory of the yeast strains used in this study with their genetic background (W303 or BY4741), the enclosed plasmids and genotypes.

OLIGONUCLEOTIDE	SEQUENCE (5'- 3')	EXPERIMENT
OHA494	GATCAAGAGACACCATTATCATCAGTTTTAGAGCTAG	Mutagenesis of <i>SNR190</i> box C by CRISPR-Cas9, cloning into pML104
OHA495	CTAGCTCTAAAACCTGATGATAATGGTGCTCTT	Mutagenesis of <i>SNR190</i> box C by CRISPR-Cas9, cloning into pML104
OHA496	GAAATTCATGACACTTTTTAAACAGAAAAGAAGATTGATTGGAACATTGATAATGGTGCTCTTCTTCTCGTCCGATTCGACCATGACGACAA	Mutagenesis of <i>SNR190</i> box C by CRISPR-Cas9, donor oligonucleotide
OHA504	GATCCGTCATGGTCGAATCGGACGTTTTAGAGCTAG	Mutagenesis of <i>SNR190</i> box A by CRISPR-Cas9, cloning into pML104
OHA505	CTAGCTCTAAAACCGTCCGATTCGACCATGACG	Mutagenesis of <i>SNR190</i> box A by CRISPR-Cas9, cloning into pML104
OHA506	AAACAGAAAAGAAGAAATTGATTGGCCCTGATGATAATGGTGCTGTTATTTGAAGATCCGATTCGACCATGACGACAAGGGATTTATCTCGTCTCTT	Mutagenesis of <i>SNR190</i> box A by CRISPR-Cas9, donor oligonucleotide
OMJ132	AAAAGAAGAAATTGATTGGCCCTGATGATAATGGTGCTCTTCTTACTCTCCGATTCGACCATGACGACAAGGGATTTATCTCGTCTCTTAATGCG	Mutagenesis of <i>SNR190</i> box A, G34C, by CRISPR-Cas9, donor oligonucleotide
OMJ122	GACGGCCAGTGAATTCATCAACTCCCTTCAAAT	Genomic amplification of <i>U14-SNR190</i> gene
OMJ123	AAGTTATTAGGTGATATCATCAATTTTTGTTAATCCCGT	Genomic amplification of <i>U14-SNR190</i> gene
OMJ124	GATCTTCAAATAACAGACACCATTATCATCAGGGCC	Mutagenesis of snR190 box A on plasmid <i>pCH32-U14-SNR190</i> by InFusion
OMJ125	TGTTATTTGAAGATCCGATTCGACCATGACG	Mutagenesis of snR190 box A on plasmid <i>pCH32-U14-SNR190</i> by InFusion
OMJ126	TAAGTGGCCGAACAAAAGTTCCCGTTTGCAAAAC	Mutagenesis of snR190 box B on plasmid <i>pCH32-U14-SNR190</i> by InFusion
OMJ127	TTGTCGGCCACTTATACAACATGCAGATCTGAGCC	Mutagenesis of snR190 box B on plasmid <i>pCH32-U14-SNR190</i> by InFusion
OMJ138	TAAAAGGTTGTTTCGTCATGGTCGAATCGGAC	Mutagenesis of snR190 internal stem on plasmid <i>pCH32-U14-SNR190</i> by InFusion
OMJ139	CGAAACAACCTTTTATCTCGTCTCTTAATGCGA	Mutagenesis of snR190 internal stem on plasmid <i>pCH32-U14-SNR190</i> by InFusion
OHA497BIS	GCCAAGCGCGCAATTAACCC	pML104 sequencing for mutagenesis by CRISPR-Cas9
OHA497	CGACTTCAGCATTGCACTCC	Genomic <i>SNR190</i> sequencing
OHA498	CCGAGAGTACTAACGATGGG	Genomic <i>SNR190</i> sequencing
OHA602	AGAATCAGTGGGAAAAGAACCCCTGTTGAG	Mutagenesis of 25S rRNA C2392U on plasmid <i>pNOY373</i> by InFusion
OHA603	TTCCCACTGATTCTGCCAAGCCCGTTC	Mutagenesis of 25S rRNA C2392U on plasmid <i>pNOY373</i> by InFusion
OHA604	AGAATCAGCGGGAAAAGAACCCCTGTTGAG	Mutagenesis of 25S rRNA U2392C on plasmids <i>Sup. #2</i> and <i>Sup. #10</i> by InFusion
OHA605	TTCCCGCTGATTCTGCCAAGCCCGTTC	Mutagenesis of 25S rRNA U2392C on plasmids <i>Sup. #2</i> and <i>Sup. #10</i> by InFusion
OHA606	CTTAGAAGCTGTACGACAAGG	Amplification and sequencing of 25S rDNA on <i>pNOY373</i>
OHA607	TCGATAGGCCACACTTTCATGG	Amplification and sequencing of 25S rDNA on <i>pNOY373</i>
RT Primer #1	TACACCCCTATGTCTTCCAC	OMJ147, methylation mapping by RT, 25S rRNA position 2434 to 2455
RT Primer #2	CACAATGTCAAAGTAGAGTCAAGC	OMJ146, methylation mapping by RT, 25S rRNA position 2413 to 2436
Nop7-HTP-Fwd	ATTGCCAAACAAAAGCTAAAAGTGAATAAACTAGATTCCAAGAAAGAGCACCATCACCATCACC	<i>NOP7::HTP</i> strain construction
Nop7-HTP-Rev	TAAAGTAATAAAGATGTTAAATTAAGACAAAATTTTGAAGGTACGACTCACTATAGGG	<i>NOP7::HTP</i> strain construction
Noc1-TAP-Fwd	ACGACAGTGAAGTTCGCTTCCG	<i>NOC1::TAP</i> strain construction
Noc1-TAP-Rev	GATGACTTGAAGAGCGCAATTCG	<i>NOC1::TAP</i> strain construction
23S.1	GATTGCTCGAATGCCCAAAG	Northern blotting probe, detection of 35S, 33S/32S, 27SA2 and 23S pre-rRNAs
rRNA2.1	GGCCAGCAATTTCAAGTTA	Northern blotting probe, detection of 35S, 33S/32S, 27SA2, 27SB and 7S pre-rRNAs
20S.3	TTAAGCGCAGGCCCGGCTGG	Northern blotting probe, detection of 35S, 33S/32S, 23S and 20S pre-rRNAs
25S	CCATCTCCGGATAAAC	Northern blotting probe, detection of mature 25S rRNA
18S middle	CATGGCTTAATCTTTGAGAC	Northern blotting probe, detection of mature 18S rRNA
5.8S	TGCGTTCAAAGATTCTGATG	Northern blotting probe, detection of mature 5.8S rRNAs
5S	CATCACCCTGGTATGCGC	Northern blotting probe, detection of mature 5S rRNA
SNR190 #1	CCTGTGCTCATGGTCGAATCG	Northern blotting probe, detection of snR190 snoRNA (nucleosides 37 to 58)
SNR190 #2	CGAGGAAAAGAAGAGACACCATTATC	Northern blotting probe, detection of snR190 snoRNA (nucleosides 10 to 34)
U14	CTCAGACATCTAGGAAGG	Northern blotting probe, detection of U14 snoRNA (nucleosides 105 to 123)
SNR37	GATAGTATTAACCACTACTG	Northern blotting probe, detection of snR37 snoRNA (nucleosides 6 to 25)
SNR38	CCATTGACAGAGGATAACTGTTTG	Northern blotting probe, detection of snR38 snoRNA (nucleosides 25 to 49)
SNR71	GATCTGAGTGAGCTGAGAAGGTT	Northern blotting probe, detection of snR71 snoRNA (nucleosides 14 to 36)
SNR5	GTCTACTCCAGCCATTTGC	Northern blotting probe, detection of snR5 snoRNA (nucleosides 71 to 90)
SNR10	CATGGGTCAAGAACGCCCGGAGGGG	Northern blotting probe, detection of snR10 snoRNA (nucleosides 54 to 79)
SNR42	TCAAACAATAGGCTCCCTAAAGCATCACAA	Northern blotting probe, detection of snR42 snoRNA (nucleosides 9 to 38)
SNR61	GGTTCAGAAGCAGAAGTGAATAG	Northern blotting probe, detection of snR61 snoRNA (nucleosides 22 to 44)

## Supplementary Table 4 Oligonucleotides used in this study

Inventory and sequence of the oligonucleotides used in this study.

## SUPPLEMENTARY REFERENCES

1. Cannone, J. J. *et al.* The comparative RNA web (CRW) site: an online database of comparative sequence and structure information for ribosomal, intron, and other RNAs. *BMC Bioinformatics* **3**, 2 (2002).
2. Lindahl, L. *et al.* RNase MRP is required for entry of 35S precursor rRNA into the canonical processing pathway. *RNA* **15**, 1407–1416 (2009).
3. de la Cruz, J., Kressler, D., Rojo, M., Tollervey, D. & Linder, P. Spb4p, an essential putative RNA helicase, is required for a late step in the assembly of 60S ribosomal subunits in *Saccharomyces cerevisiae*. *RNA* **4**, 1268–1281 (1998).
4. Rosado, I. V. *et al.* Characterization of *Saccharomyces cerevisiae* Npa2p (Urb2p) reveals a low-molecular-mass complex containing Dbp6p, Npa1p (Urb1p), Nop8p, and Rsa3p involved in early steps of 60S ribosomal subunit biogenesis. *Mol. Cell. Biol.* **27**, 1207–1221 (2007).